Wave Mechanics in Constructed Oyster Reefs and the Design of Nature-Based Coastal Adaptation

by

James Vincent Brice

B.S. Applied Physics, Rensselaer Polytechnic Institute, 2016

Submitted to the Department of Architecture and the
Department of Civil and Environmental Engineering
in partial fulfillment of the requirements for the degrees of

MASTER OF ARCHITECTURE

and

MASTER OF SCIENCE IN CIVIL AND ENVIRONMENTAL ENGINEERING

at the

MASSACHUSETTS INSTITUTE OF TECHNOLOGY

May 2024

Authored by:	James Vincent Brice Department of Civil and Environmental Engineering, Department of Architecture April 29, 2024
Certified by:	Heidi M. Nepf Professor of Civil and Environmental Engineering, Thesis Supervisor
Certified by:	Mark Jarzombek Professor of the History and Theory of Architecture, Thesis Supervisor
Accepted by:	Leslie K. Norford Chair, Department Committee on Graduate Students Professor of Building Technology
Accepted by:	Heidi M. Nepf Chair, Department Committee on Graduate Students Professor of Civil and Environmental Engineering

Thesis Supervisors

Heidi Nepf, PhD
Professor of Civil and Environmental Engineering

Mark Jarzombek, PhD
Professor of the History and Theory of Architecture

Wave Mechanics in Constructed Oyster Reefs and the Design of Nature-Based Coastal Adaptation

by

James Vincent Brice

Submitted to the Department of Architecture and the
Department of Civil and Environmental Engineering
on April 29, 2024 in partial fulfillment of the requirements for the degrees of

MASTER OF ARCHITECTURE

and

MASTER OF SCIENCE IN CIVIL AND ENVIRONMENTAL ENGINEERING

ABSTRACT

There has been great interest in the potential of constructed oyster reefs (CORs) to function as nature-based coastal protection infrastructure, but most projects to-date are designed primarily for wave attenuation and fail to consider both the environmental conditions necessary for long-term oyster reef sustainability as well as the importance of education and outreach in fostering environmental stewardship. Realizing the promise of nature-based coastal adaptation means building physical, ecological and social infrastructure simultaneously, requiring a design-research methodology that combines an understanding of biological design constraints, physical analysis and community engagement.

Physical and numerical wave flume experiments were conducted to investigate mechanisms of wave energy loss in oyster shell gabion-type CORs that place oyster biology in the foreground— particularly, the influence of across-shore width, spacing and structure porosity on wave attenuation under non-breaking wave conditions. Gabion widths of $\mathcal{O}(1)$ wavelength were found to attenuate waves by 40%. These losses were driven primarily by internal drag which was characterized experimentally and accurately modeled with the modified Ergun Equations and the *waves2Foam* library of the open-source CFD software OpenFOAM.

This research was then translated into a suite of interactive design activities, featuring a tabletop wave flume, scale models of coastal features, and a set of coastal community member cards. Through design and creative inquiry, these tools seek to communicate complex biophysical processes in coastal ecosystems while empowering communities to reimagine what it really means to *build with nature*.

Thesis supervisor: Heidi M. Nepf, Professor of Civil and Environmental Engineering

Thesis supervisor: Mark Jarzombek, Professor of the History and Theory of Architecture

Acknowledgments

This work was made possible through 4 years of reading, drawing, talking, modeling, analyzing and collaborating with friends, family and colleagues in both the Department of Architecture and Department of Civil and Environmental Engineering here at MIT. I'm grateful that I had the opportunity to work alongside so many fun, kind and brilliant people during my graduate program, and would like to personally thank the following individuals:

I would first and foremost like to thank my principle research advisor, Heidi Nepf, for welcoming me into the lab, inspiring me to pursue a career in fluid dynamics, and whose guidance, support and enthusiasm made this work as enjoyable as it was fruitful.

Many thanks as well to Mark Jarzombek for his insights and support of this entirely architectural M.Arch thesis, and to Carolina Bastidas, for our conversations about oysters and the world shellfish restoration.

Rylee Eterginoso, Donna Pagano, Susan Hogan and Jenya Frid at the Staten Island Museum, for their collaboration on the *Resilient Coast* lesson plan and invitation to the *Vulnerable Landscapes* exhibition, as well as the MIT PKG Center for financial support.

I owe much to my colleagues in the Nepf Environmental Fluid Mechanics Lab: Ernie Lee, Tian Zhao, Rachel Schaefer, Hyoungchul Park, Thomas van Veelan, Chuyan Zhao, and dear friend/collaborator, Autumn Deitrick. I would like to thank Stephen Rudolph for his help designing the mini-flume, and the undergraduate researchers who have joined the lab and worked with me: Jennifer C. Espinoza, Caroline Langmeyer and Diego Tempkin.

Bella Carriker and Amanda Ugorji for being supportive friends with great insights who made studio fun (when studio was fun).

I would like to thank the Morningside Academy for Design for financial support, and all the lovely people I met during my fellowship there for inspiring me to believe in design.

Many thanks to my loving family - my sister, my dad, and to my mom who taught me how to look at a concrete jungle and see the birds.

And finally, Noah, for being my partner, best friend and fellow oyster connoisseur through the good, bad and ugly (looking at you Covid-19) of graduate school. Looking forward to poking around in more tidepools with you.

Contents

List of Figures

All images by author

List of Tables

Chapter 1

1.1 Crassostrea virginica

The life cycle of the Atlantic Oyster begins in a rush of fluid broadcast into the water column where microscopic egg and sperm cells meet by pure statistical chance. Once fertilized, the eggs of *Crassostrea virginica* drift away from their spawning grounds on the ebb and flow of the tidal currents that characterize estuaries. Their cells divide until they become juvenile, free-swimming larvae, and for two weeks they float in the water column, eat phytoplankton and progress through various life stages. With little ability to control their movements, they are unable to defend themselves from hungry predators like copepods, larger zooplankton and marine worms—only a very small percentage of the 15-115 million eggs broadcast by a single oyster survive long enough to grow the small foot-like appendage that marks the pediveliger stage. These larvae then begin to hover above the seabed, waiting until they find a hard substrate to attach to like concrete, rock, or (more typically) oyster shell. Once a suitable substrate is found, the larvae settle and secrete a biogenic concrete mixture that fixes them in place. At this stage, they have officially become spats and will spend the rest of their lives as sessile, benthic organisms that rely on physical transport in the water to carry them the nutrients they need to thrive (Bayne, 2017).

Despite their stationary habit, oysters are far from passive in this process and take a remarkably active role in modifying their surroundings. Like most bivalves, oysters feed off of suspended particles in the water by filtering them through their gills and sorting out specific nutrients for food or excretion. They rely heavily on phytoplankton as a source of carbon which is used for general metabolic function as well as shell formation. Other forms of organic and inorganic particulate matter are filtered out of the water column as well and are either used for tissue growth or excreted as pseudofeces and passed to denitrifying bacteria living in the substrate—a critical component of aquatic nitrogen cycles (Smyth et al., 2016). This

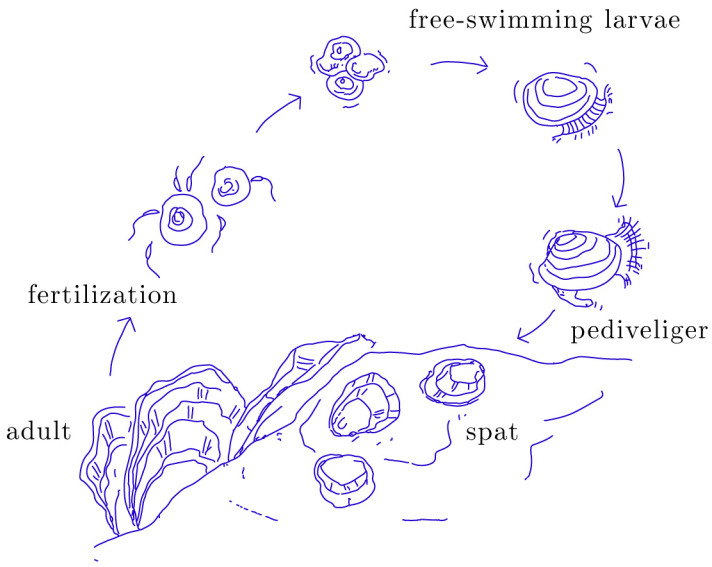

Figure 1.1: Life-cycle of the oyster

filtration process improves water clarity (turbidity), allowing sunlight to penetrate deeper in the water column and enhancing growing conditions for submerged aquatic vegetation (SAV) that rely on sunlight for photosynthesis (Newell and Koch, 2004).

By increasing habitat heterogeneity in areas of soft bottom sediment, oyster reefs also influence estuarine community composition by promoting both species diversity and abundance (Posey et al., 2003). Their complex, vertical structure acts as home and foraging ground for countless species of small marine invertebrates, larval fish, gastropods and crustaceans. Predator-prey interactions within oyster reefs can also augment the transfer of energy up the trophic web and strengthen populations of higher-order (and often commercially valuable) predators like tarpon, red drum fish and even dolphins (Peterson et al., 2003).

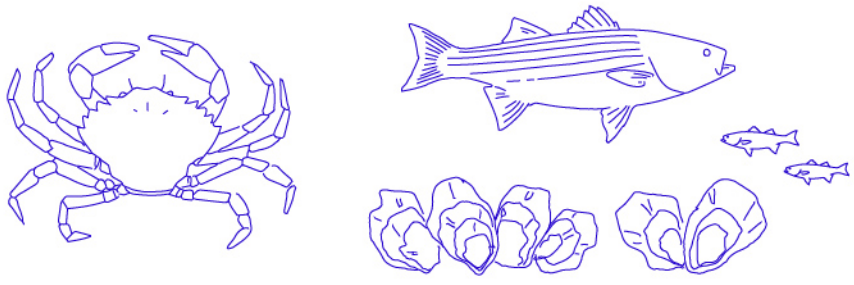

Figure 1.2: Oyster reefs as ecological infrastructure

There is a long history of influence by the oyster in human society, where evidence of oyster reefs having cultural value trace as far back as 8000 years before present (Thompson and Worth, 2011). Massive mounds of oyster shell can be found along the entirety of the eastern coast of the United States (along with many other coastal regions across the globe including Brazil, Southeast Asia and the Atlantic Sahara). Ranging in size from just a few to a few hundred meters in diameter, these mounds were once thought to be merely the leftover waste of cultures who subsided primarily on shellfish, however recent analysis indicates these sites may actually be evidence of complex building traditions: mortuary rites, cultural artifacts, heritage sites, landscape interventions and perhaps even coastal infrastructure (Ceci, 1984; Schwadron, 2010). Thousands of years later in the Southern U.S. and Puerto Rico, many shell mounds primarily composed of oyster shells were instrumental in the creation of the cement aggregate building material known as tabby concrete (Sheehan and Sickels-Taves, 2002). Coastal societies of both Native Americans and colonists have regarded the oyster as an important food source, but it wasn't until the industrial revolution that oyster farming became a commercial enterprise. Today, oyster mariculture is a global industry with a strong place in coastal marine economies (Matthiessen, 2008).

Figure 1.3: Oyster reefs as social infrastructure

Oysters also have an extraordinary ability to alter local hydrodynamic conditions across scales. At the scale of the oyster, water passing over is forced to adjust, bending around the sharp edges and crevices between oyster shells and generating small, chaotic vortices. This pulls energy away from larger, mean flows (like steady currents or periodic waves) and converts it into turbulent kinetic energy that cascades down to smaller and smaller length scales until it's dissipated as heat. By acting as a local sink of energy, oyster reefs create calm waters that stabilize shorelines, reduce edge erosion in marsh and SAV canopies, and decrease wear on coastal infrastructure.

Through the combination of these physical, ecological and social processes, oysters

Figure 1.4: Oyster reefs as physical infrastructure

heavily modify the coastal landscape at scales which we do not yet fully understand[1]. Although oysters have long been recognized as filter feeders who improve local water quality, it wasn't until the mid-20th century and the collapse of the Chesapeake Bay oyster fishery that scientists in the U.S. began to fully recognize their impact. It is estimated that during the peak of their population, oysters in Chesapeake Bay were able to filter the entire 15 trillion gallons of water in the estuary over the course of 4-5 days—a volume that would take the population recorded in 1991 over 400 days (Brooks, 1996). Following their decline, water quality in the Chesapeake suffered tremendously, phytoplankton blooms choked out SAV, water clarity plummeted, and entire regions of the bay were rendered unlivable due to hypoxic conditions at the bed (Rothschild et al., 1994).

In their seminal paper, Jones et al., 1994 coined the term "ecosystem engineer" to describe organisms that "directly or in-directly modulate the availability of resources (other than themselves) to other species... they modify, maintain and/or create habitats." Whether through their physical structure (e.g. corals) or through their actions (e.g. the beaver), all impact their local environment in ways that extend far beyond themselves. Although oysters are not specifically mentioned, the published proceedings of an oyster restoration conference held in Virginia in 1995 cite them as "potential ecosystem engineers (sensu Jones et al. 1994)" (Luckenbach et al., 1999).

This paper was part of a greater movement in restoration ecology driven by a growing understanding of the complex relationships between ecological and physical processes in the natural environment, and the benefits derived therein. Calls for oyster restoration in the

[1]The terms"physical, ecological and social" used throughout this thesis are meant to loosely categorize the reach of the oyster's influence and are not strict definitions. Other appropriate characterizations of these processes include socioeconomic, biogeochemical, etc.; the oyster, it seems, resists disciplinary boundaries.

Chesapeake Bay and other areas began to cite the ecosystem services provided by oyster reefs, a concept first introduced by John Holdren in 1974 as "natural services" (Holdren and Ehrlich, 1974) but popularized by Daily, 1997. According to Daily, ecosystem services are defined as "the conditions and processes through which natural ecosystems, and the species that make them up, sustain and fulfill human life. They maintain biodiversity and the production of ecosystem goods, such as seafood, forage, timber, biomass fuels..." etc., in addition to "actual life-support functions, such a cleansing, recycling, and renewal, and they confer many intangible aesthetic and cultural benefits as well."

Today, oysters are widely regarded as ecosystem engineers that provide a slew of ecosystem services (Grabowski and Peterson, 2007), but the context in which they are discussed is evolving. In contrast to oyster restoration efforts that focused primarily on strengthening populations for economic means, as well as those initiated in the late 20th century to restore greater ecological function and return the ecosystem to some previous or reference state (or both, as discussed in Breitburg et al., 2000), oysters are now a part of a growing effort to integrate natural ecosystems into the design of climate-resilient coastal infrastructure: a movement broadly termed *Building with Nature*.

1.2 Nature-based Solutions for Coastal Adaptation

Coastlines around the world face an uncertain future, with the impending impact of anthropogenic climate change posing a threat to human and non-human communities alike. On decadal time scales, heat trapped in the atmosphere by greenhouse gasses is causing the sea to warm and expand, melting glaciers, polar ice caps, and causing sea levels to rise (Drake, 2014). These processes have driven acute impacts and altered regional climate: wind patterns, wave action, precipitation and storm intensity (Knutson et al., 2010). The stark realities of these changes already felt around the world have spurred research into new coastal engineering solutions that can protect coastlines from climate-change related impacts.

In contemporary coastal planning, coastal adaptation is often taken to mean the unyielding fortification of the shoreline in the face of global climate change. It is typically implemented in the form of "gray infrastructure": static, hard engineering projects like seawalls, breakwaters, and multi-billion-dollar levees. Although successful in stabilizing coastlines and preventing flooding due to storm-surge, these structures are the cause of several negative externalities. They significantly inhibit access to the shore and degrade ecosystems reliant on the tidal exchange for life and sustenance (Torio and Chmura, 2013). Their totalizing approach can increase erosion by restricting the supply of sediment or redi-

recting energy that was once dissipated by coastal marshes toward areas more vulnerable (Sutherland et al., 2006). They are often singular, unmoving, and difficult to design as climate-change introduces evermore uncertainty in projections for the 2070 design flood elevation (Dedekorkut-Howes et al., 2020).

An alternative is emerging, one in which *Crassostrea virginica* plays a key role. Increased understanding within coastal management communities of the physical resilience embedded within coastal habitats like salt marshes, mangrove forests and oyster reefs has driven efforts to explore the efficacy of their implementation in the design of coastal protection infrastructure (Cheong et al., 2013; Chowdhury et al., 2021). At landscape scale, laboratory, field and modeling studies point to the ability of mangrove forests and coastal wetlands to reduce flood elevations during tropical cyclones and small tsunamis (Zhang et al., 2012; Marois and Mitsch, 2015; Rezaie et al., 2020; Fairchild et al., 2021), the global value of which may exceed 65 billion dollars USD annually (Menéndez et al., 2020). At smaller scales, coastal reefs and vegetation of various species can stabilize shorelines by dissipating wave energy (Lowe et al., 2005; Piazza et al., 2005; Gedan et al., 2011; Borsje et al., 2011), reducing wave-driven overtopping (Keimer et al., 2021) and wave loading on coastal structures (Vuik et al., 2016).

"Building with Nature", "Engineering with Nature", "Nature-based Solutions", "Ecological Engineering" and "Green Infrastructure" are just a few of the many variants of nature-driven design and planning frameworks that have gained legal, financial and cultural traction, particularly in the US and Europe (De Vriend et al., 2015; Seddon et al., 2020). Like the ideas of ecosystem services, these concepts are not new outright; most literature around green infrastructure in the U.S. emerged from the greenways movement of the 1990s, popularized by books like Greenways for America (Little, 1995), which sought to increase green spaces in cities and suburbs by preserving linear stretches of naturalized open-space along roads and river banks. The term "green infrastructure" is attributed to Buddy MacKay in 1994, then chairman of the Florida Greenways Commission, who advocated for planning initiatives that recognized natural ecosystems as critical "infrastructure" worth investing in, however human societies have been "building with nature" for millennia[2].

In this work, *building with nature* refers specifically to the contemporary movement in coastal management, defined by Dutch government-sponsored EcoShape as "a new philosophy in hydraulic engineering that utilizes the forces of nature, thereby strengthening nature, economy and society." This effort has been spearheaded by many practitioners in

[2]Particularly, indigenous societies (Berkes, 2017)

the Netherlands (in fact, "Building With Nature" is trademarked by EcoShape), but has gained momentum in the U.S. Even the United States Army Corps of Engineers (USACE), who has been responsible for the fortification of thousands of kilometers of coastal and riverine shoreline since it's founding over 200 years ago[3], has joined the effort. Their Engineering with Nature division, founded in 2014, has published hundreds of technical reports, resource guides and tools meant to accelerate the implementation of nature-based solutions for coastal adaptation. On Earth Day, April 2022, the Biden Administration issued Executive Order 14072, which stressed the importance of "deploying nature-based solutions to tackle climate change and enhance resilience." Globally, nature-based solutions have been endorsed by the IPBES Global Assessment (Díaz et al., 2019), the Climate Change and Land Report of the Intergovernmental Panel on Climate Change (IPCC) (Shukla et al., 2019), and were highlighted as one of nine key action tracks at the 2019 UN Climate Action Summit (Nations, 2019).

Reports on the physical performance of nature-based solutions for coastal adaptation are mixed, with some studies touting clear success (Gittman et al., 2014; Huynh et al., 2024) and others noting the variability in performance across geographies and adaptation strategies (Chausson et al., 2020). The primary benefit of nature-based solutions—of green vs. gray infrastructure—is not purely their capacity to replace the functionality of traditional coastal adaptation but in their ability to provide additional social and ecological co-benefits to human and non-human coastal communities. Where gray infrastructure is rigid and inflexible, green infrastructure can grow and evolve. Where gray infrastructure restricts access to the coastline, green infrastructure can facilitate this access by creating habitat and strengthening human relationships to the environment. The power of this potential has gripped the imaginations of coastal managers across the globe.

Given the clear advantage of nature-based solutions over gray infrastructure and the growing interest and support from communities, industry, state and federal governments as well as global entities, one would anticipate a surge in the design and implementation of building with nature projects; perhaps unsurprisingly, this has proven to be a challenge (Nelson et al., 2020).

1.3 How (Not) to Build a Better Breakwater

Oyster reefs have the ability to dissipate wave energy, making them a strong candidate for shoreline stabilization projects which seek to minimize erosion or mitigate wave-driven

[3]notably, the massive expansion of the levee system in the Mississippi River (Alexander et al., 2012)

overtopping of coastal structures. Furthermore, because oysters grow vertically in reef assemblages, accreting from 7 to 17 mm per year, evidence suggests that oyster reefs will be able to keep pace with future sea level rise projections, making them a resilient alternative to gray infrastructure that could degrade or be over-topped completely over time (Rodriguez et al., 2014).

Unfortunately, oysters now inhabit only a small percentage of their historic range (Rothschild et al., 1994); for oyster reefs to be a viable alternative to traditional coastal protection infrastructure at scale, a new class of *building-with-nature*-based designers need methods that synthesize expertise from ecological restoration, coastal engineering, urban planning, and landscape architecture to not only restore degraded reefs, but establish new reefs that survive in the urbanized coastal landscape (Freeman et al., 2019). To build with the oyster is to recruit the oyster - (1) to create the conditions necessary for oyster survival, growth, and reproduction, (2) to provide hard substrate for larval settlement, and (3) to ensure an adequate supply of larvae to support long-term reef sustainability (Howie and Bishop, 2021).

Research into oyster reef restoration has been going on for decades, with scientists in the Chesapeake contributing significantly to the effort. Best practices typically involve the introduction of concrete, crushed limestone, or oyster shell to a site (Breitburg et al., 2000). If there are sizeable wild populations of oyster in the area, this can be sufficient, however most restoration efforts often jump-start reef development via the seeding of oyster larvae reared in a nursery or the placement of live oyster directly on the site (either adults or "spat-on-shell" juveniles).

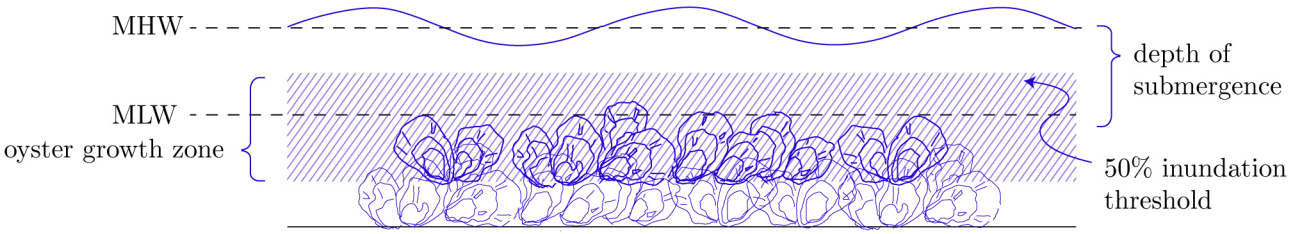

Figure 1.5: Oyster reef growth zone. The top of this region is a threshold defined as an inundation duration of <50%. MHW (mean high-water) and MLW (mean low-water) indicate the extent of the tidal range.

Although simple in theory, oyster reef restoration projects faced limited success until the mid-2000's and the adoption of new methods which considered the interaction between local hydrodynamics and reef geometry (Powers et al., 2009; Lipcius et al., 2015). Flow

velocity above the reef controls the supply of nutrients, the settlement of larvae and the deposition of sediment, with higher current velocities being linked to higher oyster growth rates. Reef crest height above the sea floor and depth of submergence (see Figure 1.5) have also been linked to reef success. When evaluating mortality rates in constructed oyster reefs, oysters have been found to grow best in a specific vertical zone of the water column termed the "oyster growth zone." The exact location of this zone is a function of local tidal range, submergence depth and the resulting time the oysters spend under the water during a tidal cycle. *Crassostrea virginica* is typically found in a zone corresponding to being submerged for 60-80% of the tidal cycle, with 50% and 90% being the respective lower and upper threshold[4] (Byers et al., 2015; Roegner and Mann, 1995; Solomon et al., 2014; Marshall et al., 2020). Reefs that spend <50% of the tidal cycle submerged ("inundation duration," Morris et al., 2021) see population declines compared to those with a longer inundation duration. Although oysters are capable of creating a water-tight seal in their shells that allows them to survive varying degrees of aerial exposure, this is a source of environmental stress that prevents feeding and larval settlement (Luckenbach et al., 1999). Conversely, reefs with very low crest height above the sea floor see similar population declines due to higher rates of sedimentation (a function of flow velocity as well as sediment characteristics) which can choke out oysters and bury them over time (Walles et al., 2016). Clearly, designing healthy, self-sustaining oyster reefs necessitates an understanding of complex biophysical interactions in the coastal landscape.

According to Ysebaert et al., 2019, over 30% of the oyster reef restoration projects currently underway in the U.S. cite coastal protection as a restoration target. This has driven the emergence of reef restoration typologies designed specifically for wave attenuation like Oyster Castles and ReefBalls (shown in Figure 1.6). It's worth emphasizing the difference in general form between oyster restoration projects with the primary aim of promoting long-term oyster reef success versus constructed oyster reefs designed for coastal protection. In this case, reef height and depth of submergence are also key design parameters, but not for the same reason. Many constructed oyster reefs that seek to attenuate wave energy and stabilize shorelines do so via a process called depth-limited breaking. This is the same process by which waves to break as they approach the shore. As water depth decreases, the effect of the seabed on the waves becomes greater and forces them to slow down or *shoal*. Neglecting friction, the total energy in the wave must be conserved, therefore this decrease

[4]This threshold was defined based on *C. virginica* populations south of and including North Carolina. There are completely subtidal oyster reefs, particularly at higher latitudes on the eastern coast of the U.S. where exposed reefs face increased environmental stresses during the winter months (Byers et al., 2015).

in speed must be balanced by an increase in wave height[5]. Eventually the wave gets so steep that it collapses on itself, losing a significant amount of energy in the process.

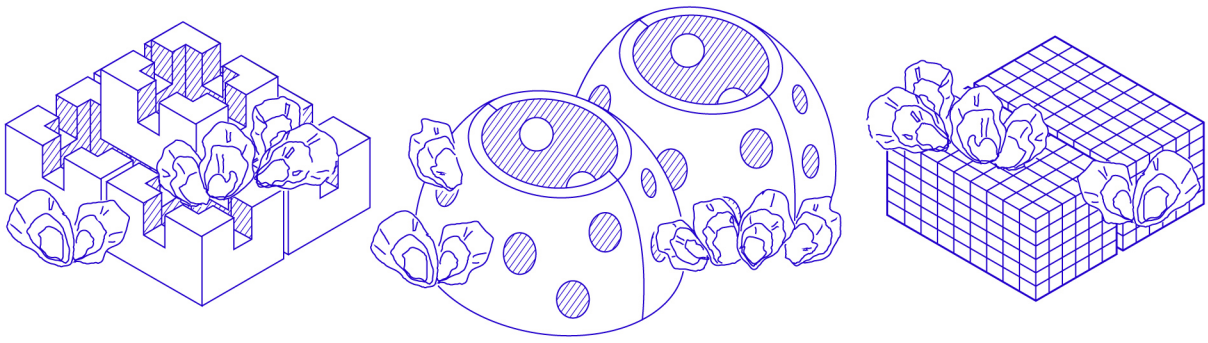

Figure 1.6: Example oyster restoration structures: Oyster Castles (left), ReefBall (center) and oyster shell gabions (right).

Even in non-breaking wave conditions, wave attenuation by submerged structures will be higher the closer the structure is to the water surface (Seabrook and Hall, 1999), so it's no wonder that typical designs of constructed oyster reefs for coastal protection are narrow in the shore-perpendicular direction with shallow submergence depths. Like breakwaters, these reefs are designed to induce depth-limited breaking by functioning as an abrupt change in local water depth and don't design explicitly for other mechanisms of energy loss like friction and internal drag[6].

If oysters prefer limited aerial exposure and deeper submergence depths, but inducing wave-breaking requires shallow submergence depths, the question arises whether it is even possible to design for both these outcomes simultaneously. Morris et al., 2019 describe this situation in their commentary aptly titled, "The application of oyster reefs in shoreline protection: Are we over-engineering for an ecosystem engineer?", highlighting the potential incongruence between constructed oyster reef design for engineering performance and that for biological persistence. Research focused on wave energy attenuation in constructed oyster reefs that fails to considers whether these reefs will be able to support living, biological communities, effectively renders their proposed interventions no different than traditional, gray infrastructure. Morris et al., 2019 argue that if we wish to truly take advantage of the ecosystem engineering ability of the oyster, we should design structures that can grow in time

[5]wave celerity $c = \omega/k$. Because wave energy flux $\frac{\partial E}{\partial x} + \nabla \cdot \vec{F} = 0$, the number of waves entering the system per unit time i.e. ω is constant. A decrease in c requires a decrease in wavelength $L = 2\pi/k$, thus for energy to be conserved, the energy $E = 1/2\rho g a^2$ per unit length must increase.

[6]A more complete discussion of the constituent mechanisms of wave energy dissipation in constructed oyster reefs is given in Chapter 2

and support healthy, self-sustaining reefs, even if this means that they will not reach their full potential as physical infrastructure for the first few years following their implementation.

1.4 Design with Living Systems

The inability of oyster reefs constructed for coastal protection to respond to the biological reality of designing with living systems is symptomatic of a larger trend in nature-based coastal adaptation. "Living shorelines" (sometimes including oyster reefs but not always) are another alternative to traditional shoreline stabilization projects that seek to soften the coastal margin through the use of natural materials and habitat like marsh vegetation (Bilkovic et al., 2016). Although there is strong evidence that living shorelines can be designed to achieve ecological functionality comparable with reference fringing marshes (Isdell et al., 2021), many projects amount to little more than traditional rock revetments with vegetation incorporated as an after-thought (Cooper and Pilkey, 2012). Firth et al., 2020 warn of a similar kind of blue-greenwashing in "integrated green-gray infrastructure" (IGGI), which is marketed as a strategy to improve the ability of traditional coastal infrastructure to function as marine habitat, but in some cases acts as a "Trojan horse to facilitate coastal development." Although these structures do often support some form of life, they tend to have a markedly different community composition compared to native populations (Burt et al., 2013) and there is some doubt as to whether they actually improve ecosystem functionality (Firth et al., 2020; Chapman and Underwood, 2011). Other projects, though well-intentioned, fail to incorporate guidance from ecological restoration practitioners in the design process, at times introducing monocultures of non-native species as "bioshields" against climate change impacts that do more harm to local ecosystems than good (Feagin et al., 2010).

There is also some doubt as to whether all nature-based solutions return their intended social co-benefits, driven in part by the lack of frameworks that consider the interaction between ecosystem function and socio-cultural factors (Raymond et al., 2017). In "Green Enough Ain't Good Enough", Meenar et al., 2022 document perceptions of green storm water infrastructure in environmental justice communities, noting that though community members may be aware of the supposed benefits of green infrastructure, they are skeptical about how they will work within their specific community. Further studies have found that a lack of understanding about nature-based coastal adaptation can undermine it's support (Josephs and Humphries, 2018). Many researchers and practitioners alike have cited the importance of community engagement and capacity building for the successful implementation of nature-based coastal adaptation (Frantzeskaki, 2019), noting that this will

require the integration of interdisciplinary expertise in physical, ecological and social science (Arkema et al., 2017).

The Billion Oyster Project in NYC is a notable example of the way oyster reef restoration can build both ecological and social infrastructure within coastal communities. This nonprofit organization is a collaboration between restoration ecologists, educators, citizen scientists and marine resource managers. In addition to leading an extensive oyster restoration effort in New York Harbor, they have worked with over 15,000 volunteers, 100 NYC schools and more than 8,000 students to educate the public about local marine ecosystems while providing pathways into green jobs (Billion Oyster Project, 2024). Critically, they recognize the importance of this effort within the community to the success of their ambitious restoration targets (one billion oysters restored) - as put succinctly on their website: "restoration without education is temporary."

The Billion Oyster Project does not seek to build physical infrastructure, not intentionally. Although coastal protection is sometimes cited as a benefit of their efforts by the media (Klinenburg, 2021), it is not framed as a part of their mission, nor is anyone on their team responsible for taking field measurements that would preclude this kind of design (e.g. local wave and velocity data). They have, however, been involved in an incredibly high-profile, high-budget project that does: *Living Breakwaters* by landscape architecture firm Scape. Winner of the Rebuild by Design competition hosted in 2015, this series of breakwaters being constructed off the coast of the southern edge of Staten Island aims to reduce wave energy at the coast while also providing suitable substrate for oyster reef restoration spearheaded by the Billion Oyster Project. Although it is often marketed as a green infrastructure project, *Living Breakwaters* is, first and foremost, a breakwater - a series of 6 very large, emergent breakwaters totaling 7200m in length. The idea here is not that oysters are attenuating any wave energy, but that once the structure is built, oysters provided by the Billion Oyster Project will be placed in the low-energy lee of the structure and colonize the surrounding base (Scape Studio, 2016). Barring custom-made concrete blocks with small depressions in them designed to increase the available surface area for tide pooling (another example of IGGI), the *Living Breakwaters* breakwaters are not very different than traditional breakwaters.

The $107 million dollar project is an impressive piece of physical infrastructure. The *Living Breakwaters* team also works to build social infrastructure through curriculum development in local schools and engagement with community stakeholders, and perhaps one day, through their collaboration with the Billion Oyster Project, the breakwater will

function as ecological infrastructure as well: it's tide pools full of marine worms, larval bass, green crabs, and it's crest a resting ground for harbor seals. It does not, however, integrate the inherent physical resilience of the oyster into it's design.

These are just a few examples of the hundreds of other oyster restoration projects that have been initiated in the U.S. within the last decade, all with their own focus and defined measure of success. Oyster reef living shorelines often prioritize coastal protection with an indifference to (and in some cases, at the expense of) ecological co-benefits, and yet there are many examples of restoration projects in which the effort is purely ecological. These cases, spearheaded by conservation groups like the Nature Conservancy and the National Oceanic and Atmospheric Administration Fisheries Department, measure success with species assemblages, biomass and biodiversity indicies (Baggett et al., 2015) with little attention placed on characterizing local hydrodynamics. Other initiatives like the Billion Oyster Project and the Louisiana Oyster Corps expand the scope of their restoration targets to include environmental stewardship, with success measured in number of volunteers or community groups engaged. Still others focus on the restoration of recreational fisheries (Gilby et al., 2018).

These projects seek to leverage the capacity of oyster reefs to function as a kind of infrastructure, be it physical, ecological or social. In some cases their functionality overlaps, and in some it does not. Although many are examples of successful oyster reef restoration based on the metrics for which they've been designed, none can say they've truly realized the promise of nature-based coastal adaption.

1.5 Physical, Ecological and Social Infrastructure

Nature-based solutions for coastal adaptation are a promising alternative to traditional, gray infrastructure that degrade coastal ecosystems, restrict access to the coast, and fail to respond to the uncertainties of design for future climate. Oyster reefs have great potential to function as coastal protection infrastructure while also providing critical ecosystem services: creating habitat and increasing biodiversity, improving water quality and water clarity, strengthening commercial fisheries and marine economies, and building social resilience through green job creation and environmental stewardship. Despite growing interest in constructing oyster reefs for this application, few projects to date successfully reconcile intended engineering outcomes and the biological reality of designing with living systems, in some instances *building with nature*-as-construction material - no different that we build breakwaters of quarried rock or concrete (e.g. oyster breakwaters). In other instances, *building with nature*-as-facade-

treatment: blue-greenwashing and the greening of gray infrastructure (e.g. IGGI). Still others, *building with nature*-as-machine, seek to harness the function of nature as a single component without consideration for the greater ecology (e.g. mangrove monocultures).

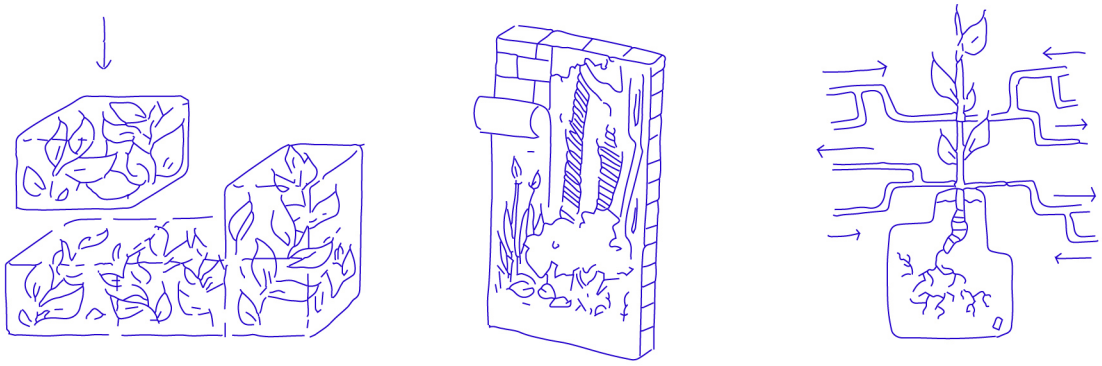

Figure 1.7: What is *building with nature?*

What makes *Living Breakwaters* effective physical infrastructure and the Billion Oyster project successful social infrastructure is their design. This thesis investigates the capacity of constructed oyster reefs to function as physical, ecological and social infrastructure *simultaneously* through a design research methodology that integrates biological constraints with physical analysis in environmental fluid mechanics and community engagement.

Chapters 2 and 3 describe physical and numerical experiments conducted at the Ralph M. Parsons Laboratory that investigate wave mechanics and energy loss mechanisms in constructed oyster reefs. In an effort to prioritize the conditions necessary for oyster survival and long-term reef sustainability, alternatives to depth-controlled attenuation processes like increased across-shore width, spacing and structure porosity are explored under non-breaking wave conditions. This works seeks to improve knowledge of the mechanisms that govern wave energy dissipation in constructed oyster reefs to inform designs that maximize energy loss while prioritizing reef persistence.

Chapter 4 presents a design, education and engagement toolkit focused on building knowledge and sparking curiosity about biophysical processes in the coastal landscape. Developed in partnership and/or with support from the Staten Island Museum in NYC, the MIT PKG Center, the MIT Department of Civil and Environmental Engineering, the Morningside Academy for Design (MAD) and the Nepf Environmental Fluid Mechanics Lab, this toolkit including physical models, interactive activities and a tabletop wave flume aimed at increasing awareness about nature-based coastal adaptation while encouraging coastal communities to reimagine what it means to *build with nature*.

Chapter 2

2.1 Introduction

Although there is considerable variability in the form of constructed oyster reefs, all are essentially porous, irregular structures on the sea floor that are submerged some or all of the time. They are often compared to submerged rubble-mound breakwaters which have been extensively studied (Seabrook and Hall, 1999; Sollitt and Cross, 1972; Van der Meer et al., 2005; Christou et al., 2008) and provide a good starting point for understanding the underlying mechanics of wave energy loss. When waves propagate over submerged structures, they transform and lose energy which manifests as a decrease in wave height. Assuming the waves are linear, wave energy $E = \frac{1}{2}\rho g a^2$ and the amount of energy lost can be quantified by the wave transmission coefficient,

$$K_t = \frac{H_t}{H_i} = \frac{a_t}{a_i} \tag{2.1}$$

in which H_i and a_i are the initial wave height and wave amplitude respectively, H_t and a_t are the transmitted wave height and wave amplitude respectively, and $H = 2a$. K_t is a function of many parameters including the incident wave characteristics (H_i, L), physical properties of the fluid (ρ, μ, g), and geometric properties of the submerged structure $(h_c, h_s, B, d, h, n, \theta)$, where L is the wavelength, ρ is the density of water, μ is the dynamic viscosity, g is the gravitational acceleration, h_c is the crest height, h_s is the freeboard, B is the structure width, d is a characteristic diameter of the porous medium, h is the total water depth, and n is the porosity and θ is the seaward structure slope (see Figure 2.1). The dimensionless structure crest height h_c/h and dimensionless width B/L [1] are understood to be the largest controls

[1] In the context of submerged porous breakwaters, crest width B is often nondimensionalized as B/H_i, however it's arguably more useful to nondimensionalize against wavelength (or wave number) when exploring wave properties in the direction of wave propagation. This investigation takes the latter approach.

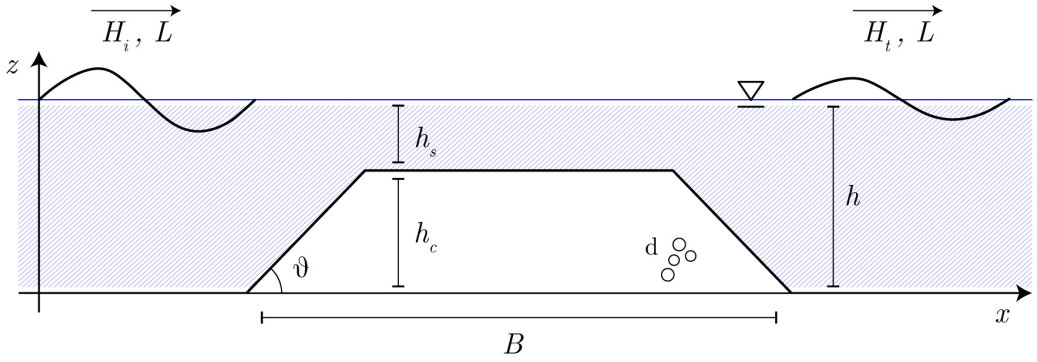

Figure 2.1: Breakwater design parameters

on wave transmission, with B becoming increasingly important as submergence increases (Seabrook and Hall, 1999).

Several studies have measured this transmission coefficient for constructed oyster reefs through field (Wiberg et al., 2019; Sigel, 2021), laboratory (Allen and Webb, 2011; Xiang et al., 2024) and numerical experiments (Salatin et al., 2022; Vona and Nardin, 2023). Xu et al., 2024 did an in-depth review of wave attenuation in constructed oyster reefs that summarized data across studies plotted against non-dimensional parameters. Although they cite previous work discussing the importance of B in controlling wave attenuation in these reefs (Seabrook and Hall, 1999; Van der Meer et al., 2005), most studies do not consider a wide range of B, with the exception of Allen and Webb, 2011 who explored wave transmission through bagged oyster shell up to $B/L = 0.88$. They found structures with larger B were able add losses of 20-40% for a given depth h_c/h, but didn't investigate specific loss mechanisms. Morris et al., 2021 conducted a large-scale comparison of 13 built oyster reef living shoreline designs along the Atlantic Coast, specifically evaluating wave attenuation in reefs with crest heights h_c above and below the critical submergence threshold required for long-term oyster reef success (an inundation duration of >50%; see Chapter 1). They found reefs that could support long-term reef success to dissipate waves by as little as 5%, noting that the designs in the field were predominantly narrow (small B) (Morris et al., 2021).

Xu et al., 2024 further mention the effect of reef porosity, which is known to influence wave attenuation, wave reflection and harmonic generation in rubble-mound breakwaters (Sollitt and Cross, 1972; Dick and Brebner, 1968; Losada et al., 1997), but which is under explored in constructed oyster reefs. They cite the need for research that investigates specific mechanisms of wave attenuation for different reef types as well as those that optimize reef layout (Xu et al., 2024). These studies, and the call for constructed oyster reef designs that

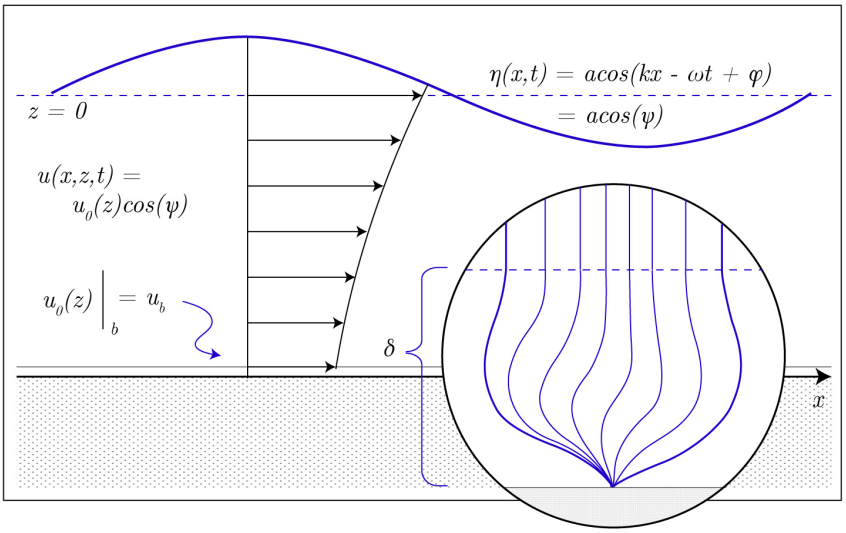

Figure 2.2: Summary of variable nomenclature. The inset illustrates the development of the wave boundary layer δ for different wave phases.

consider conditions necessary for long-term oyster reef sustainability given by Morris et al., 2019 are the primary motivations for this work.

There is significant variability in K_t across studies (Morris et al., 2021; Xu et al., 2024) in part due to the difference in bulk geometry and material characteristics across oyster reef designs. Reports of wave attenuation over commercial models made of pre-cast concrete like Reef Ball, ReefBLK (Webb and Allen, 2015) and Oyster Castle are not as generalizeable as those in the various designs that fill simple geometries with loose oyster shell (bags, gabions), hence the latter will be the focus of the current work.

To begin, it's necessary to review the underlying physical processes that drive wave energy loss in constructed oyster reefs. A diagram summarizing the variable nomenclature used in the follow discussion and throughout this thesis is presented in Figure 2.2.

2.2 Mechanisms of Energy Loss

2.2.1 Wave-breaking

Wave-breaking is a highly-energetic event that modulates the exchange of heat, gases and momentum across the air-sea interface through the entrainment of air and generation of turbulent kinetic energy (Melville, 1996; Terray et al., 1996). Although there has been considerable research into this process, the fundamental mechanisms of energy dissipation

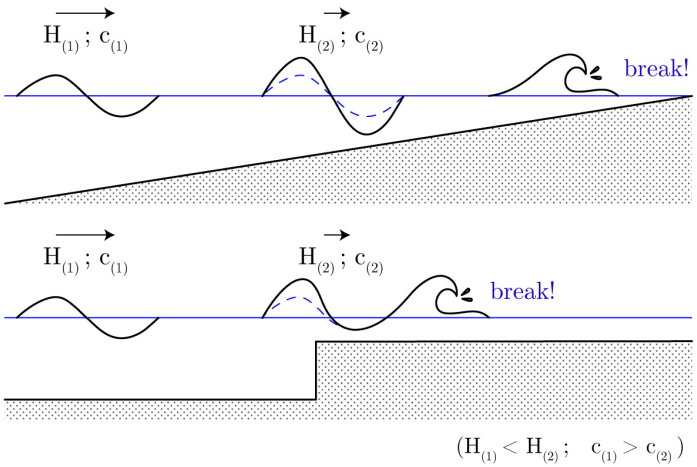

Figure 2.3: Depth-limited breaking, in which H is wave height and c is celerity.

during wave breaking are not fully understood. Experimental studies have found total energy dissipated by a single deep water breaking event to vary from 10% (spilling breaker) to 25% (plunging breaker)(Melville, 1994), however wave-breaking over a submerged structure will likely generate more losses due to interactions between the breaker jet and the structure.

When wave-breaking is present, it is said to be the controlling factor in wave energy dissipation (Xu et al., 2024). Previous studies of wave attenuation in constructed oyster reefs at relative submergence depths that imply dominance by wave-breaking ($h_s/h = 1.0$) report a wide range of values: from 40-70% for Reef Balls (Armono and Hall, 2003), 60-100% for oyster shell bags (Allen and Webb, 2011), and 30-55% for Reef BLK (Webb and Allen, 2015). The fact that these studies were conducted with different incident wave characteristics across structures that vary in shape and porosity highlights the influence of geometric factors other than h_s/h even under breaking wave conditions.

Dally et al., 1985 observed that waves stop breaking at a critical threshold of $H/h = 0.35 - 0.40$, a feature Svendsen, 2005 noted is particularly relevant in cases where a wave passes over a submerged bar, begins to break and then passes back into deep water. In these instances, wave breaking stops almost immediately when it passes into deep water. Recognizing this, maximizing energy losses in constructed oyster reefs, even in cases where wave breaking occurs, will also require consideration of width B. As previously mentioned, however, the relative submergence conditions that induce wave-breaking for significant portions of the tidal cycle are not conducive to oyster growth and long-term survival (Morris et al., 2021; Walles et al., 2016) and are therefore not considered in these experiments.

2.2.2 Friction

The low viscosity of water makes an inviscid flow assumption and the resulting potential flow theory appropriate for most water wave mechanics. However, in shallow water waves, viscous forces at the bed have a measurable effect and potential flow theory no longer holds. Because of the no-slip boundary condition, a boundary layer develops as the x-component of wave orbital velocity $u(x, z, t)$ propagates back and forth, generating vorticity. Linearized energy dissipation in the wave boundary layer is due to work done by the wave against the bed shear stress and is given by

$$\epsilon = \mu \frac{\partial u}{\partial z} \left(\frac{\partial u}{\partial z} + \frac{\partial w}{\partial x} \right) \tag{2.2}$$

or

$$\epsilon = \tau_{xz}(z, t) \frac{\partial u}{\partial z} \tag{2.3}$$

which, by integrating over the height of the boundary layer δ

$$D(t) = -\int_0^{\delta} \tau_{xz}(z, t) \frac{\partial u}{\partial z} dz \tag{2.4}$$

and averaging over a wave period T, yields

$$E_D = \frac{1}{T} \int_0^T D(t) dt = -\overline{u(t)\tau_b(t)} \tag{2.5}$$

in which the velocity $u(t) = u_b cos\omega t$ is defined as the orbital velocity at the bed predicted by potential flow theory, u_b is the maximum velocity, and $\tau_b(t)$ is the bed shear stress. In the case where the scale of roughness elements on the bed is much greater than the height of the laminar shear layer δ (e.g. oysters), this boundary layer is characterized as rough turbulent. Although the shear stress is now a function of the turbulent viscosity μ_t and cannot be determined from first principles, these boundary layers can be parameterized following Jonsson, 1967 using the maximum velocity at the bed u_b (the free stream velocity) and defining a friction factor f_w similar to the coefficient of friction C_f in stationary flows such that

$$\tau_{b,max} = \frac{1}{2} \rho f_w u_b^2 \tag{2.6}$$

Unlike stationary boundary layers, the wave boundary layer cannot grow indefinitely into the water column; it's height is limited by the oscillatory nature of the flow and can only develop while the bottom orbital velocity u_b is traveling the same direction (under 1/2 wavelength) (Trowbridge and Madsen, 1984). Because of this, wave boundary layers are far smaller than

stationary boundary layers, even in turbulent conditions (Dean and Dalrymple, 1991).

As waves pass over constructed oyster reefs, they lose energy via the boundary layer that develops at the crest of the structure. It is expected that this friction will not contribute significantly to the measured losses at the scale of the current study, however a more in-depth discussion of this assumption and wave dissipation due to friction in constructed oyster reefs is given in chapter 3.

2.2.3 Wave reflection

When a wave encounters a submerged obstruction, either built or naturally occurring, part of the wave is transmitted and part of the wave is reflected. The magnitude of this reflection can be quantified similarly to that of the transmission - via a reflection coefficient K_r defined as

$$K_r = \frac{H_r}{H_i} \tag{2.7}$$

in which H_r is the reflected wave height. For an obstruction of finite width, the magnitude of this reflection is a function of dimensionless height h_c/h, structure width B/L, the roughness of the face of the obstruction and structure porosity (Dick and Brebner, 1968).

In the idealized case of a perfectly smooth, impermeable step in bottom topography, this process does not actively dissipate wave energy but redirects it. For open-ocean coasts, waves reflected off of coastal structures are eventually dissipated offshore and are not typically of concern. For closed or semi-closed basins however, the kind of estuarine environment where oyster reefs are commonly found, these reflections can cause erosion at adjacent shorelines overtime (Allsop and Channell, 1989). Wave reflection can also drive erosion at the toe of coastal structures, undermining their stability (Zanuttigh and Van der Meer, 2007) and influencing sediment dynamics which are a known control in the success of oyster reef restoration (Breitburg et al., 2000).

2.2.4 Internal drag

Flow through porous media is a long-studied process in fluid mechanics, and a large body of work has been dedicated to describing the incidence of waves on submerged, porous structures (Dick and Brebner, 1968; Van Gent, 1995; Higuera et al., 2014). On the scale of the individual particles that make up the medium in question, be it sand grains, pebbles or oyster shell, flow is forced to adjust as it navigates around and through narrow channels of void space. The diameter of these channels (the pore size) as well as the smoothness

and shape of the particles all effect the flow velocity and subsequent pressure loss across the medium. Instead of resolving all of these processes, distributed drag models have been developed to describe these bulk losses as a function of measurable quantities like free-stream flow velocity, structure geometry and volume porosity.

If the diameter of the pore channels is on the order of the viscous boundary layer δ, turbulence cannot develop and the flow within the medium is laminar. This flow can then be modeled with Darcy's Law,

$$-\nabla p = \frac{\mu}{k} u \tag{2.8}$$

in which μ is the dynamic viscosity of water, $u = nu_p$ is the filter velocity[2], u_p is the pore velocity, n is the porosity and k is the permeability. For constructed oyster reefs, particularly those that consist of loose oyster shell, the channel diameter is large and a nonlinear correction must be introduced to account for the turbulent dissipation. The pore Reynold's number defines the point of this transition as $Re = ud/\nu \approx 100$, in which d is a representative diameter and ν is the kinematic viscosity of water.

$$-\nabla p = \frac{\mu}{k} u + \frac{\rho}{k_f} u^2 \tag{2.9}$$

in which k_f is a nonlinear analog to permeability (or "viscous permeability") called the inertial or Forchheimer permeability. Furthermore, the wave-induced velocity field is time-varying which requires consideration of inertial effects (added mass). The general governing equation for modeling porous media resistance in oscillatory flow is known as the extended Darcy-Forchheimer equation, given as

$$I = au + bu|u| + c\frac{\partial u}{\partial t} \tag{2.10}$$

in which a, b, and c are empirical coefficients that describe the permeability of the medium and I is the hydraulic gradient. The first term describes the viscous loss, the second term the turbulent loss, and the third term the added mass effects. Although they can be determined by measuring pressure losses directly, considerable effort has been placed on modeling these coefficients in terms of parameters known *a priori*. A generally accepted model is the Ergun Equations (Ergun, 1952), modified by Van Gent, 1995, which define a, b and c in terms of characteristics of the fluid, porosity, grain size or characteristic diameter d, and $KC = uT/nd$, a porous media formulation of the non-dimensional Keulegan-Carpenter number that

[2]Unless otherwise noted, filter velocity $u \equiv u(x, z, t)$ i.e. the wave orbital velocity

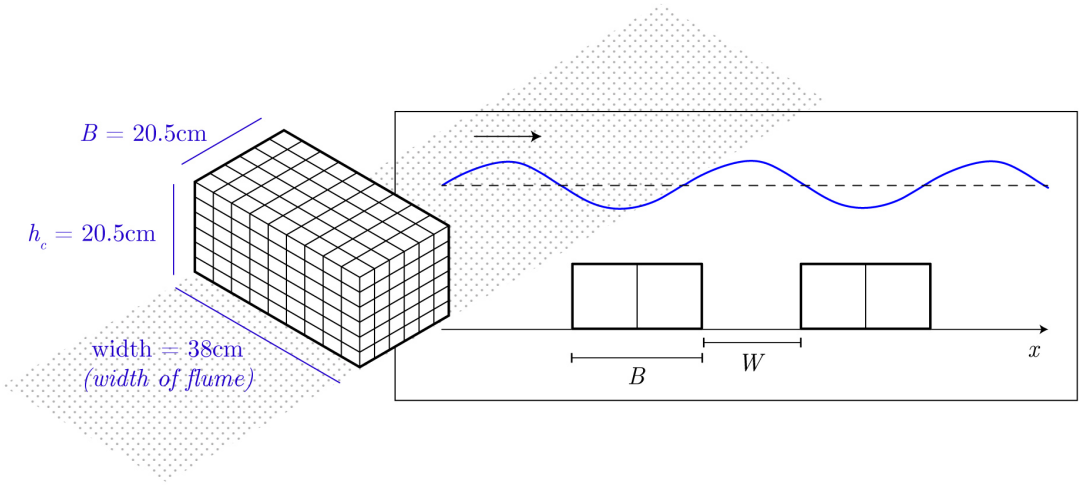

Figure 2.4: Oyster gabion design schematic.

describes the relative importance of drag over inertia in oscillatory flows.

$$a = \alpha \frac{(1-n)^2}{n^2} \frac{\nu}{gd^2} \tag{2.11}$$

$$b = \beta \left(1 + \frac{7.5}{KC}\right) \frac{1-n}{n^3} \frac{1}{gd} \tag{2.12}$$

$$c = \left(1 - \gamma \frac{1-n}{n}\right) / ng \tag{2.13}$$

Here α and β are empirical coefficients that typically take on the values 500-1000 and 1.5-3, respectively (B. Jensen et al., 2014)

2.3 Methods

2.3.1 Design prototype and scaling

Physical scale models of constructed oyster reefs allow for a detailed investigation of wave energy loss mechanisms in constructed oyster reefs (see Figures 2.4 and 2.5). The oyster gabion typology was chosen for this study, due in part to its ubiquity among oyster restoration practitioners as well as it's similarity to a design employed by the Billion Oyster Project in NYC which is always submerged.

Taking this design as a template, a series of 3:1 physical scale-models were constructed using stainless steel mesh and real oyster shell sourced from the Maine Department

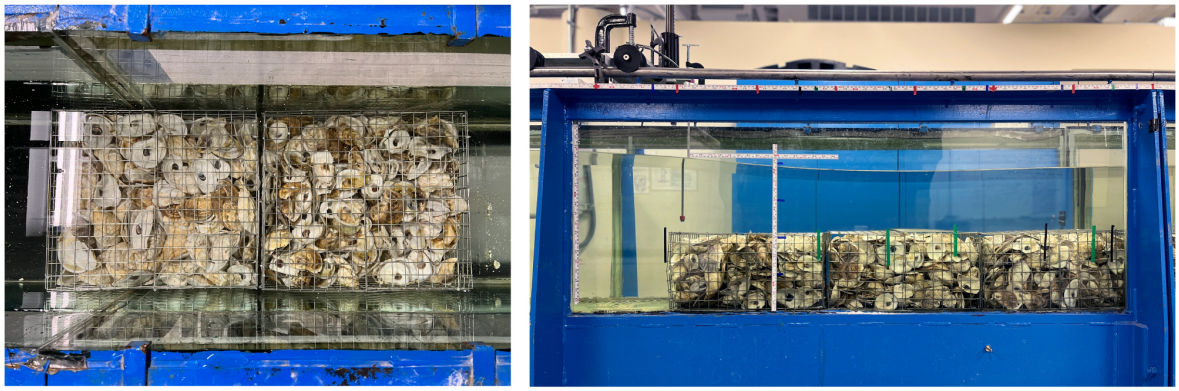

Figure 2.5: Photos of gabions in flume. Direction of wave propagation from left to right in both photos.

Table 2.1: Average oyster shell porosity across 3 trials for small, large and mixed shells with standard error SE.

Size	d (cm)	n	SE (n)
Small	3-7	0.743	0.004
Large	7-14	0.798	0.011
Mixed	3-14	0.713	0.002

of Marine Resources[3]. It is well known that applying simple Froude scaling to porous media can introduce scale effects, typically in instances where the internal flow is shifted into a different flow regime (O. J. Jensen and Klinting, 1983). In laminar flow, the measured loss or pressure drop across the medium is proportional to $u(x, z, t)$, however in turbulent flow it's proportional to u^2. This discrepancy can lead to the over-estimation of porous media resistance and wave reflection from the model compared to the prototype.

In order to ensure dynamic similarity, scaling should be based on permeability rather than porosity, requiring the hydraulic gradient in the model and the prototype to be equal (Wolters et al., 2014). Furthermore, since u varies over the course of a wave period, the hydraulic gradient must be evaluated for a range of characteristic u to fully diagnose the flow regimes present within the model, otherwise there may be times during the wave-cycle where the model no longer accurately represents the prototype (ibid). This is mostly a problem as the wave velocity approaches zero, at which time the drag can increase as the flow transitions from pressure dominated to viscous dominated. However, seeing as the velocity is near zero, the contribution to the wave-averaged dissipation is small.

[3]T. Torrent, Maine Coastal Program, personal communication, February 2023

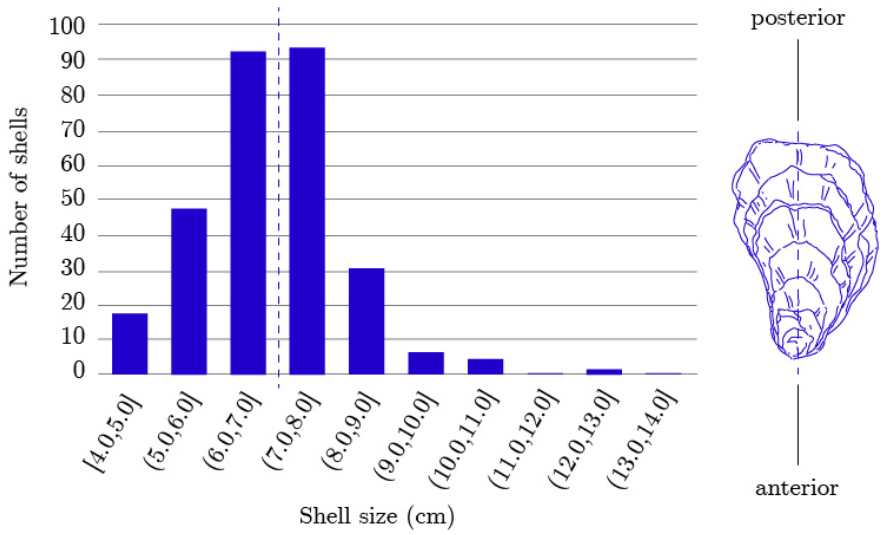

Figure 2.6: Histogram of shell diameter for a sample of 300 shells. The vertical dashed line indicates the median shell diameter 7cm which marks the division between small and large shell groups used in gabions.

To achieve this similtude, the sensitivity of the hydraulic gradient to shell size was assessed. Oysters were sorted by shell diameter measured as the maximum distance from the anterior hinge to the posterior shell edge (see Figure 2.6). Oysters with diameter greater than 7cm were labeled large and the rest were labeled small. A third group of shells were kept mixed small and large. Because these shells were recovered from restaurants in the Portland, ME area, the most common species of oyster present in the shell aggregate was *Crassostrea virginica*, however some larger shell appeared to be the Pacific oyster, *Magallana gigas* (formerly *C. gigas*). Shells that were larger than 14cm were excluded from the experiment, however since oyster shell is often obtained from similar sources, this variability is expected to be typical of stocks used in oyster restoration.

Porosity was determined by filling a single gabion with each oyster size group in turn and measuring the volume of water displaced in a container of known initial water volume. Measurement for each size group was repeated at least 3 times, with the gabion completely emptied and refilled each time to account for packing variability. The results are summarized in Table 2.1 and are in agreement with previous measurements of oyster shell porosity of 80% by (Benoit et al., 2019). The mixed shells had the lowest porosity, likely due to the ability of smaller shells to nestle in the spaces between the larger ones - a well documented phenomenon seen in sediment mixtures called *interstitiation* (Kamann et al., 2007; Glover and Luo, 2020).

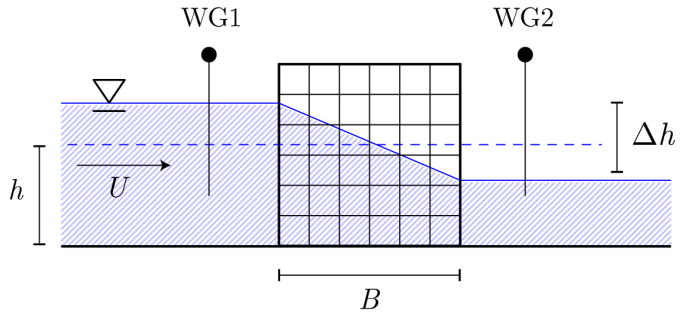

Figure 2.7: Experimental schematic for measuring hydraulic gradient.

A single oyster gabion was then placed in a recirculating current flume at the Ralph M. Parsons Laboratory, with wave gauges installed at both the leading and trailing edge of the gabion. The still water level h was held constant at 15cm depth with the gabion fully emergent and extending the entire width of the flume (see Figure 2.7). A steady current U varying from 6 to 16cm/s was introduced, causing a measurable back-water rise and accompanying pressure drop in the lee of the structure. The change in free-surface elevation measured by the wave gauges between the upstream and downstream faces was divided by width $B = 20.5$ cm to determine the hydraulic gradient as a function of velocity for small, large and mixed shell groups. This experiment was repeated 3 times for each shell size, with the oyster shells completely removed and randomly refilled each time. These data were then fit to the Darcy-Forchheimer equation and the coefficients a and b extracted (see Figure 2.8).

2.3.2 Quantifying K_t

In order to better characterize the mechanisms of wave energy loss in constructed oyster reefs, wave attenuation was quantified under non-breaking wave conditions while varying gabion width B (see Figure 2.4). Physical model flume experiments were conducted in a wave flume 24m long, 0.38m wide and 0.6m tall with a piston-type wavemaker on one end and a 1:5 sloped dissipative beach on the other. Two capacitance-type wave gauges were placed in the flume, one fixed in place at a location upstream of the influence of the gabions called WG1 ($x = -400$cm) and a second, moving wave gauge, WG2, that measured water surface elevation η in 20cm increments along the length of the test section. At $x = 0$, a series of oyster gabions filled with the mixed shell group were placed next to each other such that their collective width B varied from 41-164cm (groups of 2 – 8 gabions). These gabions extended across the entire width of the flume with gabion height $h_c = 20$cm (see Figure 2.9). For each of these width cases, the incident wave period varied from 1.54 – 2s, resulting in a total of 12 cases. These waves were chosen because of their dynamic similarity

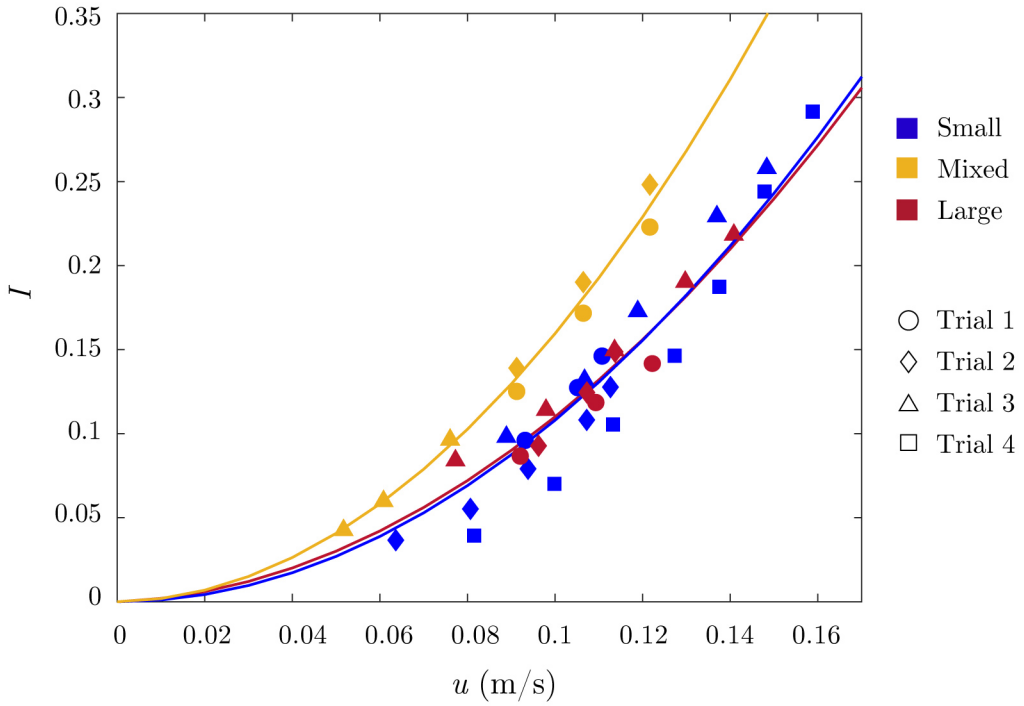

Figure 2.8: Measured hydraulic gradient as a function of measured velocity u (symbols), here in $\mathrm{m} \cdot \mathrm{s}^{-2}$. Solid lines represent best fit of Equation 2.10 to determine pre-factors a and b.

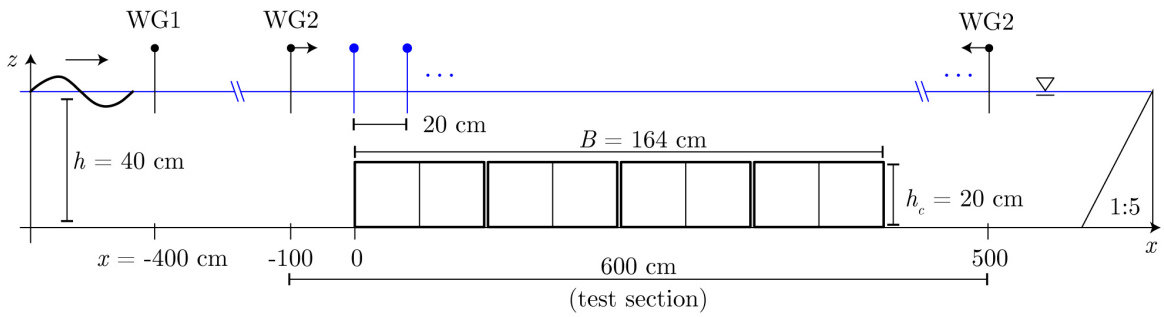

Figure 2.9: Experimental schematic for varying gabion width B.

Table 2.2: Experimental cases. Each wave period case was conducted for 4 gabion widths holding water depth constant at $h = 40$cm.

B (cm)	L (cm)	T (s)	a (cm)
41, 82, 123, 164	270	1.54	3.48
41, 82, 123, 164	298	1.67	3.16
41, 82, 123, 164	333	1.82	2.96

to typical wave conditions seen at field sites where oyster reefs are deployed (Salatin et al., 2022), achieved by scaling on h/L. The full range of experimental conditions is provided in Table 2.2.

For each case, the flume was first allowed to reach steady-state, then 60-second measurements were taken at each measurement location as well as at the reference location. The resulting timeseries of water surface elevation, which included the passage of 30-38 waves total (depending on wavelength), was then phase-averaged. Wave amplitude was calculated by taking the root-mean square of the phase-averaged free surface,

$$a = \sqrt{\frac{2}{T}\int_0^T \eta^2(t)dt} \tag{2.14}$$

with the wave attenuation quantified by dividing the wave amplitude measured at WG2 by the amplitude measured at WG1, $a(x)/a_i$. Because the wave conditions within the flume are at steady-state, verified by ensuring the standard deviation of calculated wave amplitude over the entire wave time series is less than 5%, these asynchronous measurements are treated as simultaneous and used to understand the spatial evolution of $a(x)$, and therefore wave transformation and wave energy dissipation, within the test section.

Figure 2.10 shows this spatial evolution in the bare-bed (control), 4- and 6-gabion case. The clear oscillatory pattern with increasing x-position is the result of the partial standing wave generated by constructive and destructive interference with the reflection from beach. Assuming the incident wave is of the form $\eta_i = a_i cos\,(kx - \omega t + \phi_i)$ and the reflected wave, traveling in the opposite direction, is of the form $\eta_r = a_r cos\,(kx + \omega t + \phi_r)$, a decomposition of the wave field and its constituent Fourier amplitudes following Goda and Suzuki, 1976 reveals a bare-bed reflection coefficient due to the beach $K_r = 0.08$. Not only will this beat pattern change with changing wave period, but the gabions will also generate a reflected wave that will vary with B. In order to ensure consistency across all test cases, the bare-bed beat pattern for each wave period case is fit to a sine with a linear slope

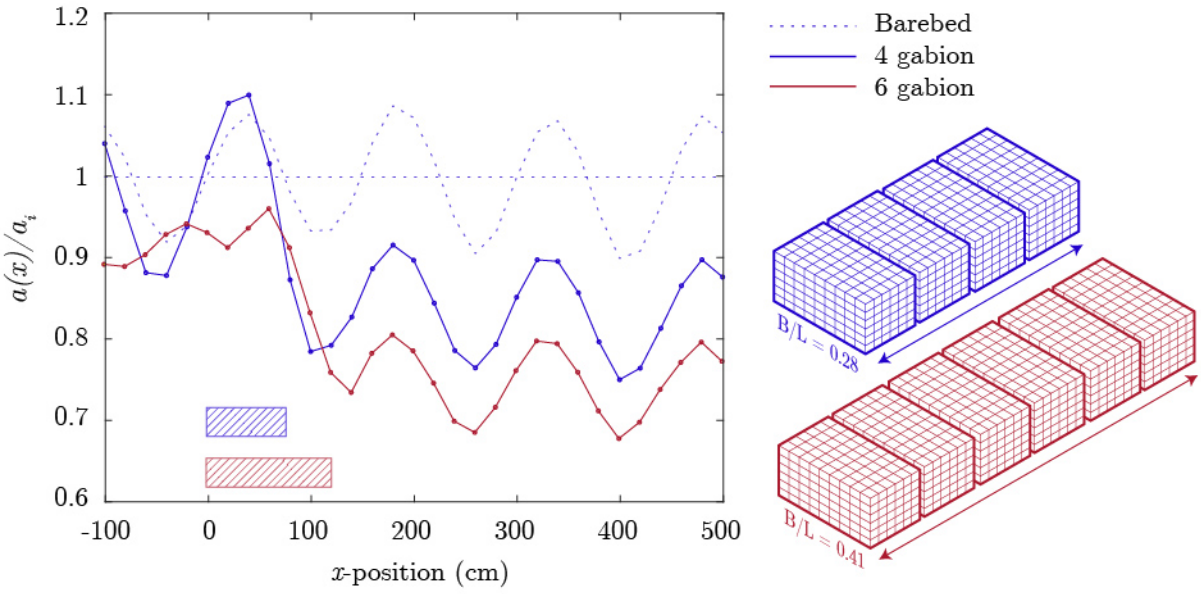

Figure 2.10: Spatial evolution of normalized amplitude $a(x)/a_i$. The hatch indicates the extent of the gabion region.

$f(x) = Ax + Bsin(kx + \phi) + C$ and a_i defined as the wave amplitude predicted by the linear component function $(Ax + B)$ at $x = -400$cm. The evolution of amplitude has a downward trend and overall loss of $\sim$10% due to frictional effects on wave propagation in the flume. This influence has been removed from the data by adding the difference between $a(x)/a_i$ =1 and the value given by the linear-fit through the downward trend in the bare-bed back to the measured amplitude. Applying this correction ε to observed losses across all test cases removes the energy loss associated with the flume bed and sidewalls along the channel (see Figure 2.11).

Wave transformation is heavily modified in the above-gabion region, but quickly recovers in the lee of the gabions and reaches a new equilibrium. Similar to the bare-bed case, a fit to $f(x)$ in the post-gabion region starting at $x = 220$cm is used to determine the transmitted wave amplitude a_t (taken as the value of this fit at $x = 400$cm). Plugging this into Equation 2.1 returns K_t which allows for a comparison of total wave energy loss across all gabion width cases.

The phase-averaging process assumes there is one wave frequency present in the time series, therefore the method of calculating wave amplitude as the root-mean-square (RMS) of the phase-averaged free surface will not capture the dynamics of any harmonic generation. In order to understand the energy contained within constituent frequencies, spectral analysis is

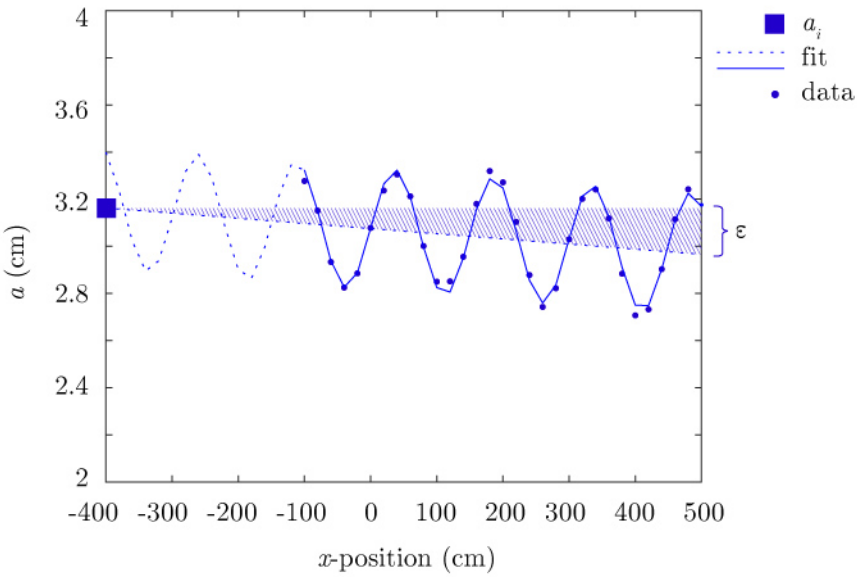

Figure 2.11: Bare-bed beat pattern, adjustment factor ε and calculation of incident wave amplitude a_i

used to determine Fourier amplitudes and the accompanying power spectrum with increasing B/L for T =1.67s.

2.4 Results

2.4.1 Gabion permeability

Figure 2.8 show the results of the gabion permeability tests (also presented in Table 2.3). The hydraulic gradient was quadratic with velocity U for both small, large and mixed shells, confirming a fully turbulent flow regime. The Darcy component was negligible and the spread of a-values large, expected since here a is merely a non-physical fitting parameter. Forchheimer resistance b is highest for the mixed shells, with b =15.6±0.7 - on the order of values for b measured in packed semi-round or irregular rock of median diameter $d_{50} \approx$ 5cm (Van Gent, 1995). The difference in hydraulic gradient across the small and large shell groups was negligible, with b = 10.0±1.9 for the large shells and b =10.8±1.0 for the small shells, suggesting that in-gabion internal drag does not scale singularly as a function of shell diameter.

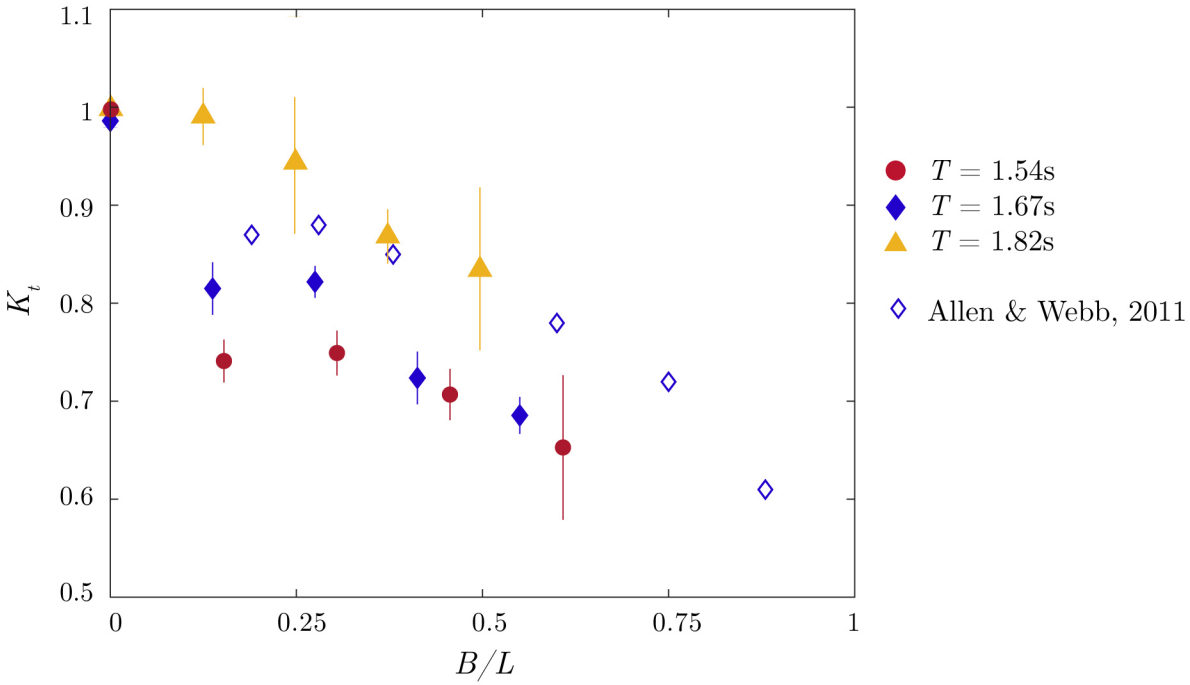

Figure 2.12: Total loss as a function of non-dimensional gabion width B/L for T =1.82s (L = 333cm), 1.54s (L =270cm), and the mean of 2 trials of T = 1.67s (L = 298cm). Outlined diamonds represent data from Allen and Webb, 2011 for the following conditions: $h_c/h \approx 0.55$, $L = 2.17$m, $T = 1.34$s, and $a = 0.05$m

Table 2.3: Fitted Darcy-Forchheimer coefficients a and b for small, large and mixed shell groups, with coefficient of determination R^2 for each fit. k and k_f are the viscous and inertial permeability given by Equation 2.9

Size	$a(\mathrm{s} \cdot \mathrm{m}^{-1})$	$b(s^2 \cdot \mathrm{m}^{-2})$	R^2	k (m^2)	k_f (m)
Small	3.41e−7	10.8	0.95	0.30	0.005
Large	0.1	10.0	0.98	9.77e−7	0.005
Mixed	0.03	15.6	0.99	3.01e−6	0.003

2.4.2 Wave transmission

Figure 2.12 describes K_t as a function of B/L across wave period cases $T = 1.54$, 1.67, 1.82s (see Table 2.4). As expected, wave transmission generally decreases with increasing gabion width B with $K_t = 0.65$ in the longest dimensionless width case $B/L = 0.6$. These data are in alignment with previous measurements of wave attenuation in bagged oyster shell by Allen and Webb, 2011 who found losses to range from 10-40% for $B/L = 0.19 - 0.89$ and $h_c/h \approx 0.55$.

While the overall magnitude of wave attenuation decreases for shorter wave periods, the trend as B/L increases is similar across cases. There is however a sharp decrease in K_t between the bare-bed and 2-gabion case for $T = 1.67$ and 1.82s not seen in the 1.54s case. The variation in this initial jump across wave period cases may be the result of increasing inertial effects at the scale of the gabion with decreasing $KC = uT/B$.

2.4.3 Wave transformation

In the above-gabion region, a steep downward trend in amplitude precedes the trailing edge of the gabion in all cases, however the width of the gabions seems to control the amplitude and number of above-gabion peaks (Figure 2.10). This is evidence of wave reflection dynamics discussed in further detail in Chapter 3.

Figure 2.13 shows the evolution of the phase-averaged free surface for the 8-gabion case. Although this data does not represent a solitary wave under transformation, presenting it in this form illustrates the spatial variability of amplitude along the test section. As the wave enters the above-gabion section, it steepens and a higher-frequency component is generated. This nonlinear transformation strengthens with increasing B, as does wave non-linearity evident in the lee of the structure (see Figure 2.14).

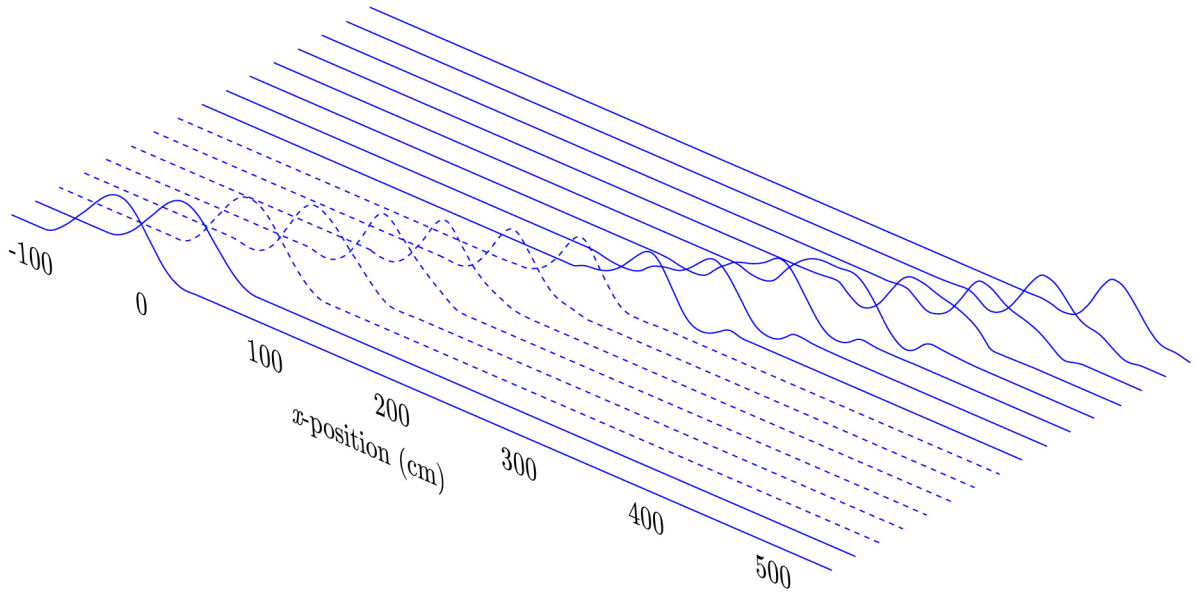

Figure 2.13: Spatial evolution of the phase-averaged free surface within a train of waves for the 8-gabion case ($B/L = 0.55$). The dashed lines indicate waves in the above-gabion region.

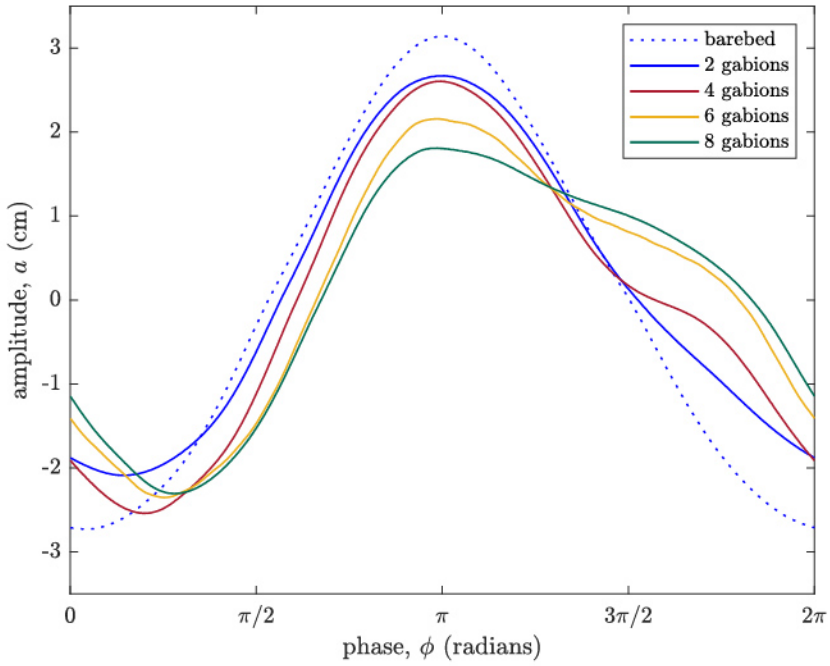

Figure 2.14: Phase-averaged free surface at $x = 400$cm for all cases B

Table 2.4: K_t measured as a function of varying gabion width B (groups of 2, 4, 6 and 8 gabions) for 3 incident wave conditions with water depth held constant at $h = 40$cm. The slight variation in a is due to the transfer function of the wave paddle. Average uncertainty in K_t was 5%

T (s)	a (cm)	B/L	K_t
1.54	3.48	0.14	0.74
1.54	3.48	0.28	0.75
1.54	3.48	0.41	0.7
1.54	3.48	0.55	0.65
1.67	3.16	0.14	0.83
1.67	3.16	0.28	0.84
1.67	3.16	0.41	0.75
1.67	3.16	0.55	0.7
1.82	2.96	0.14	0.99
1.82	2.96	0.28	0.94
1.82	2.96	0.41	0.88
1.82	2.96	0.55	0.83

2.4.4 Wave energy loss

The nonlinear transformation above the gabions is evidence of resonant triad interaction and the generation of bound (or phase-locked) waves. Spectral analysis of the wave fields presented in Figure 2.14 reveals the transfer of energy from the principal harmonic to the second harmonic that increases with nondimensional width B/L. This phenomenon has been studied extensively for waves propagating over a submerged step (Losada et al., 1997; Massel, 1983). Although not a source of wave energy loss outright, the spreading of energy into higher frequencies can reduce the impact on coastal structures in the lee of the gabions (Ting et al., 2016).

Spectral-energy at the principal and 2nd harmonic, $f = 0.6$Hz and $f = 1.2$Hz respectively, is compared to total energy determined via the RMS-amplitude a^2_{rms} at an $x-$position in the region beyond the gabions $x = 400$cm (Figure 2.15). Power is normalized to the idealized power upstream and influence of the flume removed as before. Although the magnitude of the energy transfer into the 2nd harmonic increases with increasing gabion width, the percentage of total energy shifted is negligible - on the order of 5%. Total energy lost for the 8-gabion case is over 50%.

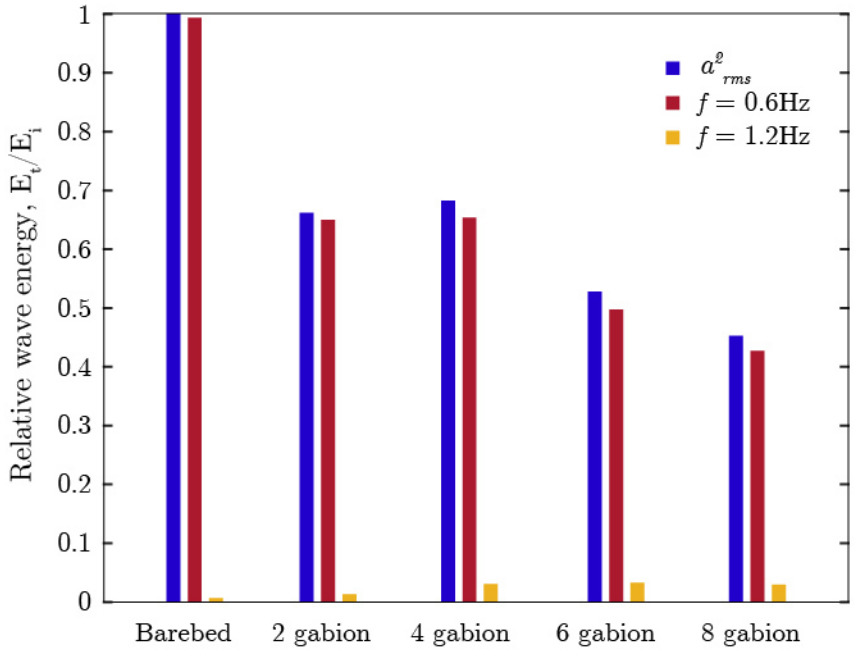

Figure 2.15: Total change in wave power at $x = 400$cm across all gabion cases compared to power spectrum in principle and second harmonic

Chapter 3

3.1 Numerical Model

In order to further investigate the influence of gabion width on wave attenuation in constructed oyster reefs, and the extension to other geometric parameters, a series of numerical experiments were carried out using the well-known open-source CFD software OpenFOAM. To model free-surface gravity waves like those generated in the previous physical experiments, a numerical wave flume of identical dimensions was created using the *waves2Foam* and *porousWaveFoam* libraries developed by Jacobsen et al., 2012. These toolboxes have been well validated for modeling a large range of flow conditions from industry-standard benchmarks (B. Jensen et al., 2014) to novel experimental investigations (Seiffert et al., 2015; W. Chen et al., 2020). Key underlying assumptions and numerical methods employed in the *waves2Foam* and *porousWaveFoam* libraries are discussed below, however a more detailed discussion including the full derivation of the governing equations can be found in B. Jensen et al., 2014.

3.1.1 Governing equations

porousWaveFoam uses the volume-averaged Reynolds-averaged Navier-Stokes (VARANS) equations discretized with a finite volume formulation on a collocated grid (B. Jensen et al., 2014). The equations are derived to compute fluid flow within the porous media zone without resolving the entire complexity of the pore geometry, greatly reducing computational cost.

Starting from the incompressible RANS equations (Ferziger et al., 2019),

$$\frac{\partial \rho \overline{u_i}}{\partial t} + \frac{\partial \rho \overline{u_j}\,\overline{u_i}}{\partial x_i} = -\frac{\partial p}{\partial x_i} + g_i x_j \frac{\partial \rho}{\partial x_i} + \frac{\partial}{\partial x_j}\mu\left(\frac{\partial \overline{u_i}}{\partial x_j} + \frac{\partial \overline{u_j}}{\partial x_i}\right) \tag{3.1}$$

$$\frac{\partial \overline{u_i}}{\partial x_i} = 0 \tag{3.2}$$

these equations are then volume averaged over a length scale defined relative to the pore length scale and macroscopic length scale using two volume-averaging operators with arbitrary tensor A

$$\langle A \rangle \equiv \frac{1}{V}\int_{V^f} A dV \tag{3.3}$$

and

$$\langle A \rangle^f \equiv \frac{1}{V^f}\int_{V^f} A dV \tag{3.4}$$

which distinguish between the total volume V and the fluid volume V^f in which $\langle A \rangle = n\langle A \rangle^f$ and porosity $n = V^f/V$. The Reynold's averaging introduces a velocity decomposition

$$u_i = \overline{u_i} + u_i' \tag{3.5}$$

in which $\overline{u_i}$ is ensemble averaged velocity and u_i' represents the temporal fluctuation. Applying these relations and the velocity decomposition introduced by Gray, 1975 to $\overline{u_i}$,

$$\overline{u_i} = \langle \overline{u_i} \rangle^f + \overline{u_i}'' \tag{3.6}$$

in which $\langle \overline{u_i} \rangle^f$ is the fluid-volume averaged, ensemble averaged velocity and $\overline{u_i}''$ is a spatial fluctuation, results in

$$(1 + C_m)\frac{\partial}{\partial t}\frac{\rho \langle \overline{u_i} \rangle}{n} + \frac{1}{n}\frac{\partial}{\partial x_i}\frac{\rho \langle \overline{u_i} \rangle \langle \overline{u_j} \rangle}{n} + \frac{1}{n}\frac{\partial \rho \langle \overline{u_i' u_j'} \rangle}{\partial x_j} = -\frac{\partial \langle \overline{p} \rangle^f}{\partial x_i} + g_i x_j \frac{\partial \rho}{\partial x_i} \tag{3.7}$$

$$+ \frac{1}{n}\frac{\partial}{\partial x_j}\mu\left(\frac{\partial \langle \overline{u_i} \rangle}{\partial x_j} + \frac{\partial \langle \overline{u_j} \rangle}{\partial x_i}\right) + F_i \tag{3.8}$$

$$\frac{\partial \langle \overline{u_i} \rangle}{\partial x_i} = 0 \tag{3.9}$$

and

$$F_i = -\frac{1}{n}\frac{\partial \rho \langle \overline{u_i}'' \overline{u_j}'' \rangle}{\partial x_j} - \frac{1}{n}\frac{1}{V}\int_{S_w} \overline{p}'' \cdot \mathbf{n} dA \tag{3.10}$$

$$+\frac{1}{n}\frac{1}{V}\int_{S_w} \mu \left\{ \left(\frac{\partial}{\partial x_j}\frac{\langle \overline{u_i} \rangle}{n} + \frac{\partial}{\partial x_i}\frac{\langle \overline{u_j} \rangle}{n} \right) + \left(\frac{\partial \overline{u_i}''}{\partial x_j} + \frac{\partial \overline{u_j}''}{\partial x_i} \right) \right\} \mathbf{n} dA \tag{3.11}$$

F_i contains terms that arise in the momentum equation during the volume averaging process that can't be solved without a closure model. Here the Darcy-Forcheimer equation defined in Chapter 2 is applied to model the porous resistance terms

$$F_i = a\rho \langle \overline{u_i} \rangle + b\rho \sqrt{\langle \overline{u_j} \rangle \langle \overline{u_i} \rangle} \langle \overline{u_i} \rangle \tag{3.12}$$

in which a and b are the resistance coefficients given by the same modified Ergun Equations proposed by Van Gent (1995) in Equation 2.11 and

$$C_m = \gamma \frac{1-n}{n} \tag{3.13}$$

where γ is a coefficient typically taken as 0.34.

The third term on the left-hand side of volume-averaged momentum equation describes the turbulent fluctuations and typically requires its own closure model. Within the gabions, this drag is captured within the empirically determined resistance coefficients a and b, and is therefore included in the resistance term F_i as well. Barring an external turbulence closure model, simulations are run as *laminar*, and eddy viscosity set to zero so that there are no frictional losses outside of the gabion (Jacobsen, 2017).

The *waves2Foam* package employs the native OpenFOAM method of free-surface tracking, namely the Volume-of-Fluid (VOF) method. In this method originally described by Berberović et al., 2009, the Navier-Stokes equations are solved for two fluids simultaneously on a single domain and tracked by a scalar field, λ. λ returns 1 for the fluid phase, 0 for the gas phase, and an intermediate value at the free surface which represents the ratio between the amount of gas and the amount of liquid present within a single computational cell. This is modified to model flow through permeable structures in the domain by limiting flow to the pore space with the advection equation

$$\frac{\partial \lambda}{\partial t} + \frac{1}{n}\frac{\partial}{\partial x_i}(\langle \overline{u_i} \rangle \lambda) + \frac{1}{n}\frac{\partial}{\partial x_i}\left(\langle \overline{u_i}^r \rangle \lambda (1-\lambda) \right) = 0 \tag{3.14}$$

also known as the volume-fraction equation, where $\langle \overline{u}^r \rangle = \langle \overline{u}^f \rangle - \langle \overline{u}^a \rangle$ describes the relative

velocity between the fluid and the air (B. Jensen et al., 2014), however in this investigation, the gabions are always submerged.

3.1.2 Boundary conditions

To accurately model waves within the numerical wave flume, boundary conditions need to be set in order to reduce wave reflection at the boundary. Two types of approaches are typically used: those that allow the wave to radiate out (the Sommerfeld radiation condition) and those that dampen the waves in a modified zone just before the boundary (Choi et al., 2020). The latter, called a relaxation zone or active sponge layer, is employed in this algorithm. Defined at both the inlet and the outlet of the computational domain, these relaxation zones reduce wave reflection at the boundaries, eliminating contamination within the domain and internal reflection at the inlet boundary which interferes with the wave maker and can lead to divergent solutions (Jacobsen et al., 2012). They can also attenuate unwanted nonlinear phenomenon like parasitic waves at the wave-maker inlet.

The explicit relaxation zone technique in *waves2Foam* works by starting with an analytical solution to the wave (given by the chosen wave theory) and then applying a weighting function

$$\chi(\xi) = 1 - \frac{exp(\xi^{\sigma} - 1)}{exp(1) - 1)} \tag{3.15}$$

in which ξ is a local coordinate in the relaxation zone valued from 1 at the inlet to 0 at the interface with the computational domain, and σ is an arbitrary shape factor. The local value of u or λ, (ϕ, generally) is then calculated as

$$\phi \;=\; \chi\phi_{computed} + (1 - \chi)\,\phi_{target} \tag{3.16}$$

in which ϕ_{target} is the analytical solution in the inlet relaxation zone and 0 in the outlet zone, and $\phi_{computed}$ is the numerical solution.

The primary drawback of the method is computational cost. In order to work effectively, relaxation zones have to be on the order of one wavelength, increasing the computational domain by at least two wavelengths in total (Mayer et al., 1998; Q. Chen et al., 2019).

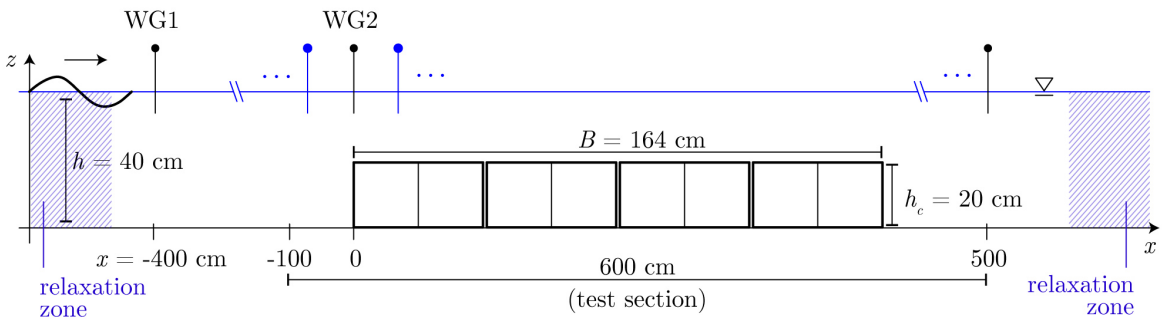

Figure 3.1: Computational domain. Each relaxation zone was 5m long.

3.2 Implementation

3.2.1 Numerical wave flume

Figure 3.1 shows a schematic of the computational domain. The total length is 24m long which results in the same working area as the physical flume when accounting for space taken up by the relaxation zones or the wave-maker and dissipative beach. As was the case in the physical experiment, the water depth was set at 40cm and the oyster gabions, included in the model as a porous media zone, varied in width B but maintained a height of $h_c = 20$cm. B ranged from 10cm to 300cm in increments of 10 cm. Simulations were validated against physical data, then extended to explore the influence of spacing W between successive gabion groups (see Figure 2.4) as well as structure porosity n on wave transmission. n varied from 0.71 (the measured porosity of the mixed oyster shell) to n =0.6, 0.4, 0.2 and 0.01, the latter treated as solid since there was no flow in the gabions. For cases that varied spacing, B was held constant for two width cases (B/L = 0.14 and 0.28, or groups of 2 and 4 gabions, respectively) and W varied from 0 to 300cm in increments of 20cm (L = 298cm). Each run ran for 90 seconds, requiring 60 seconds of spin-up to achieve steady-state.

Grid resolution was set at $\Delta x_1 = 0.05$m in the horizontal direction and $\Delta x_2 = 0.01$m in the vertical direction. In the *porousWaveFoam* library, the Courant Number is checked at every time step and Δt adjusted accordingly to stay within a defined threshold value, in this case, below 0.25. In order to limit spurious oscillations caused by this adjustment, the algorithm is implemented immediately but its effects dampened over multiple time steps (Jacobsen et al., 2012).

The governing wave theory at the wave-generation boundary was set to Stokes 2nd Order wave theory based on the guidance in Le Méhauté, 1976, with T = 1.67s and a =

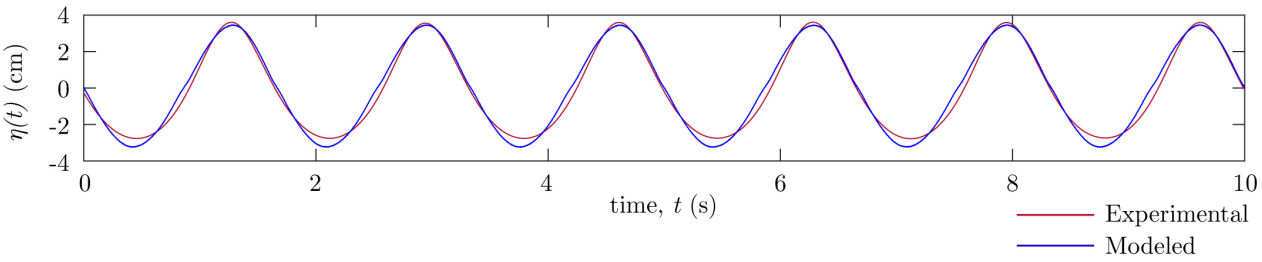

Figure 3.2: Comparison of wave time series for physical and numerical data

3.16cm (unless otherwise noted). A comparison of the wave time-series at the numerical and physical location of the reference wave gauge ($x = -100$cm) highlights the strong agreement between the simulated and measured incident wave (see Figure 3.2).

3.2.2 Characterization of oyster shell in *porousWaveFoam*

Because whole oyster shell is a highly irregular medium (see Chapter 2), the extension and applicability of the porous media formulation employed in *porousWaveFoam* to oyster shell is nontrivial. The equations employed in *porousWaveFoam* i.e. the modified Ergun Equations (Van Gent, 1995) were originally derived and validated for modeling porous media flow resistance for regular media like sand and gravel, and have been shown to underestimate pressure drops in media with non-spherical particles (Foumeny et al., 1996; Nemec and Levec, 2005). The validity of these equations for various irregular media has been studied (Li and Ma, 2011), however, to the author's knowledge, no study to-date has verified its validity for use in modeling fluid flow through collections of whole oyster shell as is found in constructed oyster reefs.

The empirical coefficients α and β were chosen as 500 and 2.0, respectively, following the results of the detailed parameter study conducted by (B. Jensen et al., 2014) for laminar, transitional and turbulent pore Reynold's number flow. For turbulent flow cases, they found the choice of α to have almost no effect on the results, and found a choice of $\beta = 2.0$ to minimize errors for both fully turbulent and laminar flow cases. Porosity n was set to 0.71, in-line with the measured volume porosity of the mixed-shell oyster gabions.

Less straightforward is the appropriate choice of d, particularly as modeled wave transmission using *porousWaveFoam* is sensitive to this parameter (see Figure 3.3). The Ergun Equations are a capillary flow model that assume the porous medium is comprised of a series of small channels where the physical meaning of d is meant to describe the average

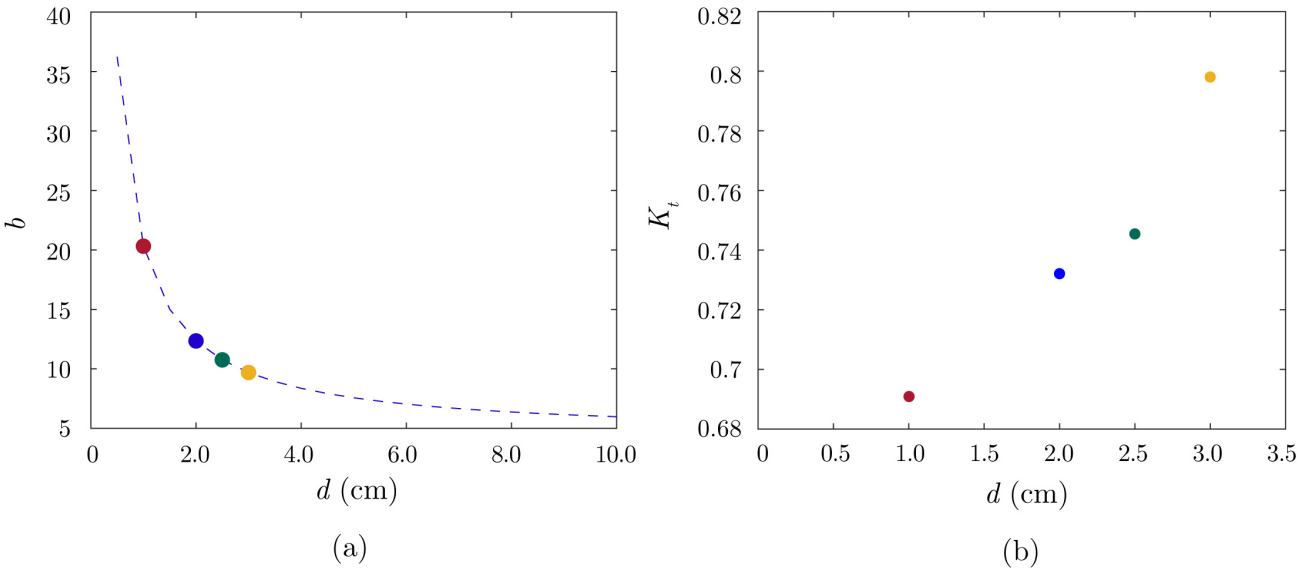

Figure 3.3: (a) Forchheimer resistance coefficient b as function of d for $n = 0.8$, β =2 and $\alpha = 500$ (Equation 2.11); (b) Modeled K_t under the same geometric and incident wave conditions ($B = 160$cm, $a = 2.64$cm). K_t is sensitive to d, varying over 10% from $d = 1$cm to d =3cm, despite increasingly small changes in b as d increases. This emphasizes the importance of accurate choice of d.

pore channel diameter. In porous media flow through regular media, this characteristic length-scale is often taken as the grain diameter which, in the case of spherical grains, sets the scale of the average pore channel diameter. However, for highly irregular grains this is no longer the case and average diameter will not yield an appropriate choice of d. This has been attributed to a number of factors depending on the characteristics of the media including the increase in tortuosity created by the irregular geometry (Foumeny et al., 1996), the increase in form drag over individual elements (Dolejs and Machac, 1995), and the change of the affected dynamic area (wetted perimeter) (Comiti and Renaud, 1989). Given the sharp, irregular edges and cupped geometry of oyster shell, it's likely that all these effects contribute to the deviation from expected resistance values for spherical-grains of an equal diameter.

Researchers have introduced various shape factors to account for this discrepancy. These models, like the equivalent diameter d_{eq} defined by Li and Ma, 2011, are typically based on the comparison of the irregular particle in question to that of a sphere with an equal ratio of volume to surface area, however these simple geometric relations are not easily defined for oyster shell. Furthermore, because the in-gabion flow is fully turbulent, contributions that result in an increase turbulent kinetic energy (TKE) like flow separation likely play a larger

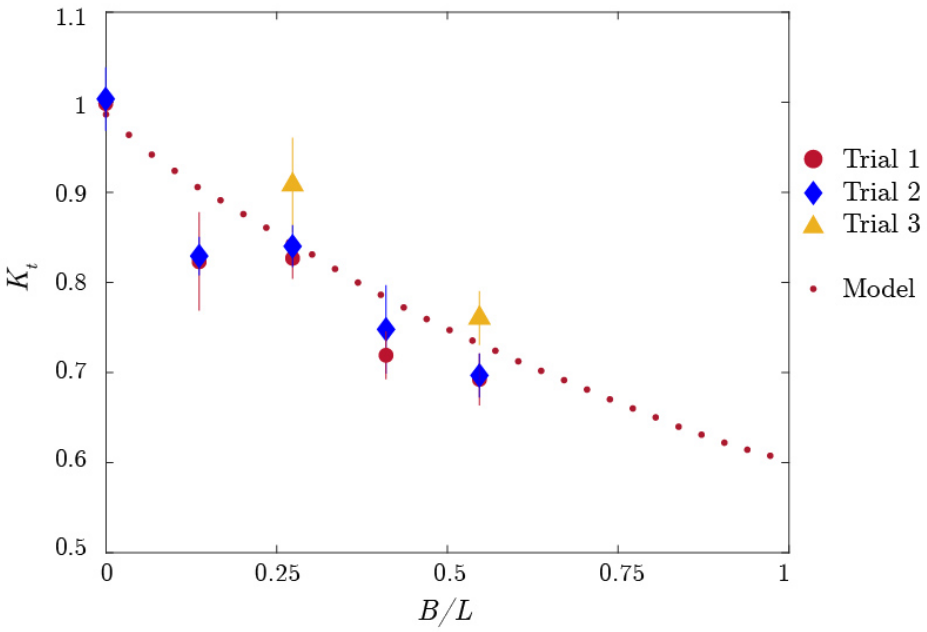

Figure 3.4: Total loss with experimental and modeled data, including all 3 experimental trials. Each red point corresponds to an individual model run.

role than those that modify viscous effects like channel diameter.

Since a and b have been determined experimentally, the effective $d \equiv d_{eff}$ can be found by matching the experimentally measured wave amplitudes to the simulated values, which can recursively verify the applicability of the modified Ergun Equations and this d_{eff} to predict a and b. The choice of $\alpha = 500$, $\beta = 2$ and $d_{eff} = 5$cm (contrary to the calculated median shell diameter $d = 7$cm) for the exact wave conditions tested in the flume results in predicted a and b values that are in agreement with experimentally determined values found in Chapter 2 (see Table 2.3).

3.3 Results

Figure 3.4 shows the transmission coefficient K_t extracted from each simulation and plotted along with the physical data for the same conditions. As expected, K_t decreases monotonically with increasing B. Although the agreement between the model and the experimental data is generally good, the model does not capture the sharp increase in loss between the bare-bed and 2-gabion experimental cases. Seeing as the model does not include an explicit turbulence closure scheme beyond the porous resistance term provided by the gabions, this

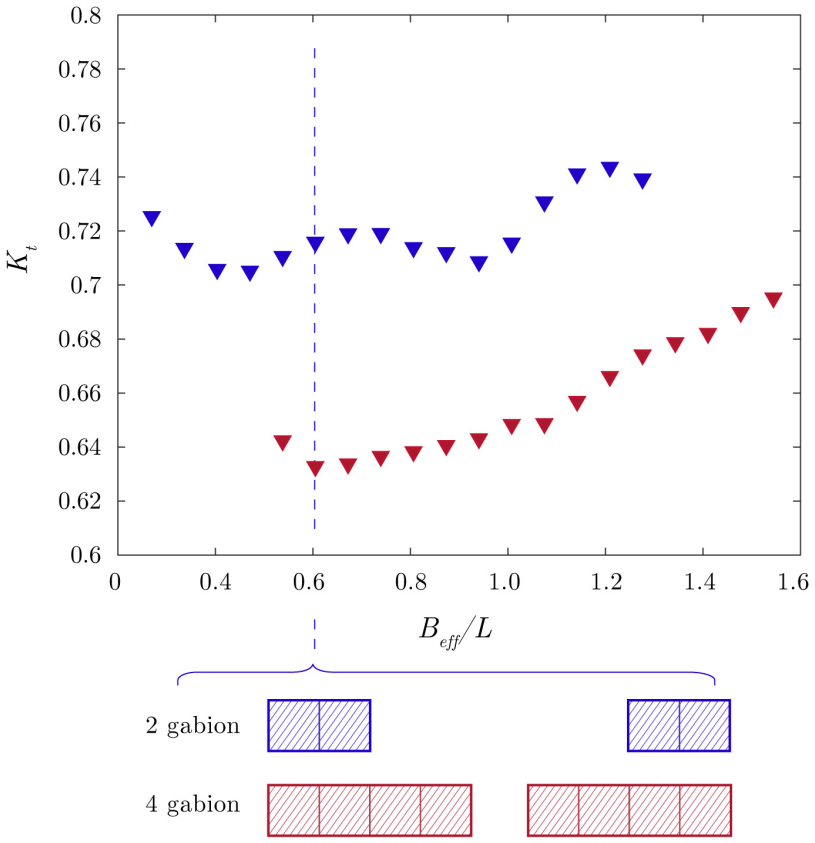

Figure 3.5: Transmission coefficient K_t as a function of nondimensional effective gabion length B_{eff}/L. Blue points refer to cases $B = 40$cm (2 gabions) while red points refer to cases $B = 80$cm (4 gabions).

suggests it may be unable to account for some form of turbulent dissipation.

Model runs also sought to explore the effect of spacing between successive gabion groups W. Data sets were produced for two gabion width cases $B/L = 0.13$ and $B/L = 0.27$, representative of the 2- and 4-gabion physical model tests, respectively, for spacing cases $W/L = 0 - 1$[1]. Figure 3.5 shows these data as a function of effective width B_{eff}, where B_{eff} is an effective gabion width defined as the sum of both gabion section widths and the space in-between them $2B + W$. Increasing gabion spacing was not found to have a notable effect on wave attenuation for this configuration, with K_t increasing 5% for the 4-gabion case and only 1% in the 2-gabion case as the spacing between the gabions grows to $B_{eff} > 1$. A slight oscillatory pattern visible in the two 2-gabion data may be evidence of resonant Bragg reflection which traditionally occurs when the distance between the leading edge of successive submerged structures is $0.5L$ (Ardhuin and Herbers, 2002; Ni and Teng, 2021).

[1]Note these tests were completed for the same wave period $T = 1.67$s but different wave amplitude than the physical experiments ($a = 2.64$cm)

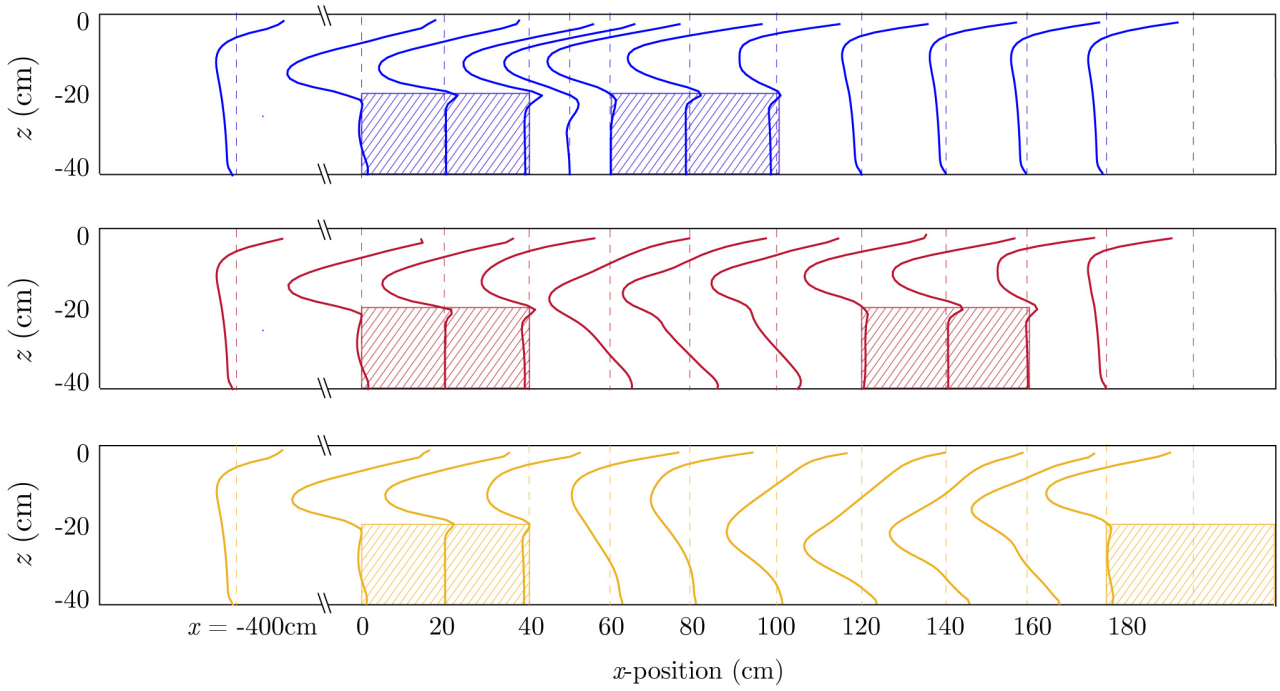

Figure 3.6: Spatial evolution of average u-velocity profile u_{avg} for $W = 0.06L$, $0.27L$, and $0.47L$ for constant B/L =0.13 ($L = 298$cm and $T = 1.67$s).

These dynamics change when the structures are porous and reflected waves are forced to propagate through the porous medium, hence the muted response in the 4-gabion width (see Section 3.4.2 for details).

To gain insight into the dynamical significance of W, the wave-induced flow field was also analyzed. Figure 3.6 shows the spatial evolution of the time-average u-velocity profile u_{avg} for $W/L = 0.06$ (blue), 2.7 (red) and 4.7 (yellow). Providing the flow is unobstructed, the wave-induced velocity recovers to its u-velocity profile upstream of the gabion's influence. This short recovery is seen in the physical data as well via the quick adjustment to a new equilibrium state in the plots of $a(x)/a_i$ (e.g. Figure 2.10). When another gabion is sufficiently close by (less than $0.5L$), this profile is influenced by a secondary circulation and cannot fully recover. For very small W (the blue case), the average velocity structure is nearly unaltered from its form within the gabions and shows no net u at the bed (see Figure 3.7).

Figure 3.8 shows the output of 4 sets of model runs for $B/L = 0 - 1$ that varied porosity $n = 0.71$, 0.6, 0.4 and 0.01 (the latter considered solid). The difference in energy loss between the $n = 0.71$ and $n = 0.6$ case is negligible, with losses decreasing across the $n = 0.4$ and solid cases. The difference in K_t between the solid case and the $n = 0.71$

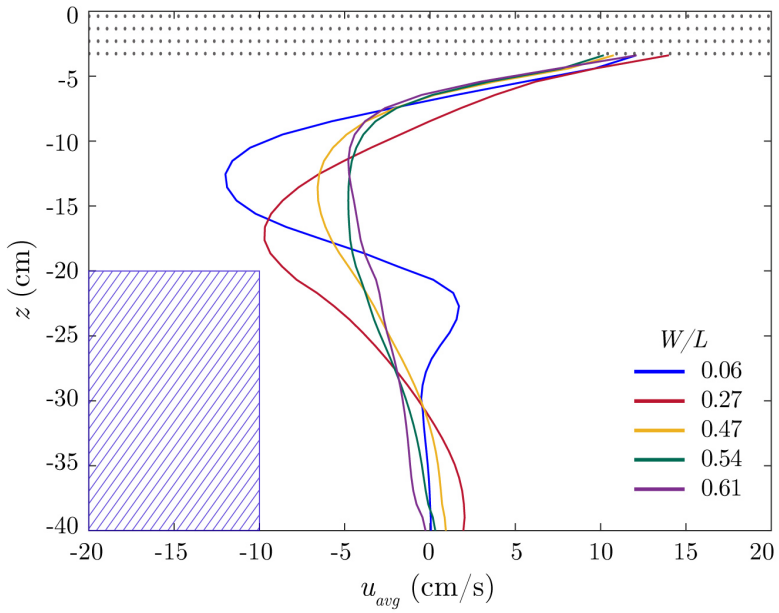

Figure 3.7: Velocity profiles at $x = 50$cm (the same distance from the edge of the gabions) for 5 different spacing cases W/L, with $B = 40$cm. Influence from secondary circulation is clear in the first two spacings ($W \lesssim 0.25L$) but decreases at $W \approx 0.5L$ and approaches the steady upstream profile.

case is $\approx 13\%$ for $B/L > 0.25$, which represents the net added wave attenuation due to the in-gabion internal drag. However, this is not a representation of the actual contribution of internal drag to energy dissipation in the $n = 0.71$ case. Increasing porosity changes the "effective relative depth" that controls the above-gabion wave characteristics (Losada et al., 1997), with this depth $h_{eff} = h_s$ when the gabion is solid and $h_{eff} \to h$ as $n \to 1$ and the wave can better penetrate the structure. For the solid, $n = 0.2$ and 0.4 cases, h_{eff} decreases enough to induce depth-controlled energy losses (particularly after $B/L \approx 0.25$) not present in the $n = 0.71$ and 0.6 case.

3.4 Discussion

Wave transmission over a constructed oyster reef under non-breaking wave conditions is controlled by mechanisms of dissipation and reflection at both the scale of the oyster and the scale of the bulk geometry. In-gabion internal drag and friction at the top of the gabion are primarily dependent on the local wave orbital velocity $u(x, z, t)$, the wave excursion $\zeta(z)$ and the characteristics of the oyster shell medium, n and d_{eff}. Wave reflection and harmonic generation in oyster gabion-type constructed oyster reefs are dependent on the bulk

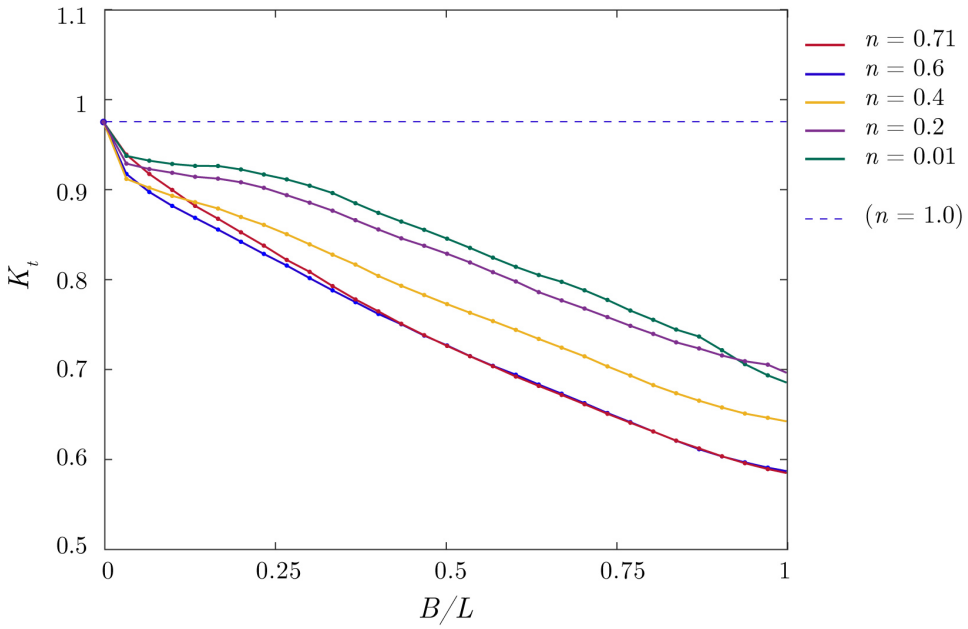

Figure 3.8: Total loss as a function of B/L with changing porosity. Points indicate individual model runs. Note the n =0.6 case (blue curve) extends the whole length of the domain but is obscured by the $n = 0.71$ case.

geometry of the gabions, particularly B/L and h_s/h. A more nuanced understanding of these mechanisms has implications for the design of constructed oyster reefs that maximizes wave energy loss while providing social and ecological co-benefits associated with long term oyster reef sustainability like water quality improvement, fisheries enhancement, and environmental stewardship. A detailed discussion is provided below.

3.4.1 Wave dissipation due to bottom friction

Recall that wave energy dissipation due to bottom friction E_D is defined as the work done by waves against the shear stress generated in the wave bottom boundary layer. It was suggested that this contribution from the top of the oyster gabion would be negligible at the scale of interest, but a quantitative understanding of the relative contribution of this energy loss in comparison to that due to in-gabion internal drag can be found as follows.

First, we can define a length scale over which the cumulative dissipation due to friction becomes important. Starting with the instantaneous bed shear stress

$$\tau_b(t) = \frac{1}{2}\rho u(t)|u(t)| \tag{3.17}$$

E_D can be defined as

$$E_D = \overline{\tau_b u_b} \tag{3.18}$$

or,

$$E_D = \frac{2}{3\pi}\rho f_w u_b^3 \tag{3.19}$$

in which u_b is amplitude of time-varying wave orbital velocity at the bed and f_w is a wave friction factor. Dean and Dalrymple, 1991 use this to define an energy balance equation where the total change in energy over distance x is due to this frictional damping,

$$\frac{dEC_g}{dx} = -E_D \tag{3.20}$$

or

$$\frac{1}{2}\rho g C_g \frac{da^2}{dx} = -\frac{\rho f_w}{6\pi}\frac{\omega^3}{sinh^3 kh}a^3 \tag{3.21}$$

Solving for the evolution of wave amplitude a as a function of x:

$$a(x) = \frac{a_i}{1 + \frac{2f_w}{3\pi}\frac{k^2 a_i x}{(2kh + sinh\ 2kh)sinh\ kh}} \tag{3.22}$$

To assess the length scale over which this frictional dissipation becomes important, we can set the wave attenuation due to friction as 5% i.e. $a(x)/a_i = 0.95$ and rearrange the equation to solve for x or $B_{f,5\%}$. The wave conditions T, a_i, and k are known, as well as the depth h which here represents the freeboard above the gabions h_s, however there is some uncertainty in the appropriate choice of friction factor f_w. Despite work quantifying frictional dissipation for unidirectional flow and the quantification of drag coefficient C_D (Reidenbach et al., 2013; Kitsikoudis et al., 2020), to the author's knowledge, no study to date has investigated frictional dissipation under oscillatory flow. Donker et al., 2013 found f_w to range from 0.1 to 0.7 in oscillatory flow over mussel beds, and typical values for f_w in coral reefs have been found to range from 0.24 – 1.8 (the upper limit from a case described as "remarkably rough" by Monismith et al., 2015), although the variation in size and shape of coral species makes this difficult to generalize. It's likely that f_w will be the same order of magnitude as mussels beds, although the sharp edges of the oyster shell, rough faces and larger size will likely enhance frictional dissipation (Hitzegrad et al., 2024).

Taking the bulk range of values reported by Donker et al., 2013 as a lower limit, $f_w = 0.5$ can give an order of magnitude estimate of the length scale over which frictional

effects will become important. Plugging the above values into the following equation

$$B_{f,5\%} = \frac{3\pi\,(0.05)\,((2kh + sinh\ 2kh)\,sinh\ kh)}{2fk^2a_i} \tag{3.23}$$

returns $B_{f,5\%} \approx 7$m or $B_{f,5\%}/L \approx 2.3$. From this, it can be concluded that frictional dissipation does not play a large roll in constructed reefs with widths $B/L < 1$, but this will depend strongly on kh.

Lowe et al., 2007 derived an equation for f_w which compared the work done against a canopy shear layer to in-canopy drag based on the original formulation by Dalrymple et al., 1984 with a modified "attenuation parameter" that accounts for the attenuated flow within the canopy $\alpha_w \equiv u_w/u_{\infty,w}$ in which u_w is the RMS-canopy wave velocity and $u_{\infty,w}$ is the above canopy velocity. This was further extended by Lowe et al., 2008 to apply to a porous media formulation in porous media flow.

$$f_w = C_f + 2bgh_cn\alpha_w^3 \tag{3.24}$$

A factor of g has been added here to account for the difference in the definition of b that either includes (following Van Gent, 1995) or excludes this factor (Lowe et al., 2008), such that b is either reported in units of $s^2 \cdot m^{-2}$ or m^{-1}, respectively. Therefore, the relative contribution of friction dissipation to internal drag is given as

$$F_d \equiv \frac{C_f}{2bgh_cn\alpha_w^3} \tag{3.25}$$

Unlike f_w, there are some studies that quantify the stationary drag coefficient over oysters, finding values for C_f range from 0.019 - 0.025 (Whitman and Reidenbach, 2012; Styles, 2015). α_w is related to the drag length scale, which is a function of porosity and gabion height h_c and the wave orbital excursion ζ, but can be found directly by looking at a representative velocity profile from the results of the numerical model (see Figure 3.9), where $u_{\infty,w}$ is defined as the RMS-velocity at $z =$-10cm and $x = 150$cm for gabion width case $B = 300$cm (chosen to minimize edge effects). Using Equation 3.24, $a_w \approx 0.55$ and the values from the current study $b = 15.6 s^2 \cdot m^{-2}$ and $h_c = 0.2$m, it's found that $f_w \approx 7$ which is two orders of magnitude larger than C_f. This is comparable to measurements of f_w found on rocky shores by Gon et al., 2020 which ranged from 4 to 34. Since F_d is very small, this suggests that even for long length scales, in-gabion drag will dominate over shear dissipation.

Previous studies have found drag coefficients in live oyster reefs to be higher than

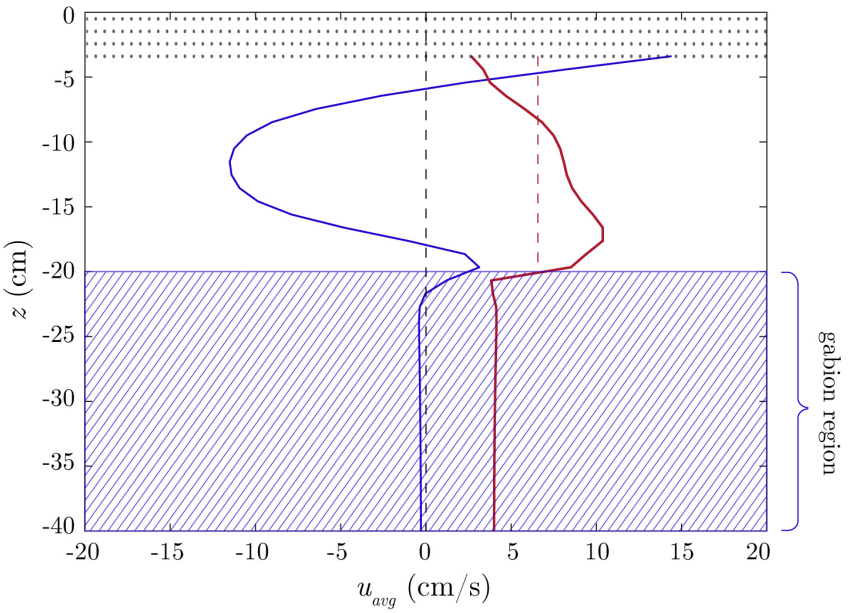

Figure 3.9: Vertical profile at $x = 150$cm for gabion width case $B = 300$cm. The blue curve is u_{avg} and the red curve u_{rms}. $u_{\infty,w}$ is taken as average of the above canopy u_{rms}.

those in dead or degraded reefs (Kitsikoudis et al., 2020). This has been attributed to the vertical orientation of live oysters in a healthy reefs when compared to loose oyster shell which increases form drag and the height of the roughness layer z_0. Live oysters also actively modify the flow field locally by filtering water. Future work should integrate an understanding of these processes with the mechanisms of energy loss explored here as they will likely increase wave attenuation ability in constructed oyster reefs.

3.4.2 Wave reflection

The measured wave reflection from the gabions is a function of width B. The oyster gabions can be modeled as a step discontinuity in the bottom topography, one at the leading edge and one at the trailing edge, with each face marking the transition between 3 distinct zones, (1), (2) and (3) (see schematic in Figure 3.10). In the simple case where the discontinuity is solid i.e., there is no in-gabion internal drag and B is short compared to $B_{f,5\%}$ (i.e. there's very little frictional dissipation), the transmitted wave height measured in the lee of the gabions H_3 will be the incident wave height H_1 minus the reflection due to the leading edge R_1 and the reflection due to the trailing edge R_2. If B is varied (while $B/L \ll B_{f,5\%}$) but all other geometric parameters are held constant, H_3 will remain constant as the magnitude of the reflection from R_1 and R_2 is constant.

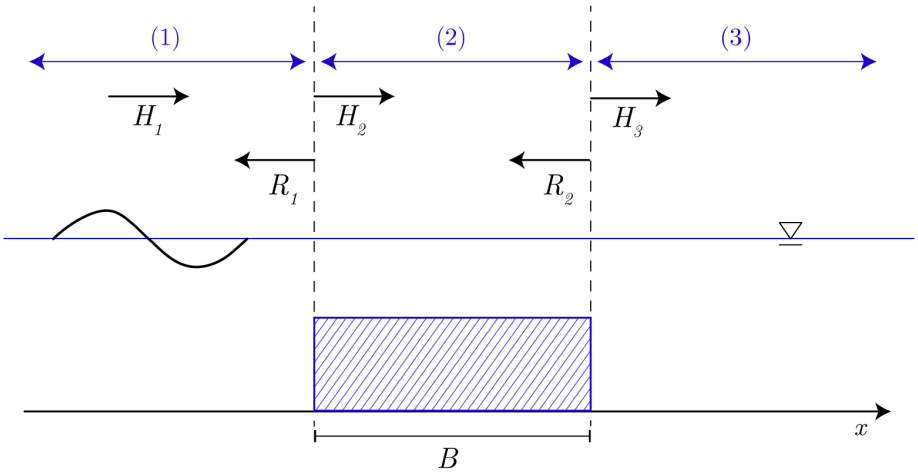

Figure 3.10: Diagram of wave reflection in the test section. The reflected wave R_1 is phase-inverted and partially cancels out H_1. Reflection from the beach is not pictured.

The magnitude of the reflection observed upstream of the gabions is, however, a function of B. This is due to the phase shift between the two reflected waves R_1 and R_2 introduced by the time-lag between each wave's generation as well as the requirement of energy conservation at the respective reflective interfaces. Suppose the incident wave H_1, reaches the leading edge of the gabions and generates the first reflected wave R_1 at $t = t_0$. Assuming shallow water waves, this step discontinuity will mark the interface between a region of higher wave celerity $c_1 = \sqrt{gh}$ and that of a lower wave celerity $c_2 = \sqrt{gh_s}$ where $h > h_s$. Continuity requires the damped force response in the low-speed region to equal the larger response from the high-speed region at the boundary, therefore R_1 must be phase-inverted. As R_1 travels in the $-x$-direction away from the interface at speed c_1, the transmitted wave H_2 will travel the length B at speed c_2 until it reaches the trailing edge of the gabions at $t_1 = B/c_2$. This step discontinuity is characterized by the opposite depth change as that of the first which, following a similar argument, will produce an R_2 that is instead in-phase with H_2. While R_1 continues to travel in the $-x$-direction at speed c_1, R_2 will begin to propagate in the $-x$-direction at speed c_2 until it reaches the leading edge of the gabions at $t_2 = 2B/c_2$. For reflected waves R_1 and R_2 to be completely out of phase such that they interfere destructively, the distance traveled by R_1 in time $t_2 - t_0$ must equal a multiple of the wavelength nL, therefore

$$\frac{2B}{\sqrt{gh_s}} = \frac{L}{\sqrt{gh}} \tag{3.26}$$

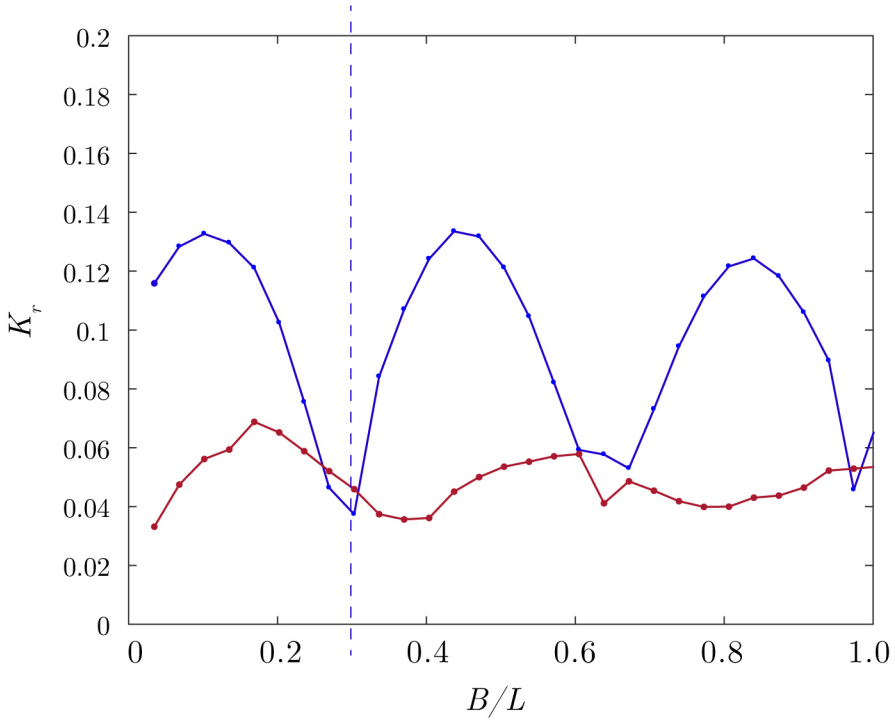

Figure 3.11: Modeled reflection coefficient K_r as a function of B/L. The curve shows the reflection coefficient measured upstream of the gabions following Goda and Suzuki, 1976 for $n = 0.71$ (red) and $n = 0.01$ (blue).

or, solving for B

$$B = \frac{1}{2}\sqrt{\frac{h_s}{h}}L \tag{3.27}$$

For the configuration considered in this study, $h_s/h = 0.5$ which predicts a minimum in the observed reflection at gabion widths $B/L = 0.35$ and 0.7. This response is seen clearly in the variation of measured wave amplitude upstream of the numerical test section for the solid-gabion case shown with the blue curve in Figure 3.11. The deviation in the predicted minima and maxima of this response is due in part to the fact that the change in wave celerity across the boundaries is not instantaneous. Porosity also influences this response, as seen in the porous gabion case (red curve in Figure 3.11). Not only does the observed minimum in the reflection coefficient lag significantly behind the predicted value, but the magnitude of the response is also damped. In this case, H_2 and R_2 propagate through the oyster gabions, changing the effective relative depth (hence $c = \sqrt{gh_{eff}}$) and losing energy due to the in-gabion internal drag. As gabion width increases, the magnitude of the reflected wave R_2 will dissipate entirely before it reaches the leading edge and the reflection coefficient will approach that of a single depth discontinuity like an infinite step.

3.4.3 Gabion spacing and wave-induced velocities

For the range of cases considered here ($W/L < 1$, $h_s/h = 0.5$, and $n = 0.71$), gabion spacing was not found to have a notable impact on wave transmission (see Figure 3.5). Although gabion spacing influences wave reflection dynamics, The primary mechanism of wave energy loss in this configuration is found to be the in-gabion internal drag, which increases at the available drag surface area increases. Increasing the spacing between gabions does not increase that available surface area, therefore energy loss does not increase.

There are other scenarios in which gabion spacing may become significant. In this investigation, gabion spacing was found to significantly modify the wave-induced flow field. When gabions were greater than 1/2 wavelength apart, the velocity profile previously modified by the gabions was allowed to recover to it's shape upstream of the influence of the gabions. A secondary circulation extending $\approx 1/2$ wavelength from the next structure was not felt. When gabion spacing decreased enough for the influence of the secondary circulation to reach the trailing-edge of the previous gabion, this circulation was constrained. In the long wave limit of wavelength $L \to \infty$, where gabion-scale $KC = uT/B$ increases and drag dominates, flow separation around individual elements and other forms of reef-scale circulation can contribute to observed energy losses. This concept applied to the arrangement of coastal structures - sometimes called "macro-scale roughness" (Sogut et al., 2019) - was found by Xiang et al., 2024 to enhance energy losses over constructed oyster reefs. By controlling the spacing between successive gabions such that a secondary circulation is generated (here $W > 0.5L$), more energy can be taken away from the mean flow. More work should be done to characterize this process, particularly for 2D wave processes.

Gabion spacing and the resulting secondary circulation may also play an important role in controlling biological processes like larval settlement and nutrient delivery in constructed oyster reefs, which depend heavily on physical transport (Whitman and Reidenbach, 2012; Wang et al., 2008).

3.4.4 Gabion permeability and porous media characteristics

Comparing the transmission coefficient K_t as a function of B/L for both the porous and solid case allows for a quantification of the relative contribution of in-gabion internal drag in total wave energy loss. For gabion widths of $\mathcal{O}(1)$ wavelength, wave reflection accounts for $\approx 5\%$ of the total wave attenuation (see Figure 3.11) and friction at the crest of the gabion is negligible (section 3.4.1), therefore porosity contributes $> 35\%$ of the active damping done by the gabions (see Figure 3.8). Wave attenuation has generally been found across studies

to be higher in oyster shell bags in comparison to Reef Balls, Reef BLK and other primarily solid, concrete structures (Allen and Webb, 2011; Xiang et al., 2024; Webb and Allen, 2015; Armono and Hall, 2003). It has been speculated that this is due to the influence of the porous media characteristics of oyster shell (Xu et al., 2024). These results confirm the high influence of internal drag on total wave energy dissipation over these reef designs while providing an in-depth characterization of internal drag and the modeling of this flow with the modified Ergun Equations (Van Gent, 1995).

The porosity of oyster shell was found to be within a dynamically optimal range for wave attenuation for these conditions. This can be explained by considering the behavior at the extreme limits. As $n \to 1$, pore pressure will increase until the resistance is high enough that flow will skim over the structure and the contribution to the total energy dissipation by in-gabion internal drag $\to 0$. Similarly, as $n \to 0$, the available surface area for drag to occur will $\to 0$ until there is nothing there, hence internal drag will also $\to 0$. Given this nonlinear trend, there must exist an optimal porosity for maximizing energy dissipation due to in-gabion internal drag between these limits, a phenomenon explored in other porous media (Huang et al., 2003) but not oyster shell. The results presented in Figure 3.8 suggest that this optimum $n^* > 0.6$ and $n^* < 1$ for oyster shell (recall the porosity of the physical oyster shell $n = 0.71$), however more experiments are required to fully characterize this transition.

The Extended-Darcy Forcheimer Equation and the accompanying Ergun Equations use the concept of a distributed drag to model small-scale interactions between the highly irregular, sharp-edged and cup-shaped oyster shells and in-gabion flow. These models do not attempt to resolve any dynamics at the scale of the oyster, therefore their ability to accurately predict pressure losses across the oyster gabion test section suggests that the exact size of the oyster shell is an irrelevant parameter in this limit. Numerical model results are sensitive to choice of d (Figure 3.3), despite there being a negligible difference between small and large shell groups (Figure 2.8). This suggests $d_{eff} = 5$cm is not only a function of other characteristics of the oyster shell, but also robust across different collections of oyster shell.

The importance of the drag response at the scale of the oyster shell will be determined by the ratio between the drag length scale and the wave-orbital excursion, ζ_b. For larger waves, this ratio will decrease as the dynamics are more controlled by drag and the waves begin to "perceive" the gabion as a solid object. Given the fact that all other aspects of the physical experiments where scaled accordingly, it is expected that any deviation at field-scale will fall in between the curve determined through the physical experiments at the lower limit

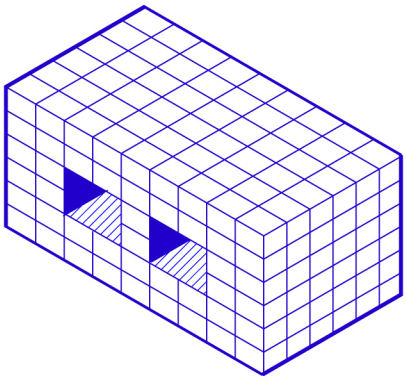

Figure 3.12: Gabion design employed by the Billion Oyster Project. The openings in the structure increase ventilation which may have implications for performance over time.

and the solid case at the upper limit.

In the field, porosity will not remain constant. Over time, oyster gabions trap sediment and become home to various species of small marine organisms (including young oysters) therefore becoming less porous. Although the latter is often a restoration target, excessive accumulation of sediment can prevent oysters from filter-feeding and lead to reef burial. As gabion-porosity decreases, wave energy dissipation due to internal drag will decrease and approach the solid limit. Gabion designs that increase structure porosity, perhaps like those employed by the Billion Oyster Project (see Figure 3.12) may achieve maximum wave energy dissipation for longer in addition to increasing ventilation and decreasing sedimentation. It will also be important to propose designs that capitalize on frictional effects to dissipate energy, which will likely increase over time as the oyster grow and orient themselves vertically, requiring even longer widths B. Current wave transmission models fail to accurately predict wave energy loss for these long crest widths (Xu et al., 2024), due both to the difficultly in modeling the nonlinear transformation in this region as well as the lack of data that characterizes friction drag in constructed oyster reefs, therefore more work must be done to explore these effects.

3.5 Conclusion

This work expands the knowledge of wave energy loss mechanisms that foreground oyster reef survival by investigating their dynamics under non-breaking wave conditions. Oyster gabion widths $B \approx \mathcal{O}(L)$ were shown to attenuate waves by 40% (or energy losses of >50%), a magnitude comparable to attenuation by some narrow design typologies when emergent (Morris et al., 2021; Webb and Allen, 2015; Armono and Hall, 2003).

This increased energy loss is attributed primarily to in-gabion internal drag which has been characterized experimentally. The ability of the modified Ergun Equations and the open-source OpenFOAM toolbox *waves2Foam* to predict the Forchheimer resistance b and model pressure losses over oyster shell was verified, with a characteristic diameter of $d_{eff} =$ 5cm found to be appropriate across large and small size shells within a sample characteristic of those used in oyster restoration. Numerical simulations explored the influence of changing porosity and found the porosity of oyster shell to be at a dynamical optimum and contribute an additional 15% to measured energy losses over solid structures at large gabion widths B. Given the non-dimensionalization of all other parameters and lack of sensitivity of b to shell diameter, these results may be scalable to larger configurations in the field, however more work would need to be done to verify this.

Spacing between successive gabion groups was found to not play a large role in modulating wave transmission for the range of spacings W explored, but was shown to play a large roll in the wave-induced flow field by constraining the development of a secondary circulation at the leading edge of the gabions. This has implications for physically-controlled biological processes in gabion-type constructed oyster reefs like larval settlement.

Chapter 4

4.1 Designing Social Infrastructure

Although practitioners can use the research presented in this thesis alongside previous work in restoration best practices to maximize wave energy dissipation under conditions that promote long-term oyster reef sustainability, this alone will not ensure the success of constructed oyster reef coastal adaptation. Oyster reef survival is dependent on more than depth of submergence; growth rates are a function of many factors including larval availability, salinity levels, temperature, nutrient availability, species and subspecies genetics, population dynamics at the community and ecosystem scale, and disease (Bayne, 2017; Breitburg et al., 2000; Powers et al., 2009; Roegner and Mann, 1995). Larval settlement in particular is controlled by oyster-scale hydrodynamics not discussed in this thesis (Fuchs et al., 2013, 2015; Powers and Grabowski, 2023). Physical dynamics within the coastal landscape are also complex, with processes spanning large spatial and temporal scales playing a role in measured wave climate[1] and water level.

In light of these inherent uncertainties, research in nature-based infrastructure must move away from design as a final, immutable product towards design as collaborative, evolving process. It is well known within restorative ecology that successful restoration often hinges upon building adaptive capacity in local communities: long-term monitoring efforts, environmental stewardship, community buy-in and, ultimately, the ability to build social infrastructure within the coastal landscape. Like the need to consider biological constraints when designing for coastal protection, design research in nature-based coastal adaptation must also see the creation of social infrastructure not just as a beneficial outcome of success-

[1]Waves in the coastal ocean are highly irregular. Dominant features of irregular wave fields like the significant wave height and dominant wave period can be statistically determined via spectral analysis of wave time series and used as the incident wave conditions in the previous analysis, however more work must be done to fully characterize irregular wave transmission in constructed oyster reefs

ful implementation, but as a *requirement* for successful implementation. Critical research that improves our ability to predict wave transformation, transmission and subsequent energy loss from oyster reefs under ideal growth conditions must therefore be combined with engagement and education practices. This will require a shift from a singularly predictive model of design towards one that integrates predictive and adaptive approaches - a process that can not only return sought for engineering outcomes but build a multi-species understanding of coastal community resilience.

This chapter presents a design research toolikit that seeks to facilitate the creation of social infrastructure around nature-based coastal adaptation by (1) challenging human-centric notions of coastal community resilience, (2) communicating and interaction between biological and physical processes in coastal landscapes, and (3) leveraging physical intuition and design to empower coastal community members to reimagine what it means to *build with nature*.

4.2 The Resilient Coast

Traditional coastal infrastructure often stabilizes shorelines and mitigates coastal flooding at the expense of coastal ecosystems (see Chapter 1). Although the immediate benefit to human coastal communities is apparent, long-term damage to the greater ecosystem (i.e. the loss of many coastal habitats) has wide-reaching impacts that decrease resilience overall. Building capacity within coastal communities for environmental stewardship of nature-based solutions should first communicate the need for an ecosystem-level perspective that challenges human-centric notions of resilience. By increasing awareness about the organisms that make up the coastal landscape - the shorebirds, the oysters, the larval fish resting in the shallows and the microphytobenthos living on the tidal flats - nature-based solutions can build a holistic understanding of the interaction between biotic and abiotic factors in these landscapes. Who and what make up the "nature" of *Building with Nature*?

These questions have been explored through the development of a lesson plan in collaboration with the Staten Island Museum (SIM) in Staten Island, NY. Coastal adaptation has received a lot of attention from the media and local government in Staten Island in the last few years (Klinenburg, 2021; Rosenzweig et al., 2011). Following the massive damages brought about by Hurricane Sandy in 2012, several initiatives in New York City have sought to improve and reimagine they city's coastal infrastructure through innovative design, with several multi-billion dollar projects currently under construction in Lower Manhattan, Jamaica Bay and Far Rockaway. Although many residents of Staten Island have heard the term

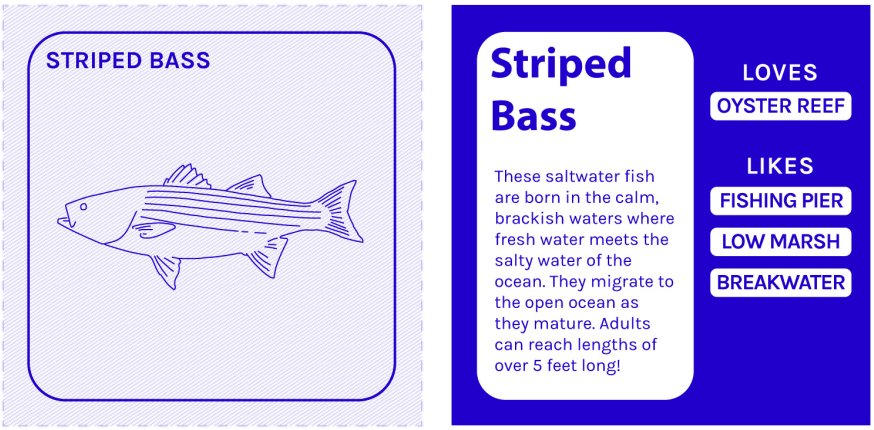

Figure 4.1: Coastal community member cards include brief descriptive text and affinity tags ("likes" and "loves") which allow students to make informed choices when designing their ideal coastline.

"nature-based solutions" (in part due to the robust media and outreach campaign of *Living Breakwaters*), it became clear in conversations with education staff at the SIM that there were gaps in understanding within the general public regarding how nature-based solutions actually work and why they are a sustainable alternative to traditional infrastructure, as well as a lack of educational materials aimed at public school students that explain these concepts and introduce them to careers in this exciting new industry. As the only major museum in New York City dedicated to both the arts and natural sciences, this museum is uniquely positioned to host conversations about this multidisciplinary topic.

The resulting lesson plan, titled *The Resilient Coast*, features a flexible, interactive design activity where students gain insight into the physical, ecological and social resilience embedded in New York's coastal ecosystems through role play and creative inquiry. It is divided into two modules: "The Coastal Landscape" and "Living with Nature: a Pathway Towards a Sustainable Coast." The former focuses on introducing students to northeastern coastal habitats as they are, highlighting important physical processes and features (the ocean, the beach, waves, the low marsh and high marsh, estuaries and river mouths) as well as the human and non-human inhabitants of these ecosystems. The latter gives students the opportunity to imagine their own coastline, placing coastal feature cards in positions on a shoreline cross-section while challenging notions of human-centric development by designing for a set of coastal community members that include shore birds, oysters, horseshoe crabs, and fish as well as the fisherman, artist, student, and park ranger (see Figures 4.1 and 4.2). Each zone on the cross-section (corresponding to the subtidal, intertidal and upland) can

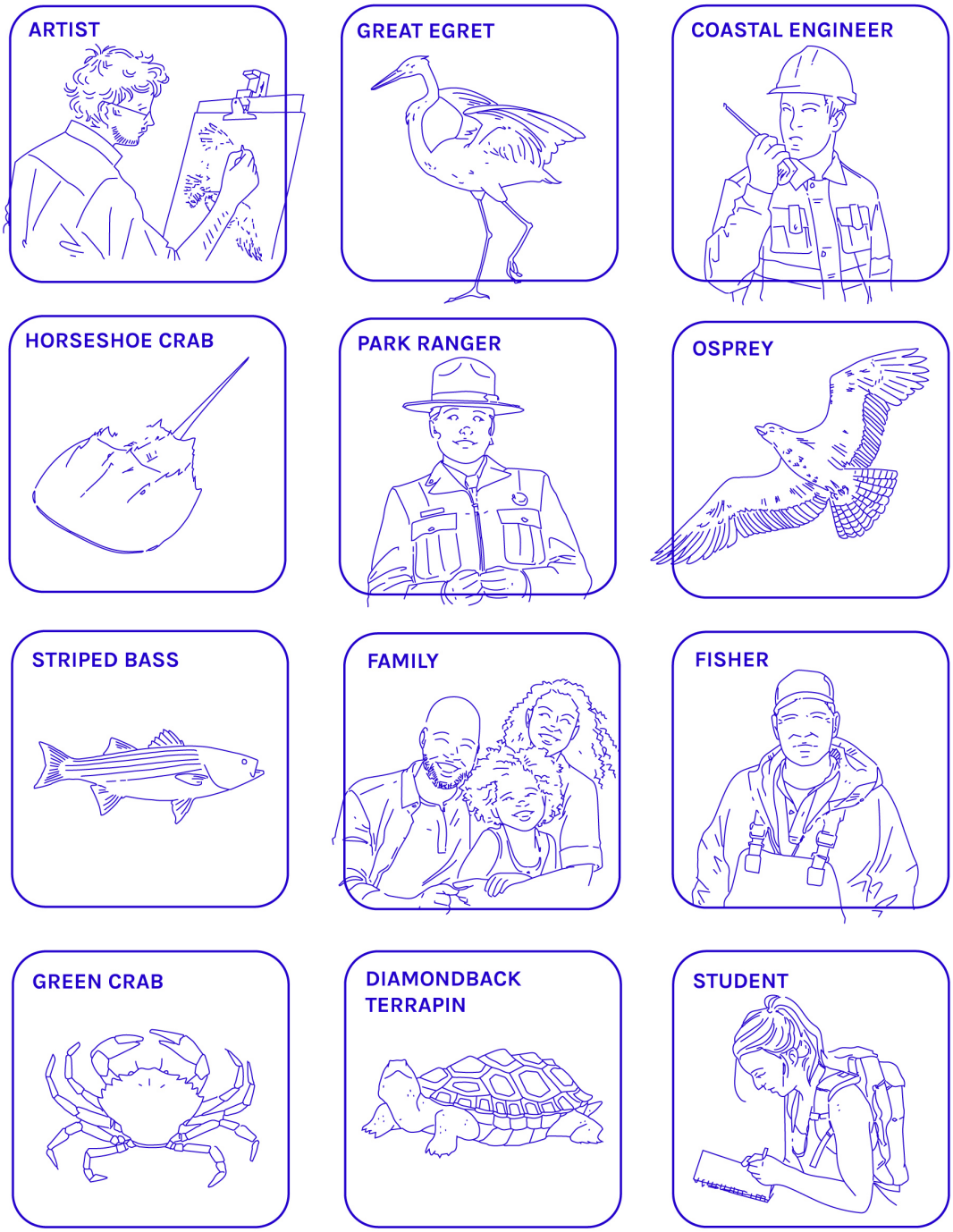

Figure 4.2: There are 12 community member cards in total, each with their own affinity tags.

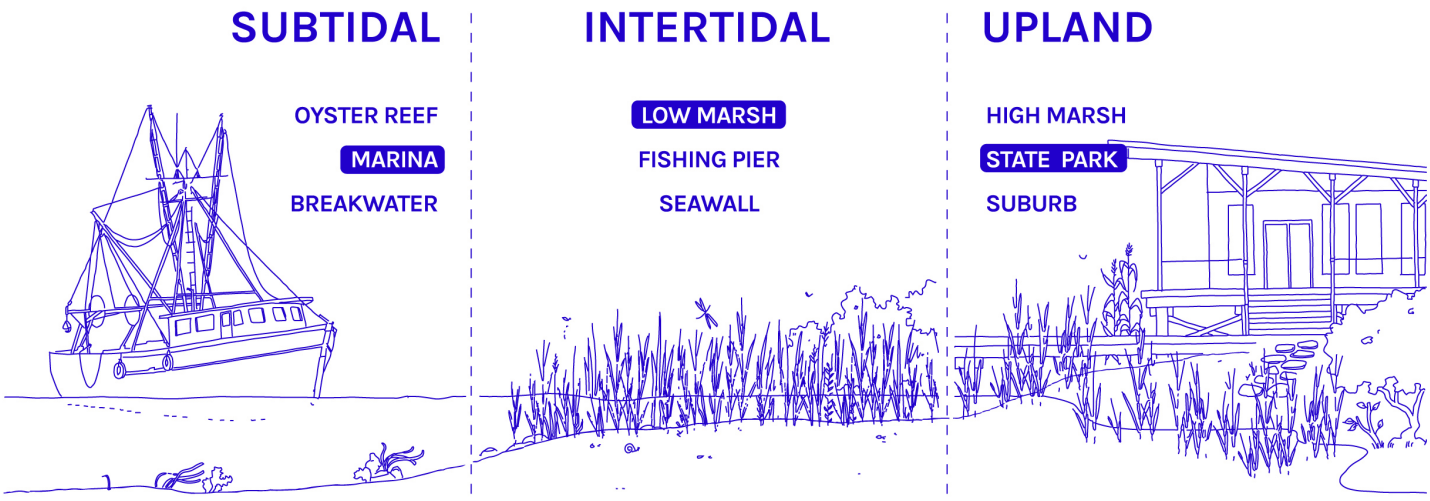

Figure 4.3: Coastal zones: subtidal, intertidal and upland

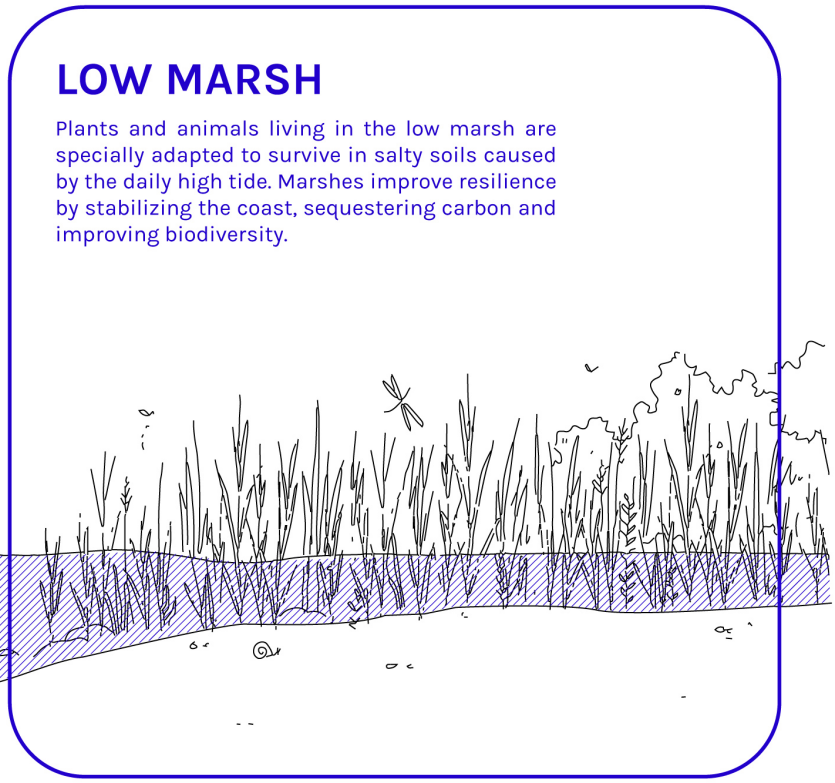

Figure 4.4: Example coastal feature card. There are 9 coastal feature cards in total, 3 for each of the coastal zones: subtidal, intertidal and upland.

only fit certain features, with the option to choose from heavily developed options like a marina, to lighter developments like a fishing pier, to wild landscapes like a full marsh (see Figures 4.4 and 4.3), which are then matched to affinity tags on the accompanying coastal community cards. Students choose coastal features cards and match to tags on the coastal community cards, gaining an appreciation for those who their coastline can support and those who it can't.

These programs reach over 2000 New York City public students each year, a number which is steadily growing as the Staten Island Museum expands its scope in preparation for a new and highly-anticipated natural sciences wing. Initial feedback from education staff was positive, paving the way for further engagements with environmental educators across New York City through the Green Umbrella Coalition.

4.3 Visualizing Coastal Processes

Successful physical, ecological and social design in nature-based coastal adaptation requires a deeper understanding of the way these processes interact and feedback on one another across scales. Although crafted with the intent of communicating with an multidisciplinary audience, many of diagrams thus far presented in this thesis are of a type of visualization designed for specialists. Graphs effectively communicate data, but a deeper, more intuitive appreciation of the complex systems at play in nature-based coastal infrastructure requires a multimedia approach.

A 4 ft. by 1 ft. topographic shoreline model was CNC-milled out of solid maple wood and painted with fabric dye (Figures 4.5, 4.6, 4.7 and 4.10). Illustrations of the physical and ecological processes present in the coastal landscape were laser-scored into 6 in. by 4 ft. acrylic sheets placed on either side of the model (Figure 4.8 and Figure 4.9, respectively). This piece was shown from April 22nd to December 30th, 2023 as a part of the Staten Island Museum's *Vulnerable Landscapes* Exhibition with the accompanying text:

> *Staten Island is home to a rich collection of coastal ecosystems, primarily found in the form of beaches and tidal salt marsh estuaries like Lemon Creek, Saw Mill Creek, and Fresh Kills. These landscapes tell a story of inter-species relationships spanning multiple scales: from the migratory bird reliant on the eggs of the horseshoe crab to fuel a long journey ahead, to the larval fish taking refuge within the porous structure of shellfish reefs. They also bear the mark of human influence; we are a part of these landscapes, our role within them not singularly defined by degradation or decline, but in many instances by appreciation and stewardship and care.*

Figure 4.5: Photo of shoreline model in exhibition

> *The landscape tells another story – a hidden resilience rooted in the meeting of physics and ecology. A story of flows and energy and forces.*
>
> *The way oyster reefs and marsh grasses dissipate wave energy generated during storms.*
>
> *The way wetlands trap carbon-rich sediments and prevent them from entering the atmosphere.*
>
> *The way vegetation filters runoff before it enters the watershed.*
>
> *To understand the true value of our coastal ecosystems is to be able to toggle between these alternative modes of seeing, to view the landscape through the lens of the ecological and the physical simultaneously. To see the social resilience embedded in both.*
>
> *Based on the Lemon Creek tidal estuary and its history as a working waterfront, Resilient Landscapes seeks to reveal the physical, ecological, and social resilience embedded within the coastal landscapes of Staten Island, asking how we can leverage a deeper understanding of these phenomena to design a better future.*

This multidisciplinary exhibition, curated by Rylee Eterginoso of the SIM, aimed to convey the vulnerability of Staten Island's landscapes through contemporary art works, stories of resistance, change and scientific investigation, while strengthening the connection between the Staten Island coastal community and their environment ("Vulnerable Landscapes", 2023). A quote by founding member of the local North Shore Waterfront Conservancy, Beryl Thur-

Figure 4.6: Photo of shoreline model *(plan view)*

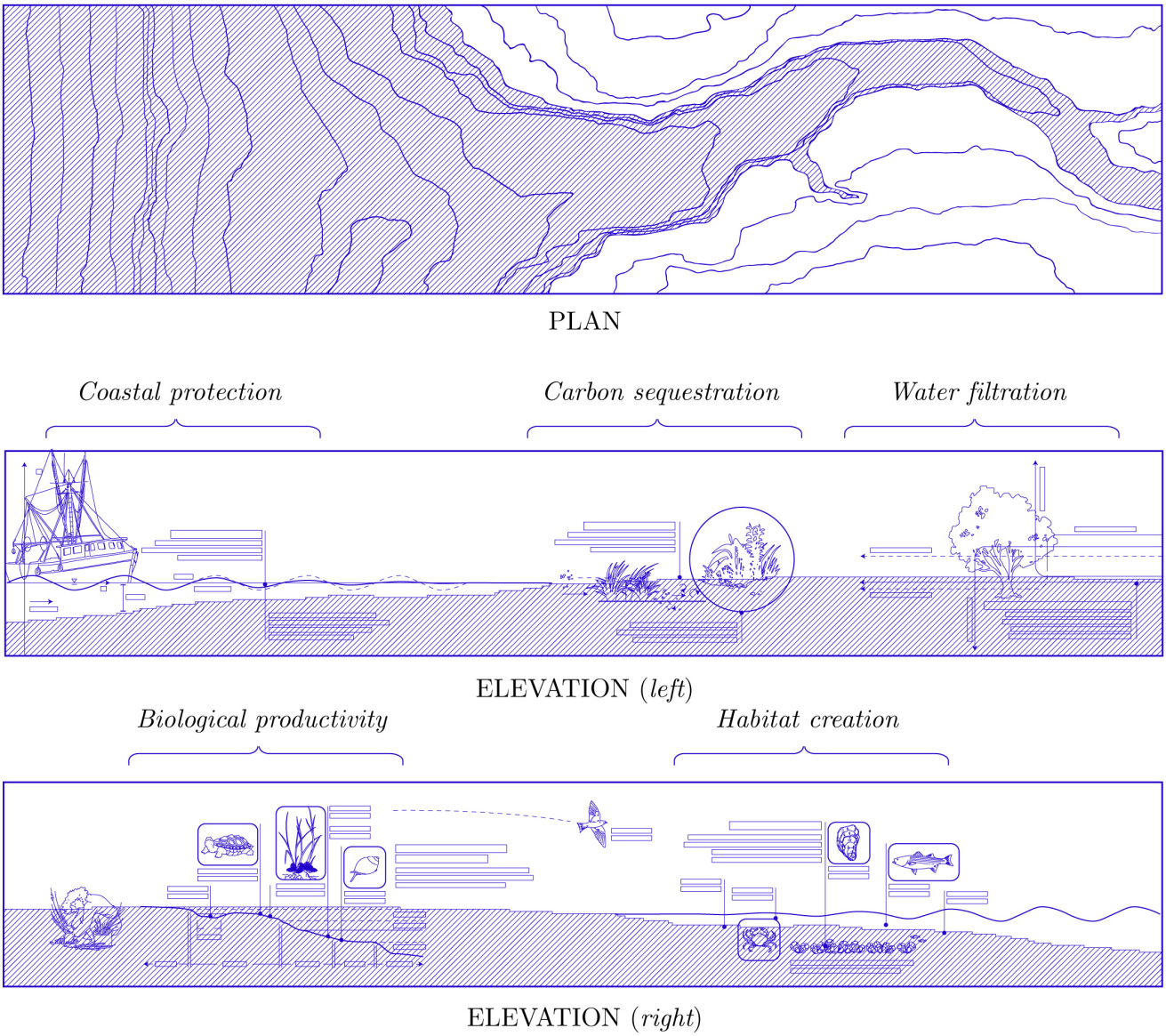

Figure 4.7: Plan and elevation drawings for shoreline model

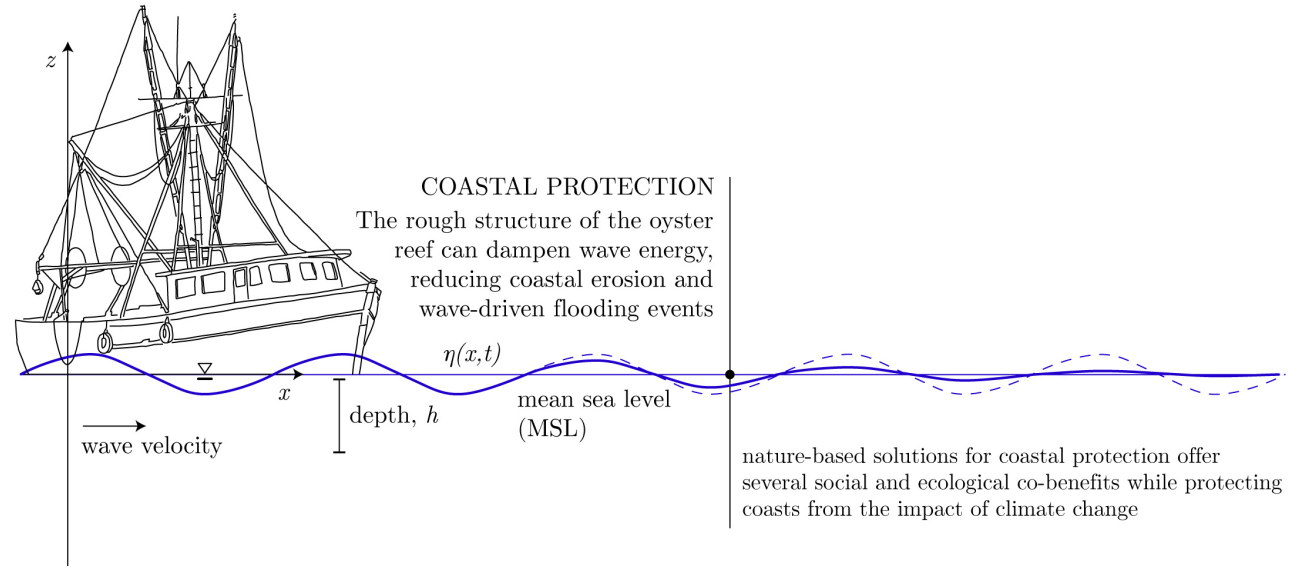

Figure 4.8: Example drawing of the physical resilience embedded in coastal landscapes

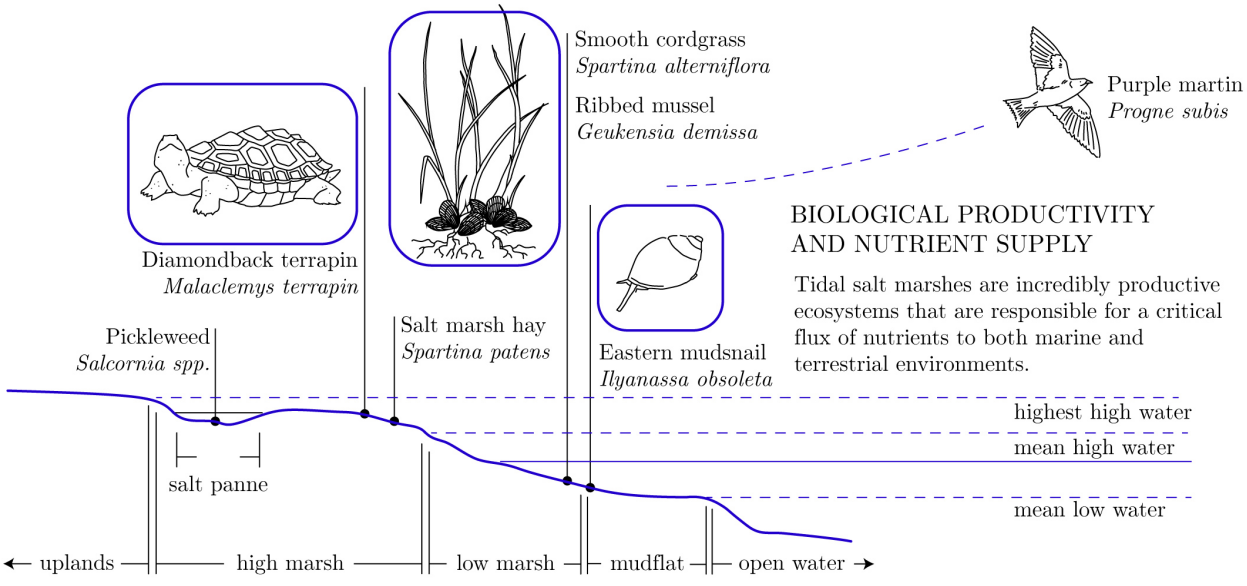

Figure 4.9: Example drawing of the ecological resilience embedded in coastal landscapes

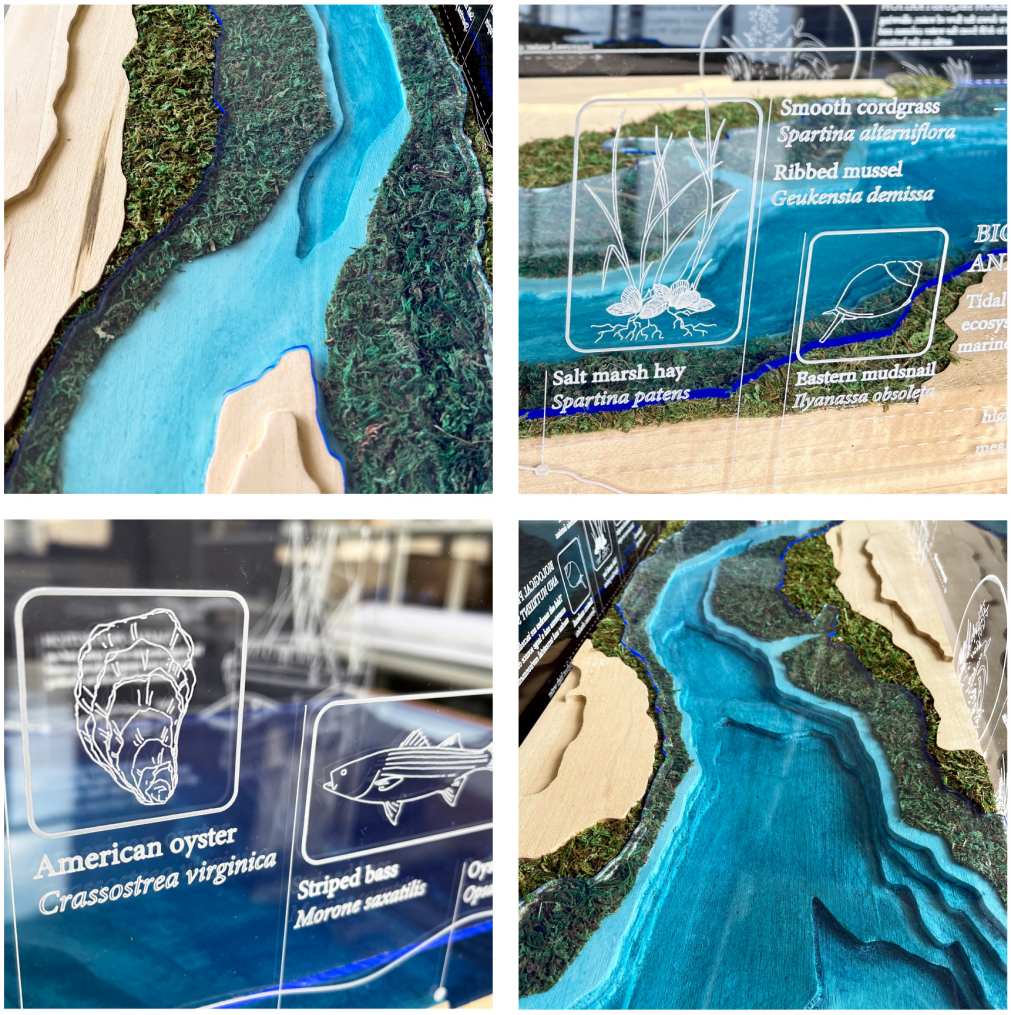

Figure 4.10: Detail images

man, accompanied the exhibition's website: "The more you know about your environment, the better advocate you can be for Staten Island. And that's what Staten Island really needs, it needs more advocates, it needs more people that think through the process."

4.4 Building Physical Intuition Through Design

Process-based diagrams can captivate audiences and spark curiosity, but active demonstrations build a more intuitive understanding of the physical resilience embedded in coastal ecosystems. The following interactive activity was originally co-developed with Autumn Deitrick for the 2022 Cambridge Science Festival and 2022 MIT Splash (a high school outreach program hosted by MIT annually), but has since been reconceptualized by the author.

Figure 4.11: Photo from original demonstration at Cambridge Science Festival

This activity consists of a 7.5 ft. tabletop wave flume with two parallel channels and a hand-held wave paddle accompanied by a coastal adaptation kit-of-parts (see Figure 4.14). Participants have the opportunity to design their own coastline adaptation, choosing from models of gray infrastructure like seawalls and breakwaters to green infrastructure like marsh grasses, mangroves and oyster gabions (Figure 4.12).

Waves pass over participant designs with varying levels of energy dissipation or reflection. The difference in response between the models of green infrastructure and those of grey infrastructure is visually striking - the latter case often producing a clear reflected wave and the former dissipating the wave substantially. Although the scale of the demonstration prevents dramatic wave breaking events, submerged models sufficiently close to the water surface can induce spilling and the development of a bore. This allows for a more nuanced conversation about *how* nature-based solutions work in which concepts like wave energy, reflection and turbulence are discussed. Furthermore, the split nature of the flume allows participants to test a hypothesis, exploring wave attenuation by sparse vs. dense vegetation, or oyster gabions combined with vegetation vs. seawalls. Wave heights can be measured qualitatively by taping a piece of construction paper just above the still water elevation to the far wall and noting the extent of the wave run-up (the wet edge). More quantitative

Figure 4.12: Photos of flume inserts

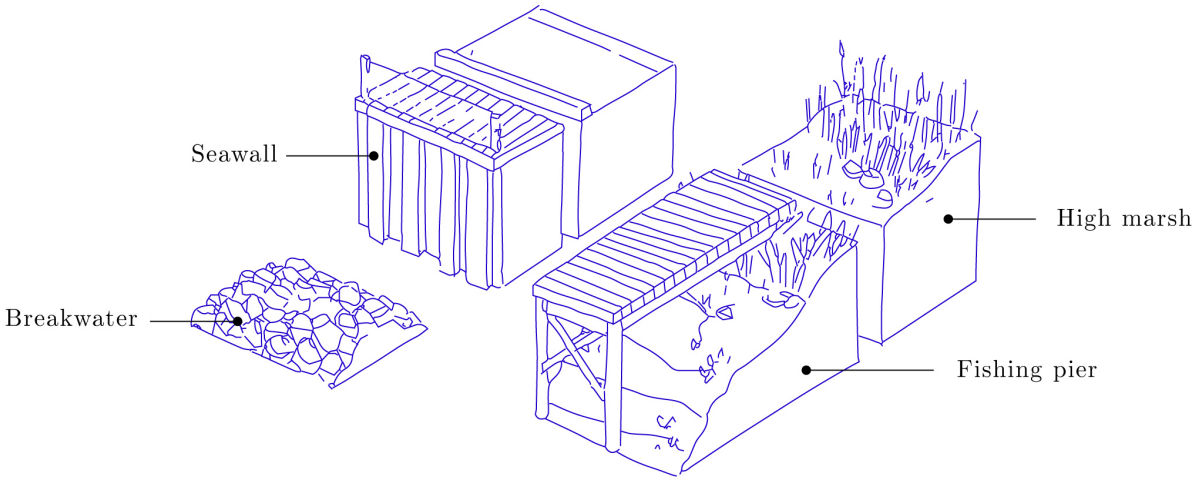

Figure 4.13: Physical models of the Coastal Feature cards

measurements can be gained with sensors[2].

It is also a unique opportunity to increase awareness about scientific research in nature-based coastal adaptation. Including scale models from actual experiments (like the oyster gabions from Chapters 2 and 3) and pictures or video of full-scale wave flumes can introduce the science of physical model testing and environmental fluid mechanics.

Combining this activity with the *Resilient Coast* card deck allows for a nuanced conversation about the interaction of physical, ecological and social processes in the coastal landscape through the lens of design. Instead of using the Coastal Feature Cards, physical models of coastal features (see Figure 4.13) allow participants to design their ideal coastline

[2]A simple but effective method explored with the help of Diego Tempkin, Caroline Langmeyer and Stephen Rudolf of the Department of Civil and Environmental Engineering involved recalibrating a pair of soil moisture sensors to act wave gauges.

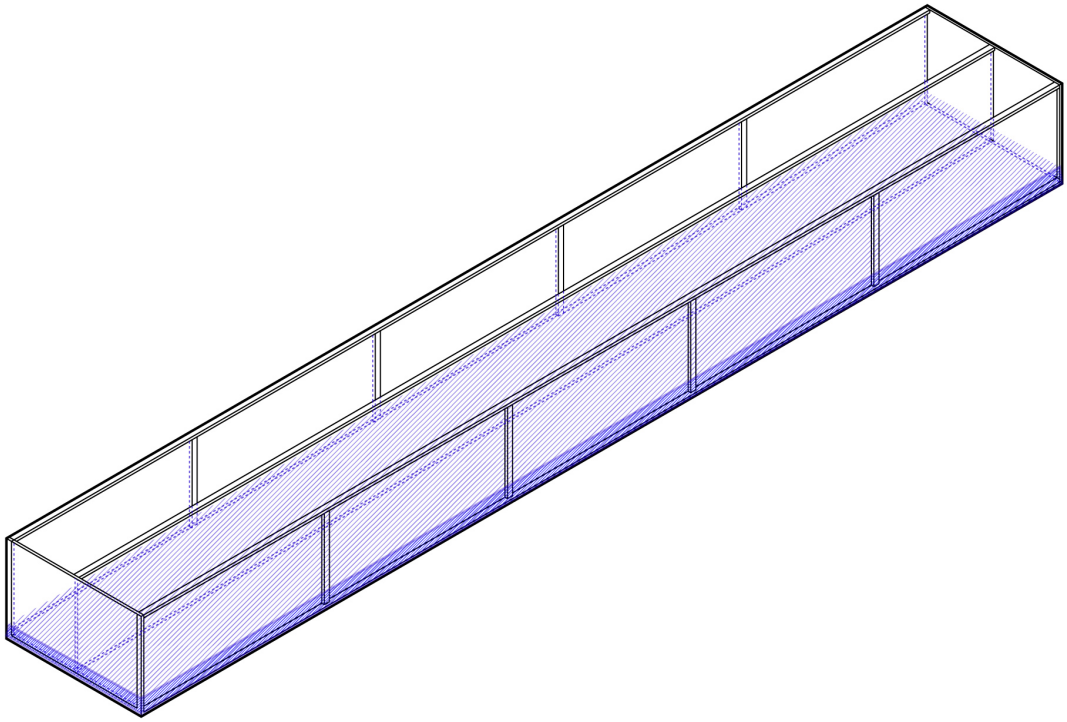

Figure 4.14: Table-top wave flume schematic

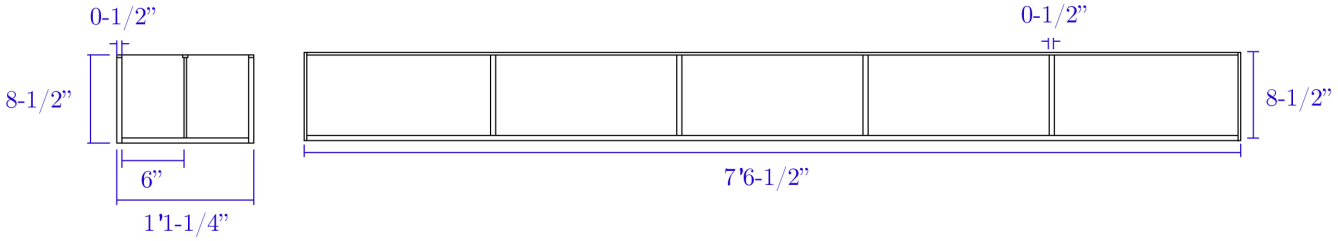

Figure 4.15: Table-top wave flume dimensions

based on personal priorities and value systems, which they can then test directly. Who are the human and non-human actors in these systems and what are their needs? Which coastal features support life and which do not? What are the mechanics of ocean waves and how to they interact with various forms of green and gray infrastructure? By allowing participants to engage in these questions simultaneously, this suite of engagement tools aims to educate coastal communities about nature-based coastal adaptation (and all the nuance that goes with it) while empowering them to make informed decisions about its application.

References

Bayne, B. L. (2017). *Biology of oysters*. Academic Press.

Smyth, A. R., Geraldi, N. R., Thompson, S. P., & Piehler, M. F. (2016). Biological activity exceeds biogenic structure in influencing sediment nitrogen cycling in experimental oyster reefs. *Marine Ecology Progress Series*, *560*, 173–183.

Newell, R. I., & Koch, E. W. (2004). Modeling seagrass density and distribution in response to changes in turbidity stemming from bivalve filtration and seagrass sediment stabilization. *Estuaries*, *27*, 793–806.

Posey, M. H., Alphin, T. D., Powell, C. M., & Townsend, E. (2003). Use of oyster reefs as habitat for epibenthic fish and decapods. *Oyster Reef Habitat Restoration: A Synopsis and Synthesis*, 229.

Peterson, C. H., Grabowski, J. H., & Powers, S. P. (2003). Estimated enhancement of fish production resulting from restoring oyster reef habitat: Quantitative valuation. *Marine Ecology Progress Series*, *264*, 249–264. https://doi.org/10.3354/meps264249

Thompson, V. D., & Worth, J. E. (2011). Dwellers by the sea: Native american adaptations along the southern coasts of eastern north america. *Journal of Archaeological Research*, *19*(1), 51–101. https://doi.org/10.1007/s10814-010-9043-9

Ceci, L. (1984). Shell midden deposits as coastal resources. *World Archaeology*, *16*(1), 62–74.

Schwadron, M. (2010). *Landscapes of maritime complexity: Prehistoric shell work sites of the ten thousand islands, florida* [Doctoral dissertation, University of Leicester].

Sheehan, M. S., & Sickels-Taves, L. B. (2002). Vernacular building materials and the factors conditioning their use: Tabby, a case study. *Material Culture*, *34*(2), 16–28.

Matthiessen, G. C. (2008). *Oyster culture*. John Wiley & Sons.

Brooks, W. K. (1996). *The oyster*. JHU Press.

Rothschild, B. J., Ault, J. S., Goulletquer, P., & Héral, M. (1994). Decline of the chesapeake bay oyster population: A century of habitat destruction and overfishing. *Marine Ecology Progress Series*, *111*(1/2), 29–39.

Jones, C. G., Lawton, J. H., & Shachak, M. (1994). Organisms as ecosystem engineers. *Oikos*, *69*(3), 373–386. https://doi.org/10.2307/3545850

Luckenbach, M. W., Mann, R., & Wesson, J. A. (1999). Oyster reef habitat restoration: A synopsis and synthesis of approaches; proceedings from the symposium, williamsburg, virginia, april 1995. https://doi.org/10.21220/V5NK51

Holdren, J. P., & Ehrlich, P. R. (1974). Human population and the global environment: Population growth, rising per capita material consumption, and disruptive technologies have made civilization a global ecological force. *American Scientist*, *62*(3), 282–292.

Daily, G. C. (1997). Introduction: What are ecosystem services? In *Societal dependence on natural ecosystems* (pp. 1–10). Island Press.

Grabowski, J. H., & Peterson, C. H. (2007). Restoring oyster reefs to recover ecosystem services. In K. Cuddington, J. E. Byers, W. G. Wilson, & A. Hastings (Eds.), *Ecosystem engineers* (pp. 281–298, Vol. 4). Academic Press. https://doi.org/10.1016/S1875-306X(07)80017-7

Breitburg, D., Coen, L. D., Luckenbach, M., Mann, R., Posey, M., & Wesson, J. (2000). Oyster reef restoration: Convergence of harvest and conservation strategies. *Journal Of Shellfish Research*, *19*(1), 371–377.

Drake, F. (2014). *Global warming*. Routledge.

Knutson, T. R., McBride, J. L., Chan, J., Emanuel, K., Holland, G., Landsea, C., Held, I., Kossin, J. P., Srivastava, A. K., & Sugi, M. (2010). Tropical cyclones and climate change. *Nature Geoscience*, *3*(3), 157–163. https://doi.org/10.1038/ngeo779

Torio, D. D., & Chmura, G. L. (2013). Assessing coastal squeeze of tidal wetlands. *Journal of Coastal Research*, *29*(5), 1049–1061. https://doi.org/10.2112/JCOASTRES-D-12-00162.1

Sutherland, J., Obhrai, C., Whitehouse, R. J. S., & Pearce, A. (2006). Laboratory tests of scour at a seawall. *Proceedings 3rd International Conference on Scour and Erosion, CURNET, Gouda, The Netherlands*. https://eprints.hrwallingford.com/591/

Dedekorkut-Howes, A., Torabi, E., & Howes, M. (2020). When the tide gets high: A review of adaptive responses to sea level rise and coastal flooding. *Journal of Environmental Planning and Management*, *63*(12), 2102–2143.

Cheong, S.-M., Silliman, B., Wong, P. P., van Wesenbeeck, B., Kim, C.-K., & Guannel, G. (2013). Coastal adaptation with ecological engineering. *Nature Climate Change*, *3*(9), 787–791. https://doi.org/10.1038/nclimate1854

Chowdhury, M. S. N., La Peyre, M., Coen, L. D., Morris, R. L., Luckenbach, M. W., Ysebaert, T., Walles, B., & Smaal, A. C. (2021). Ecological engineering with oysters enhances

coastal resilience efforts. *Ecological Engineering*, *169*, 106320. https://doi.org/10.1016/j.ecoleng.2021.106320

Zhang, K., Liu, H., Li, Y., Xu, H., Shen, J., Rhome, J., & Smith III, T. J. (2012). The role of mangroves in attenuating storm surges. *Estuarine, Coastal and Shelf Science*, *102*, 11–23.

Marois, D. E., & Mitsch, W. J. (2015). Coastal protection from tsunamis and cyclones provided by mangrove wetlands–a review. *International Journal of Biodiversity Science, Ecosystem Services & Management*, *11*(1), 71–83.

Rezaie, A. M., Loerzel, J., & Ferreira, C. M. (2020). Valuing natural habitats for enhancing coastal resilience: Wetlands reduce property damage from storm surge and sea level rise. *PLoS One*, *15*(1), e0226275.

Fairchild, T. P., Bennett, W. G., Smith, G., Day, B., Skov, M. W., Möller, I., Beaumont, N., Karunarathna, H., & Griffin, J. N. (2021). Coastal wetlands mitigate storm flooding and associated costs in estuaries. *Environmental Research Letters*, *16*(7), 074034.

Menéndez, P., Losada, I. J., Torres-Ortega, S., Narayan, S., & Beck, M. W. (2020). The global flood protection benefits of mangroves. *Scientific reports*, *10*(1), 1–11.

Lowe, R. J., Falter, J. L., Bandet, M. D., Pawlak, G., Atkinson, M. J., Monismith, S. G., & Koseff, J. R. (2005). Spectral wave dissipation over a barrier reef. *Journal of Geophysical Research: Oceans*, *110*(C4).

Piazza, B. P., Banks, P. D., & La Peyre, M. K. (2005). The potential for created oyster shell reefs as a sustainable shoreline protection strategy in louisiana. *Restoration Ecology*, *13*(3), 499–506.

Gedan, K. B., Kirwan, M. L., Wolanski, E., Barbier, E. B., & Silliman, B. R. (2011). The present and future role of coastal wetland vegetation in protecting shorelines: Answering recent challenges to the paradigm. *Climatic change*, *106*, 7–29.

Borsje, B. W., van Wesenbeeck, B. K., Dekker, F., Paalvast, P., Bouma, T. J., van Katwijk, M. M., & de Vries, M. B. (2011). How ecological engineering can serve in coastal protection. *Ecological Engineering*, *37*(2), 113–122.

Keimer, K., Schürenkamp, D., Miescke, F., Kosmalla, V., Lojek, O., & Goseberg, N. (2021). Ecohydraulics of surrogate salt marshes for coastal protection: Wave–vegetation interaction and related hydrodynamics on vegetated foreshores at sea dikes. *Journal of Waterway, Port, Coastal, and Ocean Engineering*, *147*(6), 04021035.

Vuik, V., Jonkman, S. N., Borsje, B. W., & Suzuki, T. (2016). Nature-based flood protection: The efficiency of vegetated foreshores for reducing wave loads on coastal dikes. *Coastal engineering*, *116*, 42–56.

De Vriend, H. J., van Koningsveld, M., Aarninkhof, S. G., de Vries, M. B., & Baptist, M. J. (2015). Sustainable hydraulic engineering through building with nature. *Journal of Hydro-environment research*, *9*(2), 159–171.

Seddon, N., Chausson, A., Berry, P., Girardin, C. A. J., Smith, A., & Turner, B. (2020). Understanding the value and limits of nature-based solutions to climate change and other global challenges. *Philosophical Transactions of the Royal Society B: Biological Sciences*, *375*(1794), 20190120. https://doi.org/10.1098/rstb.2019.0120

Little, C. E. (1995). *Greenways for america*. JHU Press.

Berkes, F. (2017). *Sacred ecology*. Routledge.

Alexander, J. S., Wilson, R. C., & Green, W. R. (2012). *A brief history and summary of the effects of river engineering and dams on the mississippi river system and delta* (tech. rep.). US Geological Survey.

Díaz, S. M., Settele, J., Brondízio, E., Ngo, H., Guèze, M., Agard, J., Arneth, A., Balvanera, P., Brauman, K., & Butchart, S. (2019). The global assessment report on biodiversity and ecosystem services: Summary for policy makers. https://ri.conicet.gov.ar/handle/11336/116171

Shukla, P. R., Skea, J., Buendia, E. C., Masson-Delmotte, V., Pörtner, H. O., Roberts, D. C., Zhai, P., Slade, R., Connors, S., & Van Diemen, R. (2019). Ipcc, 2019: Climate change and land: An ipcc special report on climate change, desertification, land degradation, sustainable land management, food security, and greenhouse gas fluxes in terrestrial ecosystems. https://spiral.imperial.ac.uk/bitstream/10044/1/76618/2/SRCCL-Full-Report-Compiled-191128.pdf

Nations, U. (2019). *2019 climate action summit*. https://www.un.org/en/climatechange/2019-climate-action-summit

Gittman, R. K., Popowich, A. M., Bruno, J. F., & Peterson, C. H. (2014). Marshes with and without sills protect estuarine shorelines from erosion better than bulkheads during a category 1 hurricane. *Ocean & Coastal Management*, *102*, 94–102.

Huynh, L. T. M., Su, J., Wang, Q., Stringer, L. C., Switzer, A. D., & Gasparatos, A. (2024). Meta-analysis indicates better climate adaptation and mitigation performance of hybrid engineering-natural coastal defence measures. *Nature Communications*, *15*(1), 2870.

Chausson, A., Turner, B., Seddon, D., Chabaneix, N., Girardin, C. A., Kapos, V., Key, I., Roe, D., Smith, A., Woroniecki, S., et al. (2020). Mapping the effectiveness of nature-based solutions for climate change adaptation. *Global Change Biology*, *26*(11), 6134–6155.

Nelson, D. R., Bledsoe, B. P., Ferreira, S., & Nibbelink, N. P. (2020). Challenges to realizing the potential of nature-based solutions. *Current Opinion in Environmental Sustainability*, *45*, 49–55. https://doi.org/10.1016/j.cosust.2020.09.001

Rodriguez, A. B., Fodrie, F. J., Ridge, J. T., Lindquist, N. L., Theuerkauf, E. J., Coleman, S. E., Grabowski, J. H., & et al. (2014). Oyster reefs can outpace sea-level rise. *Nature Climate Change*, *4*(6), 493–497. https://doi.org/10.1038/nclimate2216

Freeman, L. A., Corbett, D. R., Fitzgerald, A. M., Lemley, D. A., Quigg, A., & Steppe, C. N. (2019). Impacts of urbanization and development on estuarine ecosystems and water quality. *Estuaries and Coasts*, *42*, 1821–1838.

Howie, A. H., & Bishop, M. J. (2021). Contemporary oyster reef restoration: Responding to a changing world. *Frontiers in Ecology and Evolution*, *9*, 689915.

Powers, S. P., Peterson, C. H., Grabowski, J. H., & Lenihan, H. S. (2009). Success of constructed oyster reefs in no-harvest sanctuaries: Implications for restoration. *Marine Ecology Progress Series*, *389*, 159–170.

Lipcius, R. N., Burke, R. P., McCulloch, D. N., Schreiber, S. J., Schulte, D. M., Seitz, R. D., & Shen, J. (2015). Overcoming restoration paradigms: Value of the historical record and metapopulation dynamics in native oyster restoration. *Frontiers in Marine Science*, *2*, 65.

Byers, J. E., Grabowski, J. H., Piehler, M. F., Hughes, A. R., Weiskel, H. W., Malek, J. C., & Kimbro, D. L. (2015). Geographic variation in intertidal oyster reef properties and the influence of tidal prism. *Limnology and Oceanography*, *60*(3), 1051–1063.

Roegner, G. C., & Mann, R. (1995). Early recruitment and growth of the american oyster crassostrea virginica (bivalvia: Ostreidae) with respect to tidal zonation and season. *Marine Ecology Progress Series*, *117*, 91.

Solomon, J. A., Donnelly, M. J., & Walterst, L. J. (2014). Effects of sea level rise on the intertidal oyster crassostrea virginica by field experiments. *Journal of Coastal Research*, (68), 57–64.

Marshall, D. A., La Peyre, M. K., & Walters, K. (2020). Effects of inundation duration on southeastern louisiana oyster reefs. *Experimental Results*, *1*, e30.

Morris, R. L., La Peyre, M. K., Webb, B. M., Marshall, D. A., Bilkovic, D. M., Cebrian, J., McClenachan, G., Kibler, K. M., Walters, L. J., Bushek, D., et al. (2021). Large-scale variation in wave attenuation of oyster reef living shorelines and the influence of inundation duration. *Ecological Applications*, *31*(6), e02382.

Walles, B., Fodrie, F. J., Nieuwhof, S., Jewell, O. J. D., Herman, P. M. J., & Ysebaert, T. (2016). Guidelines for evaluating performance of oyster habitat restoration should

include tidal emersion: Reply to baggett et al. *Restoration Ecology*, *24*(1), 4–7. https://doi.org/10.1111/rec.12328

Ysebaert, T., Walles, B., Haner, J., & Hancock, B. (2019). Habitat modification and coastal protection by ecosystem-engineering reef-building bivalves. https://doi.org/10.1007/978-3-319-96776-9_13

Seabrook, S. R., & Hall, K. R. (1999). Wave transmission at submerged rubblemound breakwaters. In *Coastal engineering 1998* (pp. 2000–2013).

Morris, R. L., Bilkovic, D. M., Boswell, M. K., Bushek, D., Cebrian, J., Goff, J., Kibler, K. M., & et al. (2019). The application of oyster reefs in shoreline protection: Are we over-engineering for an ecosystem engineer? *Journal of Applied Ecology*, *56*(7), 1703–1711. https://doi.org/10.1111/1365-2664.13390

Bilkovic, D. M., Mitchell, M., Mason, P., & Duhring, K. (2016). The role of living shorelines as estuarine habitat conservation strategies. *Coastal Management*, *44*(3), 161–174.

Isdell, R. E., Bilkovic, D. M., Guthrie, A. G., Mitchell, M. M., Chambers, R. M., Leu, M., & Hershner, C. (2021). Living shorelines achieve functional equivalence to natural fringe marshes across multiple ecological metrics. *PeerJ*, *9*, e11815.

Cooper, J. A. G., & Pilkey, O. H. (2012). *Pitfalls of shoreline stabilization: Selected case studies* (Vol. 3). Springer Science & Business Media.

Firth, L. B., Airoldi, L., Bulleri, F., Challinor, S., Chee, S.-Y., Evans, A. J., Hanley, M. E., Knights, A. M., O'Shaughnessy, K., Thompson, R. C., et al. (2020). Greening of grey infrastructure should not be used as a trojan horse to facilitate coastal development. *Journal of Applied Ecology*, *57*(9), 1762–1768.

Burt, J. A., Feary, D. A., Cavalcante, G., Bauman, A. G., & Usseglio, P. (2013). Urban breakwaters as reef fish habitat in the persian gulf. *Marine Pollution Bulletin*, *72*(2), 342–350.

Chapman, M., & Underwood, A. (2011). Evaluation of ecological engineering of "armoured" shorelines to improve their value as habitat. *Journal of experimental marine biology and ecology*, *400*(1-2), 302–313.

Feagin, R. A., Mukherjee, N., Shanker, K., Baird, A. H., Cinner, J., Kerr, A. M., Koedam, N., Sridhar, A., Arthur, R., Jayatissa, L. P., et al. (2010). Shelter from the storm? use and misuse of coastal vegetation bioshields for managing natural disasters. *Conservation Letters*, *3*(1), 1–11.

Raymond, C. M., Frantzeskaki, N., Kabisch, N., Berry, P., Breil, M., Nita, M. R., Geneletti, D., & Calfapietra, C. (2017). A framework for assessing and implementing the co-benefits of nature-based solutions in urban areas. *Environmental Science & Policy*, *77*, 15–24.

Meenar, M., Heckert, M., & Adlakha, D. (2022). "green enough ain't good enough:" public perceptions and emotions related to green infrastructure in environmental justice communities. *International Journal of Environmental Research and Public Health*, *19*(3), 1448.

Josephs, L. I., & Humphries, A. T. (2018). Identifying social factors that undermine support for nature-based coastal management. *Journal of Environmental Management*, *212*, 32–38.

Frantzeskaki, N. (2019). Seven lessons for planning nature-based solutions in cities. *Environmental science & policy*, *93*, 101–111.

Arkema, K. K., Griffin, R., Maldonado, S., Silver, J., Suckale, J., & Guerry, A. D. (2017). Linking social, ecological, and physical science to advance natural and nature-based protection for coastal communities. *Annals of the New York Academy of Sciences*, *1399*(1), 5–26.

Billion Oyster Project. (2024). *Billion oyster project*. https://www.billionoysterproject.org/

Klinenburg, E. (2021). The seas are rising. could oysters protect us? *The New Yorker*, *97*(24), 30–39. https://www.newyorker.com/magazine/2021/08/09/the-seas-are-rising-could-oysters-protect-us

Scape Studio. (2016). *Living breakwaters*. https://www.scapestudio.com/projects/living-breakwaters/

Baggett, L. P., Powers, S. P., Brumbaugh, R. D., Coen, L. D., DeAngelis, B. M., Greene, J. K., Hancock, B. T., Morlock, S. M., Allen, B. L., Breitburg, D. L., et al. (2015). Guidelines for evaluating performance of oyster habitat restoration. *Restoration Ecology*, *23*(6), 737–745.

Gilby, B. L., Olds, A. D., Peterson, C. H., Connolly, R. M., Voss, C. M., Bishop, M. J., Elliott, M., Grabowski, J. H., Ortodossi, N. L., & Schlacher, T. A. (2018). Maximizing the benefits of oyster reef restoration for finfish and their fisheries. *Fish and Fisheries*, *19*(5), 931–947.

Sollitt, C. K., & Cross, R. H. (1972). Wave transmission through permeable breakwaters. In *Coastal engineering 1972* (pp. 1827–1846).

Van der Meer, J. W., Briganti, R., Zanuttigh, B., & Wang, B. (2005). Wave transmission and reflection at low-crested structures: Design formulae, oblique wave attack and spectral change. *Coastal Engineering*, *52*(10-11), 915–929.

Christou, M., Swan, C., & Gudmestad, O. (2008). The interaction of surface water waves with submerged breakwaters. *Coastal Engineering*, *55*(12), 945–958.

Wiberg, P. L., Taube, S. R., Ferguson, A. E., Kremer, M. R., & Reidenbach, M. A. (2019). Wave attenuation by oyster reefs in shallow coastal bays. *Estuaries and Coasts*, *42*, 331–347.

Sigel, L. (2021). Effect of an artificial oyster reef on wave attenuation.

Allen, R. J., & Webb, B. M. (2011). Determination of wave transmission coefficients for oyster shell bag breakwaters. In *Coastal engineering practice (2011)* (pp. 684–697).

Xiang, T., Bryski, E., & Farhadzadeh, A. (2024). An experimental study on wave transmission by engineered plain and enhanced oyster reefs. *Ocean Engineering*, *291*, 116433.

Salatin, R., Wang, H., Chen, Q., & Zhu, L. (2022). Assessing wave attenuation with rising sea levels for sustainable oyster reef-based living shorelines. *Frontiers in Built Environment*, *8*, 884849.

Vona, I., & Nardin, W. (2023). Oysters' integration on submerged breakwaters offers new adaptive shoreline protection in low-energy environments in the face of sea level rise. *Journal of Geophysical Research: Earth Surface*, *128*(11), e2023JF007249.

Xu, W., Tao, A., Wang, R., Qin, S., Fan, J., Xing, J., Wang, F., Wang, G., & Zheng, J. (2024). Review of wave attenuation by artificial oyster reefs based on experimental analysis. *Ocean Engineering*, *298*, 117309.

Dick, T. M., & Brebner, A. (1968). Solid and permeable submerged breakwaters. In *Coastal engineering 1968* (pp. 1141–1158).

Losada, I., Patterson, M. D., & Losada, M. (1997). Harmonic generation past a submerged porous step. *Coastal Engineering*, *31*(1-4), 281–304.

Webb, B. M., & Allen, R. (2015). Wave transmission through artificial reef breakwaters. *Coastal Structures and Solutions to Coastal Disasters Joint Conference 2015*, 432–441.

Melville, W. K. (1996). The role of surface-wave breaking in air-sea interaction. *Annual review of fluid mechanics*, *28*(1), 279–321.

Terray, E. A., Donelan, M., Agrawal, Y., Drennan, W., Kahma, K., Williams, A. J., Hwang, P., & Kitaigorodskii, S. (1996). Estimates of kinetic energy dissipation under breaking waves. *Journal of Physical Oceanography*, *26*(5), 792–807.

Melville, W. K. (1994). Energy dissipation by breaking waves. *Journal of Physical Oceanography*, *24*(10), 2041–2049.

Armono, H., & Hall, K. (2003). Wave transmission on submerged breakwaters made of hollow hemispherical shape artificial reefs. *Canadian coastal conference*, 313–322.

Dally, W. R., Dean, R. G., & Dalrymple, R. A. (1985). A model for breaker decay on beaches. In *Coastal engineering 1984* (pp. 82–98).

Svendsen, I. A. (2005). *Introduction to nearshore hydrodynamics* (Vol. 24). World Scientific Publishing Company.

Jonsson, I. G. (1967). Wave boundary layers and friction factors. In *Coastal engineering 1966* (pp. 127–148).

Trowbridge, J., & Madsen, O. S. (1984). Turbulent wave boundary layers: 1. model formulation and first-order solution. *Journal of Geophysical Research: Oceans*, *89*(C5), 7989–7997.

Dean, R. G., & Dalrymple, R. A. (1991). *Water wave mechanics for engineers and scientists* (Vol. 2). world scientific publishing company.

Allsop, W., & Channell, A. (1989). Wave reflections in harbours: Reflection performance of rock armoured slopes in random waves.

Zanuttigh, B., & Van der Meer, J. W. (2007). Wave reflection from coastal structures. In *Coastal engineering 2006: (in 5 volumes)* (pp. 4337–4349). World Scientific.

Van Gent, M. (1995). Porous flow through rubble-mound material. *Journal of waterway, port, coastal, and ocean engineering*, *121*(3), 176–181.

Higuera, P., Lara, J. L., & Losada, I. J. (2014). Three-dimensional interaction of waves and porous coastal structures using openfoam®. part i: Formulation and validation. *Coastal Engineering*, *83*, 243–258.

Ergun, S. (1952). Fluid flow through packed columns. *Chemical engineering progress*, *48*(2), 89.

Jensen, B., Jacobsen, N. G., & Christensen, E. D. (2014). Investigations on the porous media equations and resistance coefficients for coastal structures. *Coastal Engineering*, *84*, 56–72.

Jensen, O. J., & Klinting, P. (1983). Evaluation of scale effects in hydraulic models by analysis of laminar and turbulent flows. *Coastal Engineering*, *7*(4), 319–329.

Wolters, G., Van Gent, M., Hofland, B., & Wellens, P. (2014). Wave damping and permeability scaling in rubble mound breakwaters. *Proc., 5th Int. Conf. on the Application of Physical Modelling to Port and Coastal Protection, Coastlab14*, 1–11.

Benoit, M., Molin, B., Remy, F., & Durand, N. (2019). Experimental tests and numerical modeling of submerged wave attenuators made of cages filled with oyster shells in shallow water. *Coastal Structures 2019*.

Kamann, P. J., Ritzi, R. W., Dominic, D. F., & Conrad, C. M. (2007). Porosity and permeability in sediment mixtures. *Groundwater*, *45*(4), 429–438.

Glover, P. W., & Luo, M. (2020). The porosity and permeability of binary grain mixtures. *Transport in Porous Media*, *132*(1), 1–37.

Goda, Y., & Suzuki, Y. (1976). Estimation of incident and reflected waves in random wave experiments. In *Coastal engineering 1976* (pp. 828–845).

Massel, S. (1983). Harmonic generation by waves propagating over a submerged step. *Coastal Engineering*, *7*(4), 357–380.

Ting, C.-L., Chao, W.-T., & Young, C.-C. (2016). Experimental investigation of nonlinear regular wave transformation over a submerged step: Harmonic generation and wave height modulation. *Coastal Engineering*, *117*, 19–31.

Jacobsen, N. G., Fuhrman, D. R., & Fredsøe, J. (2012). A wave generation toolbox for the open-source cfd library: Openfoam®. *International Journal for numerical methods in fluids*, *70*(9), 1073–1088.

Seiffert, B. R., Ertekin, R. C., & Robertson, I. N. (2015). Wave loads on a coastal bridge deck and the role of entrapped air. *Applied Ocean Research*, *53*, 91–106.

Chen, W., Warmink, J., van Gent, M., & Hulscher, S. (2020). Modelling of wave overtopping at dikes using openfoam. *Coastal Engineering Proceedings*, (36v), 27–27.

Ferziger, J. H., Perić, M., & Street, R. L. (2019). *Computational methods for fluid dynamics*. springer.

Gray, W. G. (1975). A derivation of the equations for multi-phase transport. *Chemical Engineering Science*, *30*(2), 229–233.

Jacobsen, N. G. (2017). Waves2foam manual. *Deltares, The Netherlands*, *570*.

Berberović, E., van Hinsberg, N. P., Jakirlić, S., Roisman, I. V., & Tropea, C. (2009). Drop impact onto a liquid layer of finite thickness: Dynamics of the cavity evolution. *Physical Review E*, *79*(3), 036306.

Choi, Y.-M., Kim, Y. J., Bouscasse, B., Seng, S., Gentaz, L., & Ferrant, P. (2020). Performance of different techniques of generation and absorption of free-surface waves in computational fluid dynamics. *Ocean Engineering*, *214*, 107575.

Mayer, S., Garapon, A., & Sørensen, L. S. (1998). A fractional step method for unsteady free-surface flow with applications to non-linear wave dynamics. *International Journal for Numerical Methods in Fluids*, *28*(2), 293–315.

Chen, Q., Kelly, D. M., & Zang, J. (2019). On the relaxation approach for wave absorption in numerical wave tanks. *Ocean Engineering*, *187*, 106210.

Le Méhauté, B. (1976). *An introduction to hydrodynamics and water waves*. Springer Science & Business Media.

Foumeny, E., Kulkarni, A., Roshani, S., & Vatani, A. (1996). Elucidation of pressure drop in packed-bed systems. *Applied Thermal Engineering*, *16*(3), 195–202.

Nemec, D., & Levec, J. (2005). Flow through packed bed reactors: 1. single-phase flow. *Chemical Engineering Science*, *60*(24), 6947–6957.

Li, L., & Ma, W. (2011). Experimental study on the effective particle diameter of a packed bed with non-spherical particles. *Transport in porous media*, *89*, 35–48.

Dolejs, V., & Machac, I. (1995). Pressure drop during the flow of a newtonian fluid through a fixed bed of particles. *Chemical Engineering and Processing: Process Intensification*, *34*(1), 1–8.

Comiti, J., & Renaud, M. (1989). A new model for determining mean structure parameters of fixed beds from pressure drop measurements: Application to beds packed with parallelepipedal particles. *Chemical Engineering Science*, *44*(7), 1539–1545.

Ardhuin, F., & Herbers, T. (2002). Bragg scattering of random surface gravity waves by irregular seabed topography. *Journal of Fluid Mechanics*, *451*, 1–33.

Ni, Y.-L., & Teng, B. (2021). Bragg resonant reflection of water waves by a bragg breakwater with porous rectangular bars on a sloping permeable seabed. *Ocean Engineering*, *235*, 109333.

Reidenbach, M. A., Berg, P., Hume, A., Hansen, J. C., & Whitman, E. R. (2013). Hydrodynamics of intertidal oyster reefs: The influence of boundary layer flow processes on sediment and oxygen exchange. *Limnology and Oceanography: Fluids and Environments*, *3*(1), 225–239.

Kitsikoudis, V., Kibler, K. M., & Walters, L. J. (2020). In-situ measurements of turbulent flow over intertidal natural and degraded oyster reefs in an estuarine lagoon. *Ecological Engineering*, *143*, 105688.

Donker, J., Van der Vegt, M., & Hoekstra, P. (2013). Wave forcing over an intertidal mussel bed. *Journal of Sea Research*, *82*, 54–66.

Monismith, S. G., Rogers, J. S., Koweek, D., & Dunbar, R. B. (2015). Frictional wave dissipation on a remarkably rough reef. *Geophysical Research Letters*, *42*(10), 4063–4071.

Hitzegrad, J., Köster, S., Windt, C., & Goseberg, N. (2024). Understanding the role of sharp edges in the propagation of surface gravity waves. *Journal of Geophysical Research: Oceans*, *129*(2), e2023JC020336.

Lowe, R. J., Falter, J. L., Koseff, J. R., Monismith, S. G., & Atkinson, M. J. (2007). Spectral wave flow attenuation within submerged canopies: Implications for wave energy dissipation. *Journal of Geophysical Research: Oceans*, *112*(C5).

Dalrymple, R. A., Kirby, J. T., & Hwang, P. A. (1984). Wave diffraction due to areas of energy dissipation. *Journal of waterway, port, coastal, and ocean engineering*, *110*(1), 67–79.

Lowe, R. J., Shavit, U., Falter, J. L., Koseff, J. R., & Monismith, S. G. (2008). Modeling flow in coral communities with and without waves: A synthesis of porous media and canopy flow approaches. *Limnology and Oceanography*, *53*(6), 2668–2680.

Whitman, E. R., & Reidenbach, M. A. (2012). Benthic flow environments affect recruitment of crassostrea virginica larvae to an intertidal oyster reef. *Marine Ecology Progress Series*, *463*, 177–191.

Styles, R. (2015). Flow and turbulence over an oyster reef. *Journal of Coastal Research*, *31*(4), 978–985.

Gon, C. J., MacMahan, J. H., Thornton, E. B., & Denny, M. (2020). Wave dissipation by bottom friction on the inner shelf of a rocky shore. *Journal of Geophysical Research: Oceans*, *125*(10), e2019JC015963.

Sogut, E., Sogut, D. V., & Farhadzadeh, A. (2019). Effects of building arrangement on flow and pressure fields generated by a solitary wave interacting with developed coasts. *Advances in water resources*, *134*, 103450.

Wang, H., Huang, W., Harwell, M. A., Edmiston, L., Johnson, E., Hsieh, P., Milla, K., Christensen, J., Stewart, J., & Liu, X. (2008). Modeling oyster growth rate by coupling oyster population and hydrodynamic models for apalachicola bay, florida, usa. *Ecological Modelling*, *211*(1), 77–89. https://doi.org/10.1016/j.ecolmodel.2007.08.018

Huang, C.-J., Chang, H.-H., & Hwung, H.-H. (2003). Structural permeability effects on the interaction of a solitary wave and a submerged breakwater. *Coastal engineering*, *49*(1-2), 1–24.

Fuchs, H. L., Hunter, E. J., Schmitt, E. L., & Guazzo, R. A. (2013). Active downward propulsion by oyster larvae in turbulence. *Journal of Experimental Biology*, *216*(8), 1458–1469.

Fuchs, H. L., Gerbi, G. P., Hunter, E. J., Christman, A. J., & Diez, F. J. (2015). Hydrodynamic sensing and behavior by oyster larvae in turbulence and waves. *The Journal of Experimental Biology*, *218*(9), 1419–1432.

Powers, S. P., & Grabowski, J. H. (2023). Changes in water flow alter community dynamics in oyster reefs. *Ecosphere*, *14*(4), e4405.

Rosenzweig, C., Solecki, W. D., Blake, R., Bowman, M., Faris, C., Gornitz, V., Horton, R., Jacob, K., LeBlanc, A., Leichenko, R., et al. (2011). Developing coastal adaptation to climate change in the new york city infrastructure-shed: Process, approach, tools, and strategies. *Climatic change*, *106*, 93–127.

Vulnerable landscapes. (2023). https://www.statenislandmuseum.org/exhibitions/vulnerable-landscapes/